EXPERIMENTAL AND COMPUTATIONAL STUDIES ON THE STRUCTURE-REACTIVITY RELATIONSHIP OF SOME RHODIUM- AND IRIDIUM-BASED COMPLEXES AND THEIR CATALYTIC ACTIVITY IN HYDROGEN TRANSFER REACTIONS

BY

SAHEED ABIODUN POPOOLA

A Dissertation Presented to the

DEANSHIP OF GRADUATE STUDIES

KING FAHD UNIVERSITY OF PETROLEUM & MINERALS

DHAHRAN, SAUDI ARABIA

In Partial Fulfillment of the
Requirements for the Degree of

DOCTOR OF PHILOSOPHY

In

CHEMISTRY

MAY 2016

KING FAHD UNIVERSITY OF PETROLEUM & MINERALS

DHAHRAN- 31261, SAUDI ARABIA

DEANSHIP OF GRADUATE STUDIES

This thesis, written by **Saheed Abiodun Popoola** under the direction his thesis advisor and approved by his thesis committee, has been presented and accepted by the Dean of Graduate Studies, in partial fulfillment of the requirements for the degree of **DOCTOR OF PHILOSOPHY IN CHEMISTRY**.

Dr. Abdulaziz Al-Saadi
(Advisor)

9/5/2016

Dr. Abdulaziz Al-Saadi
Department Chairman

Prof. Luis A. Oro
(Member)

Dr. Salam A. Zummo
Dean of Graduate Studies

Dr. Nisar Ullah
(Member)

9/5/16

Date

Dr. Bassam El Ali
(Member)

Dr. Anvarhusein Isab
(Member)

This Dissertation is dedicated to my Almighty Allah, the Lord of universe.

Without His permission this work would not have been successful

ACKNOWLEDGMENTS

To Almighty Allah be all the glories and adorations. I give thanks to Him for His mercy, blessing and protection over since I was born into this world.

My sincere appreciation goes to my advisor and mentor Dr. Abdulaziz Al-Saadi for his immense contribution towards the success of this research work. Without him I would have been a lost sheep in the wilderness. His tenderness, humility, moral and financial supports are incomparable. Sir, I shall forever be grateful to you. I am also grateful to Prof. Luis A. Oro from the University of Zaragoza for his unquantifiable contributions to the success of this research work. Sir, your fatherly role towards the success of this work lives forever in my memory. My sincere gratitude also goes to the wonderful members of my committee, Dr Nisar Ullah, Dr Bassam El Ali and Anvarhusein Isab for their immense contributions. I also want to thank Dr Jaseer of Center for Refining and Petrochemical for the training as well as support and encouragement.

I wish to register my since gratitude to all the faculties and staffs of Chemistry Department, KFUPM, for their cooperation and support during my programme.

My heartfelt appreciation goes to my wife, Bilikisu Popoola, my two daughters Maryam and Zainab Popoola for their endurance, understanding, supports and prayers. Also, my humble gratitude goes to my mother, uncles Mr. Azeez O. Musbaudeen, Mr. Azeez O. Akeem and my siblings Selimat, Rafiat, Samsideen and Khadijat for their understanding and prayers. I also appreciate kind gesture of all my friends and colleagues at KFUPM.

Finally, I want to thank the Deanship of Graduate Studies, KFUPM for awarding me the scholarship.

TABLE OF CONTENTS

LIST OF TABLES

LIST OF FIGURES

LIST OF SCHEMES

ABSTRACT

Full Name : Saheed Abiodun Popoola

Thesis Title : Experimental and Computational Studies on the Structure-Reactivity Relationship of Some Rhodium- and Iridium-Based Complexes and Their Catalytic Activity in Hydrogen Transfer Reactions

Major Field : Chemistry

Date of Degree : April, 2016

Owing to the significance of 1,5-cyclooctadiene (COD) complexes of iridium and rhodium metal as precursors for most of important catalysts, comprehensive studies were carried out on them. Single-molecule vapor-phase density functional theory (DFT) calculation revealed lower symmetry D_2 and C_2 for $[Rh(\mu\text{-}Cl)(COD)]_2$ and $[Ir(\mu\text{-}Cl)(COD)]_2$, respectively, in addition to their X-ray reported configurations and they were predicted to be more stable by 7 kcal/mol. On the part spectroscopic studies, analysis affirms the presence of lower symmetry in trace amount along with the dominant higher symmetry in the solid phase of the two complexes. However, NMR results agreed only with higher symmetry as the complex configuration. In addition to chloro, the study was extended to methoxo and amido-bridged cyclooctadiene complexes of the two metals. With respect to the bridging ligands, theoretical energetics evaluation revealed that the magnitude of binding energy was in the order of $NH_2 < OCH_3 < Cl$ while that of coordination energy was $OCH_3 < NH_2 < Cl$. The use of Dewar-Chatt-Duncanson (DCD) model for metal-olefin interaction prediction, showed that the interaction was in the order of $NH_2 < Cl < OCH_3$ which is quite agreeable with the trend of $(\pi+\sigma)$ metal-olefin interaction predicted by using the frequency shifts obtained from detailed vibrational assignment. On the other hand, the π components in the interaction was in the order of $NH_2 < OCH_3 < Cl$. On the issue of reactivity, complex ionization potentials and absolute

electronegativity were found to be in the order of $NH_2 < OCH_3 < Cl$ but in general, amido bridged dinuclear complexes of both metals were found to more reactive than others. For easy handling, chloro and methoxo bridged COD complexes of iridium were used with monodentate P-donor ancillary ligands for transfer hydrogenation reaction of acetophenone. Methoxo-bridged complex was found to be more catalytically beneficial with the order of activity of ancillary ligands being $P(p\text{-}OMeC_6H_4)_3 > PPh_3 > P(p\text{-}FC_6H_4)_3$. However, the replacement of COD with tetrafluorobenzobarrelene (TFBB), an electron withdrawing diolefin, caused a reversal in the activity of the ancillary ligands. While the theoretical investigation into the reaction mechanism showed the involvement of stepwise mechanism where the participation of metal hydride was the most probable reaction path for both COD and TFBB systems in the transfer hydrogenation of acetophenone. Similar to monodentate, ancillary bidentate diphosphine ligands were also used with both COD and TFBB methoxo- bridged complex systems. It was found that catalytic activity of systems was dependent on the interplay of electronic and steric properties of ligands together with nature of diolefin. The order of performance for the COD system was found to be dppp > dppm > dppb > dppe, whereas a different trend was recorded for TFBB. Consequently, the results obtained affirmed the coordination of diolefin during the course of catalytic reaction. In case of study on phosphinic acids, substituents bulkiness was found to play a significant role in their conformations. In addition, the presence of OH and P=O in their functional groups led to dimerization through hydrogen bonding. Moreover, natural bond orbital analysis was carried out to evaluate their reactivity which revealed their order to be phosphinic acid > dimethylphosphinic > bis(4-methoxyphenyl)phosphinic > diphenylphosphinic >

phenylphosphinic acid. Based on the theoretical revelation, dimethylphosphinic acid was used for the synthesis of di-μ-dimethylphos-phinate bis(1,5-cycloocadiene) di-rhodium(I).

ملخص الرسالة

الإسم : سعيد أبيدون بوبولا

إسم الأطروحة: الدراسات التجريبية والحسابية على العلاقة بين بنية الهيكل والنشاط الحفزي لبعض مركبات الريديم والإريديم وإمكانياتهم التحفيزية في تفاعل نقل الهيدروجين

القسم : الكيمياء

التاريخ: أبريل 2016

نظرا لأهمية 1-5 أوكتاداايين الحلقي المكون من مركبات معادن الإريديم و الروديم كمون أساسي لأغلب المحفزات ، أجريت العديد من الأبحاث المهمة عليها. كشفت نظرية الكثافة الوظيفية للطور البخاري على الجزئي اللآحادي انخفاض التماثل د2 و س2

$[Rh(\mu\text{-}Cl)(COD)]_2$ and $[Ir(\mu\text{-}Cl)(COD)]_2$

بالإضافة لذلك فإن الأشعة السينية أظهرت ظهور تكوينات و يتوقع لها أن تكون أكثر استقرارا بنسبة 7 كيلو كالوري / مول . بالنسبة لجانب دراسات الجزئية الطيفية فإن التحليلات تؤكد وجود انخفاض في التماثل في كمية بسيطة أثر جنبا إلى جنب مع التماثل العالي السائد في المرحلة الصلبة من المركبين. ومع ذلك، وافقت نتائج الرنين المغناطيسي فقط مع ارتفاع التماثل كما في التكوينات المعقدة. بالإضافة إلى الكلور،إمتدت هذه الدراسة أيضا لتشمل مركبات الميثوكسي والأميدو المتصلة بالأوكتاداايين الحلقي. بالنسبة لهذه الروابط المتصلة أظهرت تحليلات الطاقة النظرية أن حجم طاقة الربط كان حسب الترتيب الكلور > الميثوكسي > الأميدو. إستخدام نموذج التبنؤ برد الفعل بين المعادن والأوليفات ديور- شات- دنكانسون و أظهر أن رد الفعل كان حسب الترتيب التالي الميثوكسي > الكلور > الأميدو بما يطابق نوعا ما اتجاه ($\pi+\sigma$) لرد الفعل بين المعادن والأوليفينات المتحصل عليه بإستخدام إزاحة الذبذات بأستعمال دراسة الإهتزازات المفصلة. في الجانب الاخر، مكون π بين رد الفعل كان حسب الترتيب الكلور > الميثوكسي > الأميدو. وفيما يتعلق بمسألة التفاعل، تم العثور على إمكانات التأين معقدة والكهربية المطلق فكانت حسب الترتيب الكلور > الميثوكسي > الأميدو، لكن على العموم وجد أن رابطة الأميدو ثنائية النووية لكلا المعدنين لها قدرة أعلى على التفاعل بالمقارنة مع بقية الروابط. لتسهيل التعامل فإن رابطة الكلور والميثوكسي مع الإريديم إستخدمت كمانح أحادي لتفاعل هدرجة الأستوفينون. رابطة الميثوكسي وجدت أكثر فائدة حفزيا حسب ترتيب التالي

$P(p\text{-}OMeC_6H_4)_3 > PPh_3 > P(p\text{-}FC_6H_4)_3$

ومع ذلك تسبب إستبدال 1-5 أوكتاداايين الحلقي برباعي فلورو بنزين بارلين بفقدان إلكترون ثنائي الأولفين مما تسبب بنقص في النشاط التفاعلي للرابطة. بينما كشف البحث النظري في آلية التفاعل على أن هدرجة المعادن كانت المساهم المحتمل الغالب بالنسبة لمسار تفاعل 1-5 أوكتاداايين الحلقي و رباعي فلورو بنزين بارلين وهدرجتها إلى

أستوفينون. وبالمثل بالنسبة للمونودينتيت، أستخدمت رابطة البايندتيت دايفسفين مع كل من 1-5 أوكتاداايين الحلقي برباعي فلورو بنزين بارلين. وجد أن النشاط التفاعلي في هذا النظام كان يعتمد على الخصائص الإلكترونية والفراغية معا بالإضافة الى طبيعة الدايأولفين. ترتيب أداء هذه 1-5 أوكتاداايين الحلقي كان

dppp > dppm > dppb > dppe

وهو مغاير تماما لما لوحظ عند رباعي فلورو بنزين بارلين. فتبعا لذلك فإن النتائج المتحصل عليها تؤكد على تنسيق الدايأولفين خلال التفاعل. وفي بحث دراسي لحمض الفوسفينك وجد أن البدائل الضخمة تلعب دورا مهما في تأكيد ذلك. بالإضافة الى ذلك فإن ظهور

OH and P=O

ومجموعاتهم الوظيفية أدى إلى حدوث تأين من خلال رابطة الهيدروجين. وزيادة على ذلك فإن تحليل مجال الرابطة الطبيعي والذي استخدم لتقييم النشاط التفاعلي أوضح أن ترتيب النشاط هو

phosphinic > diphenylphosphinic > phenylphosphinic acid

بناءا على التبنؤ النظري فإن حمض ثنائي ميثيل فوسفينك أستخدم في تحضير ثنائي مايكرو ثنائي ميثيل فوسفنيت و 1-5 أوكتاداايين الحلقي ثنائي الريديم.

CHAPTER 1

INTRODUCTION

The impressive developments of organometallic chemistry during the past decades have allowed the preparation of a wide variety of soluble metal complexes useful for organic transformations under mild conditions. This, in turn has opened door for field of research in homogenous catalysis. Homogeneous catalysis is considered one of the very active areas of applied research in chemistry and has shown an outstanding development in recent years, not just because of the great number of applications in terms of selective preparation of high value added chemicals, but also its interdisciplinary characters which link both the academic and industrial interests together. Additionally, the high atom economy usually enjoyed with homogenous catalysis by avoiding waste formation significantly contribute to green chemistry and make this field a highly desirable area of research. Applications of homogenous catalysis extend from bulk to fine chemistry products. Among these applications, transfer hydrogenation has found applications in the production of alcohol, drugs, scents as well as fragrance.

In the field of homogenous catalysis, transition metals play a key role in the design and synthesis of catalysts. Among these transition metals, rhodium and iridium, are mostly used for catalyst synthesis due to their high electronegativity and presence of relatively low energy orbitals whose energies match or are closer to that of the ligands. Subject to this electronegative nature, late transition metals tend to retain their valence electrons and form stable complexes at low oxidation states. Unlike the early transition metals, back donation is not so much remarkable with late metals and therefore any unsaturated ligands attached to them would bear resultant positive charges which are prone to

nucleophilic attacks in organic synthesis [1]. In addition, the development of homogenous catalysts is linked to the design of ligands that are able to influence the properties of the metallic center. The ligand topology determines the catalyst structure while the electronic character of the coordination centers as well as its size or flexibility governs the affinity for a particular substrate which eventually determines the stability, reactivity and catalytic activity of complexes. Hence, the success of homogeneous catalyzed reactions relies primarily on the proper combination of a metal and a ligand system. With this understanding, considerable efforts have been directed towards the development of transition metal complexes as catalysts. This has led to an extensive use of iridium and rhodium metals in combination with a variety of ligands such as phosphine, carbene and amine in the formation of metal complexes and their subsequent use in various catalytic reactions [2–7]. In the same sense, a vast number of mono- and binuclear iridium and rhodium based complexes have been prepared using diolefinic ligands such as norbornadiene and 1,5-cycloctadiene. These diolefins might remained coordinated during the course of catalytic reaction in some cases as being proposed by Noyori *et al*, [8–10] while in others they get replaced. Unlike the aforementioned ligands, phosphinic acid and its derivatives have not been widely used as ligands in homogeneous catalytic reactions. Only few reports are available on their catalytic applications as ligands. In one report, rhodium (II) phosphinate was used [11] in rhodium-mediated carbenoid reactions to facilitate series of cyclopropanation reactions, while in an another report diphenylphosphinic acid [12] was used as a promoter in the carbonylation of nitroarenes to diarylureas catalyzed by palladium based catalytic system.

The success of homogenous catalysis relies upon the appropriate combination of metals and ligands. Therefore several tools have been used to study the suitability of metal complexes and ligands for a particular reaction. Spectroscopy and computational techniques have also been employed to understand the nature of the electronic and steric influence of ligands on the metal centre [13–20] . Infrared and Raman methods can provide rich information regarding the nature of coordination, electronic properties of the metal, σ-donation ability, and others by inspecting the spectral fingerprints of these complexes. In addition, vibrational spectroscopy is used to assess the nature of the metal-olefin bonds in which the magnitude of changes in carbon-carbon double bond stretching frequency are compared to free ligands [13]. In another method, this technique is used to estimate metal-metal bond strength in binuclear complexes via reliance on force constants k [15] which is considered to be a more sensitive indicator of metal-metal bond strength than frequencies. The understanding of the interactions in the molecules affords better prediction of their chemistries. On the other hand, computational technique has been helpful in the study of steric effects of ligands. The cone angle for monodentate ligand as well as bidentate ligand bite angles have been established via theoretical calculations.

A wide number of catalytic systems using different rhodium and iridium complexes have been employed in hydrogen transfer reaction [4, 21–27]. In hydrogen transfer reaction, a hydrogen is transferred from hydrogen donor, usually an alcohol, to a hydrogen acceptor with the use of suitable catalyst. The result is the addition of hydrogen to a multiple bond of unsaturated substrate yielding a hydrogenated product. Transfer hydrogenation is a process with a high atom economy. In addition, although, it is second to catalytic molecular hydrogen addition but due to its risk reduction as well as elimination of safety

restriction, transfer hydrogenation is advantageous over catalytic hydrogenation which involves use of pressure vessel [28]. It is considered an important methodology for reduction of organic double bonds by hydrogen addition donated from organic or inorganic sources (alcohols, formic acid, hydrazine, etc.) under mild reaction conditions. The use of cationic Ir(I) compound of the type $[Ir(cod)(L)_2]^+$ (L = N-, P- donor) and Ir(III) in hydrogen transfer reactions have been reported and their catalytic activities have been found to depend on the activity and selectivity of the electronic and steric properties of the N- or P- donor ligands [29–32]. Moreover, the substitution of phosphines by carbene ligands (NHC), has led to the emergence of a second generation catalysts which are frequently used for hydrogen transfer reactions. These types of catalysts as well as iridium(III) complexes containing bis-NHC ligands have shown excellent activities in hydrogen transfer reactions to imines, C=O and C=C [29–33].

An interesting part in the homogenous catalysis is the prediction of probable reaction mechanisms. However, the short lifetime of intermediates makes the understanding of mechanistic pathways a challenging task. The use of *Ab initio* calculations have been helpful in providing a reasonable understanding about the pathways followed by catalytic reactions. Among the three established mechanisms for hydrogen transfer reaction, the inner-sphere mechanism follows hydrido route whose formation is a critical step in the cycle involving participation of metal centre. Scheme 1, illustrates a typical inner-sphere hydrogen transfer reaction mechanism.

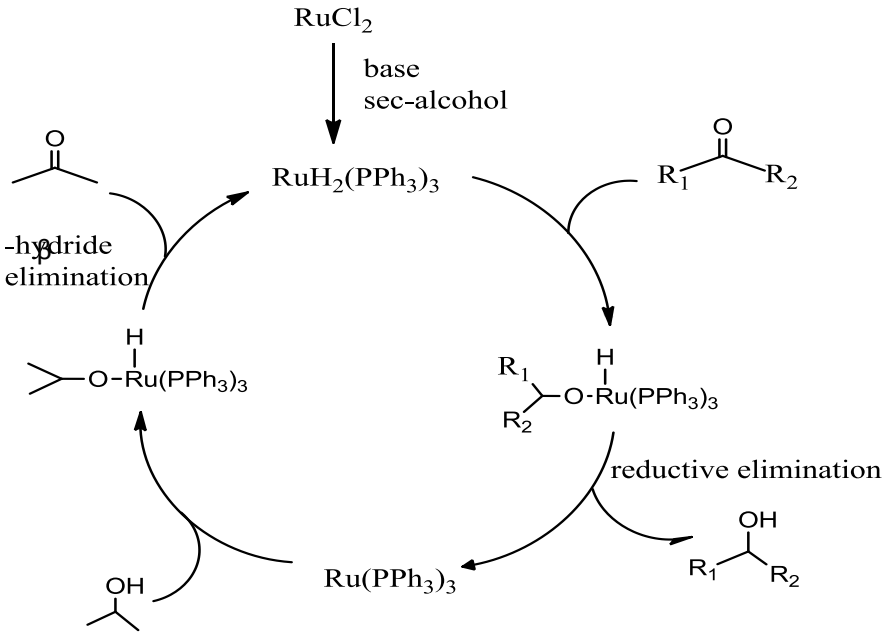

Scheme 1. Hydrido route mechanism of hydrogen transfer reaction

The second mechanism proposed by Meerwein-Ponndorf-Verley (MPV) is an outer sphere mechanism that proceeds via a six membered ring transition state without the coordination of hydrogen donor to the metal (Scheme 2) [22]. This mechanism involves direct hydrogen transfer.

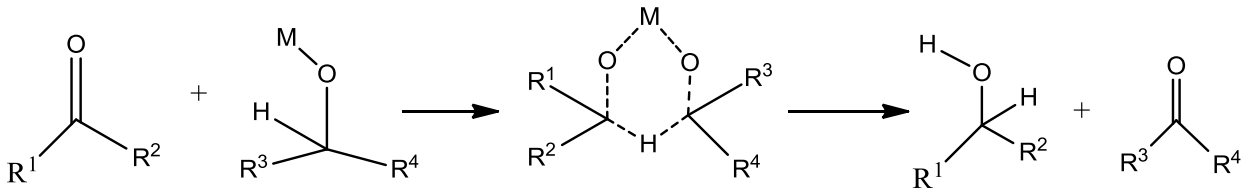

Scheme 2. Meerwein-Ponndorf-Verley (MPV) hydrogen transfer reaction mechanism

The third type of the mechansim is also an outer-sphere mechanism but is bifunctional. A typical example established by Noyori (see Scheme 3) where the catalyst ligand sites

act as a basic centre interacting with the alcohol via a hydrogen bonding and hence realizing the hydride transfer [22].

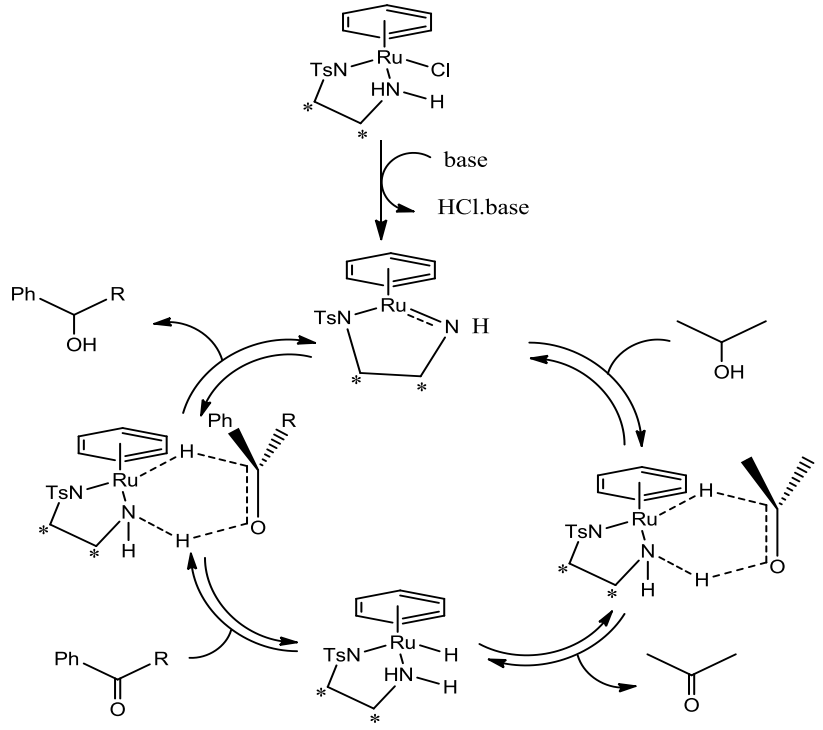

Scheme 3. Bifunctional mechanism for hydrogen transfer reaction

In a generalized sense, the mechanisms for transition-metal-catalyzed hydrogen transfer reactions are usually consist of oxidative addition, reductive elimination, migratory insertion and β-hydrogen elimination reactions as illustrated:

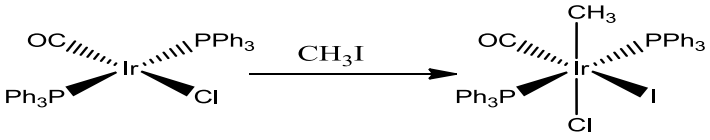

Scheme 4: Oxidative Addition Reaction

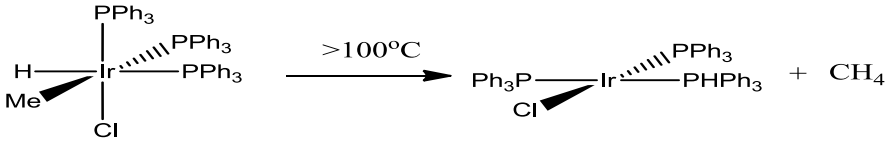

Scheme 5: Reductive Elimination Reaction

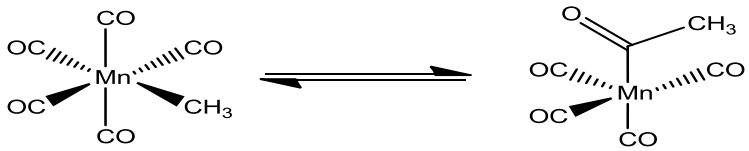

Scheme 6: Migratory Insertion Reaction

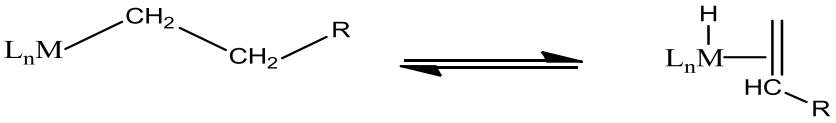

Scheme 7: β-elimination

CHAPTER 2

METHODOLOGY

Both experimental and computational methods have been employed in this work to fulfill our research objectives. As a general view, this work has gone through three main stages: (i) the synthesis and characterization of some dinuclear iridium and rhodium based complexes, (ii) the study of their structure-reactivity relationship with the help of spectroscopic and computational tools, (iii) the application of these complexes in some hydrogen transfer reactions. Scheme 8 summarizes the flow of the objectives of this work and main techniques utilized at each stage.

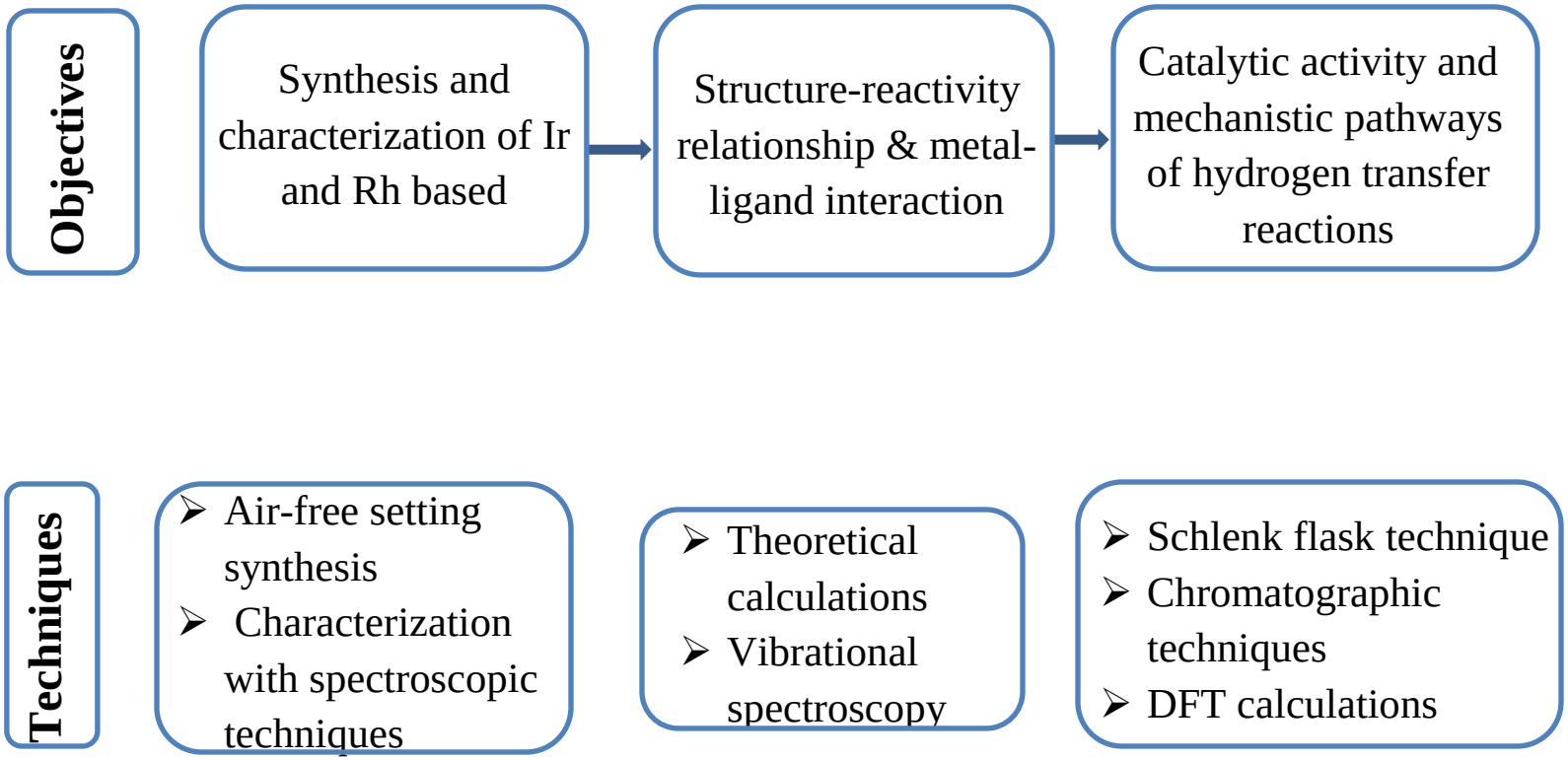

Scheme 8: Objectives followed and techniques used to execute the tasks of this work.

2.1. Experimental

For the experimental part, all the chemicals were purchased from Sigma Aldrich Chemicals and used without further purification. In addition, all the solvents used for both complex synthesis and hydrogen transfer reactions were first purified using standard procedures and distilled under argon prior to use. Furthermore, the synthesis of the complexes was carried out under an inert atmosphere with use of schlenk-tube technique [34] following standard procedure.

2.2. Synthesis of Dinuclear Iridium and Rhodium Based Complexes

2.2.1. Synthesis of $[Ir(\mu\text{-}Cl)COD]_2$

6 mL of distilled water, 2.2 mL of isopropanol and 1.2 mL of 1,5-cyclooctadiene were mixed into 50 mL two neck round bottomed flask. The solvent mixture was first purged with argon after which a condenser was connected to the flask. Then, the mixture was refluxed for 1 hour prior to the addition of 1 g of $IrCl_3.3H_2O$ and further refluxed for 8 hours after the addition, under strong stirring. The suspended liquid was removed via cannula and the cold methanol was added to red oil left to effect formation of red crystalline solid. The solid was later filtered, washed with cold methanol and dried under vacuum [35].

2.2.2. Synthesis of $[Rh(\mu\text{-}Cl)COD]_2$

1 g of $RhCl_3.3H_2O$ was weighed in 50 mL two neck round bottomed flask fitted with condenser, then vacuumed and filled with argon. Then, 10 mL of ethanol, 2 mL of distilled water and 1.4 mL of 1,5-cyclooctadiene were added into the flask. Thereafter, the reaction mixture was refluxed for 8 hours under strong stirring. The resulting yellow

precipitate was filtered, washed with distilled water and ethanol and dried under high vacuum [36].

2.2.3. Synthesis of $[M(\mu\text{-}OMe)(COD)]_2$ (M=Rh, Ir)

1 g of $[M(\mu\text{-}Cl)COD]_2$ and 1 g of Na_2CO_3 were mixed into 100 mL two neck round bottomed flask. Then vacuum was applied and filled with argon prior to the addition of 40 mL of methanol. Thereafter, the reaction mixture was stirred at room temperature for 2 hour before the addition of small volume of water to dissolve Na_2CO_3 and further stirred the mixture for 30 mins. The solution was then filtered, washed with water and methanol and dried under vacuum in a round bottom flask [37].

2.2.4. Synthesis of $[Ir(\mu\text{-}OMe)(TFBB)]_2$ (TFBB = Tetrafluorobenzobarrelene)

40 mL of methanol was measured in to 100 mL round bottomed flask under an inert atmosphere. Then 1 g of K_2CO_3 was dissolved in it, followed by the addition of 1 g of $[Ir(Cl)(TFBB)_2]_2$ [38]. The reaction mixture was stirred overnight at room temperature and the resulting orange precipitate was filtered, washed with methanol and diethyl ether and dried under vacuum [38].

2.2.5. Synthesis of $[M(\mu\text{-}NH_2)(COD)]_2$ (M=Rh, Ir)

1.5 mmol of $[M(\mu\text{-}OMe)COD]_2$ was weighed into schlenk flask. It was then vacuumed and purged with nitrogen gas. Thereafter, 8 mL of ether was added and the flask was kept at -15 ^oC (ice + acetone). Ammonia gas was later bubbled into the flask through needle for 30 mins. The reaction was then stopped and the supernatant was removed via cannula

at -10 ^{o}C. Thereafter, the solid obtained was kept under vacuum for 1 hour before being transferred into glove box [4].

2.2.6. Preparation of Di-μ-dimethylphosphinate bis(1,5-Cyclooctadiene) Di-Rhodium(I)

0.64 mmol of $[Rh(\mu\text{-}OMe)(COD)]_2$ was added to dichloromethane (10 ml) solution of 1.28 mmol of dimethylphosphinic acid and the reaction mixture was stirred at room temperature for 18 hours. The solvent was thereafter evaporated under reduced pressure and a bright yellow solid was obtained at the yield of 83%. The resulting solid was then characterized using mass spectrometry, crystallography and elemental analyzer.

2.3. Characterization

The NMR analysis of the deuterated chloroform solution of all the synthesized complexes were carried out using NMR of 500 MHz. The infrared spectrum of 1,5-cyclooctadiene was recorded through smart orbit technique while those of the complexes were sampled in KBr pellets. Moreover, the Raman spectrum for the cyclooctadiene as well as those of complexes was recorded via a 1 mm glass tube using a laser source of 1064 nm with 0.3 W power.

2.4. Hydrogen Transfer Reaction

0.03 mmol of the catalyst and 0.06 or 0.12 mmol of the ligand were weighed into a schlenk flask inside a glove box. Also, 0.09 mmol of KOH was weighed into another schlenk flask. Then, both flasks were vacuumed and purged with argon. Thereafter, 2 mL of *i*-PrOH was added into the schlenk flask containing catalyst and ligand while 1 mL was added into that of KOH through syringe. The two solutions were then stirred for 30 mins at room temperature, after which the base solution was quantitatively transferred to

the catalyst schlenk flask and the resulting mixture was further stirred for 30 mins prior to the addition of 3 mmol of acetophenone and 3 mmol of internal standard mesitylene. The reaction mixture was then placed in a thermostated oil bath at 60 ^{o}C with strong stirring. The progress of reaction was then monitored through GC [4].

2.5. Computation

All the theoretical calculations were carried out using Ab initio density functional theory (DFT) method provided by Gaussian 09 program [39]. B3LYP level was used for all the calculation while the basis sets were chosen based on target. For the Optimization calculation, basis set of SDD was chosen for metals while 6-311++g(d,p) was used for nonmetals with the inclusion of Grimme dispersion correction [40] and the convergence was checked through the frequency calculation analysis. The vibrational frequencies and population analysis being undertaken through full Natural Bond Orbital (NBO) analysis were also calculated using the same basis set. The Raman intensities were computed according to:

$$I_n = f \frac{(\nu_{ex}-\nu_n)^4}{\nu_n(1-e^{-(hc\nu_n/KT)})} S_n \quad (1)$$

Where ν_{ex} is excitation wavenumber with the value of 18798 cm^{-1}, ν_n is the nth normal mode harmonic frequency, S_n is the nth normal mode Raman activity, T is the temperature set at 25 ^{o}C while f is a normalization factor used for all the mode intensity.

The proton NMR shifts were computed using Gauge-Independent Atomic Orbital (GIAO) method. The Polarizable Continuum Model (PCM) using the integral equation formalism variant (IEF) was implemented to predict the solvent effect on the theoretical

NMR spectral data for both complexes. The incorporation of Grimme dispersion correction [40] was found to produce more reliable results in better agreement with experimental values.

For the reaction mechanism, a basis set of def2svp with the incorporation of Grimme dispersion correction was used for all atoms in optimizing all the intermediates and calculating for transition states. Furthermore, the nature of transition states was checked using the negative frequency analysis.

CHAPTER 3

STUDIES ON CHLORO-BRIDGED CYCLOOCTADIENE COMPLEXES OF RH AND IR METALS

3.1. Introduction

The complexes of di-μ-chloro bis(1,5-cyclooctadiene) di-rhodium(I); $[Rh(\mu\text{-}Cl)(COD)]_2$, and di-iridium(I); $[Ir(\mu\text{-}Cl)(COD)]_2$ have shown prominent activities in a number of catalytic reactions. There are different reports where they were used as precursor catalysts in the development of catalytic systems for particular reactions application [41–43]. In another report, the iridium complex was used as a sole catalyst for ligand free transfer hydrogenation of ketones and aldehydes [23]. Over the past years, attention has been shifted to exploration of structural and vibrational properties of the two complexes. Crystallography studies had been used to establish the symmetry of $[Rh(\mu\text{-}Cl)(COD)]_2$ in the solid phase as D_{2h} [44, 45] . The same D_{2h} was also first reported for the ruby form of $[Ir(\mu\text{-}Cl)(COD)]_2$ [46] before being latter established to be C_{2v} [47]. On the other hand, vibrational spectroscopy was used for vibrational assignments of ν(C=C), ν(M-Cl) and ν(M-olefin) vibrations in $[Rh(\mu\text{-}Cl)(COD)]_2$ [48] as well as correlating frequencies shift between the free and coordinated diolefin to the strength of metal-olefin bond interaction [13]. The magnitude of shifts in ν(C=C) mode and in-plane C-H wagging mode were made to correspond to total (σ+π) metal-olefin interaction while the π contribution to the interaction was investigated by examining metal-olefin mode associated with the movement of olefinic carbon atom in and out of π-electron density section [13, 49]. In addition, out-of-plane olefinic C-H wagging mode is another indicator for π-electron

density as its magnitude directly related to amount of electron density in the π component [13].

The concept of molecular symmetry is essential in mastering the electronic, structural properties and catalytic activity of complexes. Likewise, the symmetry of the diolefin ligand used in the complex build-up plays a significant role in defining the structure of resultant complex. The tub form of 1,5-cyclooctadiene (COD), the diolefin for these complexes, was earlier reported to adopt higher symmetry C_{2v} in both liquid and solid phases; a feat which makes it mostly used for complexation [13, 48]. However, a later study revealed that its structure was actually C_2 [50]. This shows the possibility of having D_2 being formed in addition to higher symmetry D_{2h} earlier reported for di-μ-chloro bis(1,5-cyclooctadiene) di-rhodium(I) [13, 48] while C_2 could also be possible for Ir complex along with C_{2v}. Hence, it can be hypothetically assumed that coordinated COD would maintain C_2 symmetry in D_2 structure while C_{2v} would be for D_{2h} structure.

Development of an effective catalytic system requires an in-depth knowledge of HOMO-LUMO energy gap of the complex as well as ligands. A close energy gap between the HOMO of the ligands which are the σ-donors and LUMO of the metal of organometallic complexes facilitate easy orbital overlap. In the same sense, the LUMO of ligand should be close to HOMO of the metal for easy back donation from the occupied d_π of the metal [1]. Besides, another parameters worthy of considering in catalytic system design are the absolute electronegativity and absolute hardness, both of which give insight into the metal-ligand bond polarity [51]. They are related to ionization potential and electron affinity which depict acidity and basicity of molecule respectively [52]. However, the

absolute hardness is essential in catalyst development as the soft ligands always go with soft metals while hard ones go with hard metals [51].

This work aims at using theoretical calculation to establish the possible geometry for di-μ-chloro bis(1,5-cyclooctadiene) di-iridium(I) and di-rhodium(I), detailed vibrational assignment as well as assessment of their catalytic properties.

3.2. Results and Discussion

3.2.1. Molecular Geometry

The concept of molecular symmetry is essential in understanding the electronic properties and catalytic activity of metal complexes. At the same time, the structure of diolefin ligands used in the complex build-up plays a significant role in determining the overall symmetry as well as predicting reasonable mechanistic pathways involving particular catalyst precursors. Chloro-bridged complexes of Rh and Ir metals are common catalyst precursors used in many catalytic applications. The symmetry of their isolated structure is governed by two factors which are (1) the arrangement of the binuclear center with respect to the bridging chlorine atoms, and (2) the configuration of the COD rings. Based on these, different symmetries could arise theoretically (see Figure 1). Four possible conformations for each system were fully optimized and their relative energies are given in Table 1. It can be seen that both C_2 and D_2 symmetries are predicted to be more stable by 6-7 kcal/mol than the corresponding C_{2v} and D_{2h} symmetries. However, empirical report revealed that both complexes adopt their higher symmetries at the solid phase: C_{2v} for Ir complex [47] while Rh adopts D_{2h} [13, 48]. This indicates that the intermolecular packing outweighs the intramolecular forces and that the strained COD form is more

preferable in the solid phase of the two complexes. For the iridium complex, both planar and folded geometries were reported [46, 47] which is in agreement with the calculated 1 kcal/mol energy difference between the two forms (Table 1). While in the case of the rhodium complex the calculated relative stability is almost negligible, and the complex would prefer to adopt the more symmetrical configuration. Moreover, the coordination energies corresponding to the gas phase for the eight possible structures listed in Table 1 predicts a higher stability of the Ir complex. The geometrical parameters obtained for both complexes from calculation compared with reported experimental crystallography data [44, 47] are presented in Table 2 and 3. Thorough examination of the reported solid-phase structures reveals that are not perfect C_{2v} and D_{2h} symmetries. For the Rh complex, the crystallography data used for comparison happened to be the latest. Though it was aimed to correct the symmetry previously reported by two different research groups [45, 53], but point of inversion, one of the important properties of D_{2h} symmetry cannot be easily justified, due to difference in the values reported for some two similar bond angles which are supposed to be the same. Never the less, the structural parameters of solid-phase structures are in better agreement with the single-molecule DFT data of higher symmetries than the C_2 and D_2, respectively. The folded configuration in the Ir complex results with an intermetallic distance of 0.5 Å shorter than the flat configuration of the Rh complex. In order to gain more insight into their structure nuclear magnetic resonance (NMR) analysis was carried out on the complexes. The chemical shifts for different sets of hydrogens are presented in Table 4. The result shows a good agreement between experimental and calculated NMR for Rh complex. While for Ir complex, the three set of 8H atoms in the experimental result indicates that NMR recorded average chemical shift

of two pairs of 4H atoms. More importantly, the symmetry and identity of metal centers were found more influential on the paraffinic hydrogen chemical shifts where the values dropped by about 0.2 ppm (see Scheme 8). The calculation method estimated the chemical shift values of the paraffinic hydrogen in good agreement with experimental results.

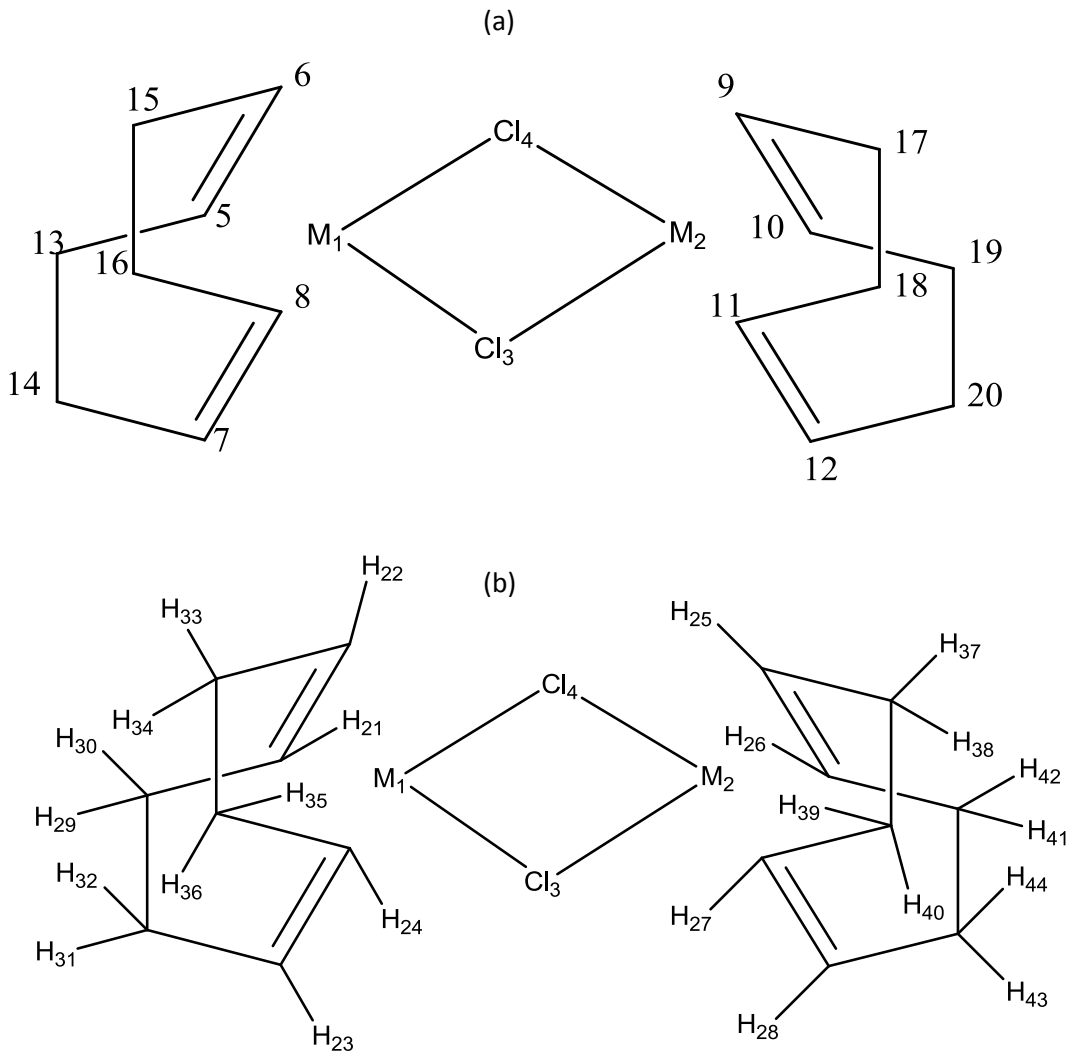

Scheme 9: Atom numbering of $[Ir(\mu\text{-}Cl)(COD)]_2$ and $[Rh(\mu\text{-}Cl)(COD)]_2$

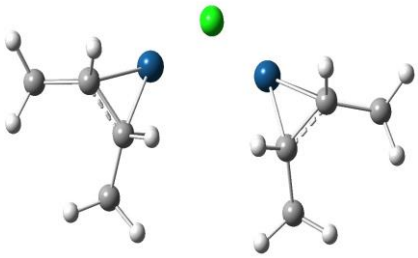	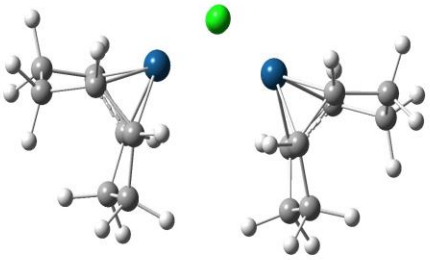
C_{2v}	C_2
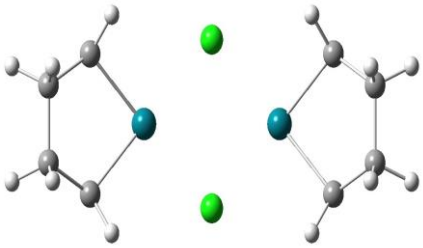	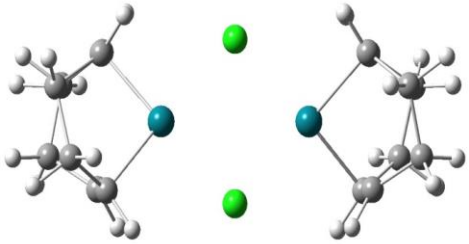
D_{2h}	D_2

Figure 1. Possible symmetries for $[Rh(\mu\text{-}Cl)(COD)]_2$ and $[Ir(\mu\text{-}Cl)(COD)]_2$ complexes

Table 1. Relative and coordination energies for different configurations of $[Rh(\mu\text{-}Cl)(COD)]_2$ and $[Ir(\mu\text{-}Cl)(COD)]_2$ complexes calculated at the B3LYP/6-311++g(d,p) level for non-metals and SDD for metals

Symmetry	$[Rh(\mu\text{-}Cl)(COD)]_2$			$[Ir(\mu\text{-}Cl)(COD)]_2$		
	Rel. Energy (kcal/mol)	Coord.Energy (kcal/mol)	Dihedral Angle (°)[c]	Rel. Energy (kcal/mol)	Coord. Energy (kcal/mol)	Dihedral Angle (°)[c]
C_2	0.00	357	44.9	0.00	405	46.9
D_2	0.33	356	0.0	1.04	404	0.0
C_{2v}	6.49	364	45.7	5.66	412	46.7 (46.5)[b]
D_{2h}	6.73	363	0.0 (8)[a]	6.69	411	0.0

[a] Ref. [44]

[b] Ref. [47]

[c] Dihedral angle $M_1Cl_3M_2Cl_4$ in Scheme 9a

Table 2. Bond distances (A^o) in $[Rh(\mu\text{-}Cl)(COD)]_2$ and $[Ir(\mu\text{-}Cl)(COD)]_2$ complexes compared with X-ray crystallography data

	M=Rh			M=Ir		
Bond Length	D_2	D_{2h}	Experiment[a]	C_2	C_{2v}	Experiment[b]
M_1-M_2	3.596	3.601	–	2.982	2.990	2.910(1)
M_1-Cl_3	2.462	2.465	2.4020(10)	2.482	2.485	2.399(5)
M_1-Cl_4	2.462	2.465	2.4150(10)	2.482	2.485	2.400(5)
M_1-C_5	2.143	2.122	2.104(7)	2.132	2.117	2.09(2)
M_1-C_6	2.123	2.122	2.097(6)	2.113	2.114	2.08(2)
M_1-C_7	2.143	2.122	2.108(5)	2.129	2.114	2.11(2)
M_1-C_8	2.123	2.122	2.126(6)	2.116	2.117	2.08(2)
M_2-Cl_3	2.462	2.465	2.4030(10)	2.482	2.485	2.408(4)
M_2-Cl_4	2.462	2.465	2.4210(10)	2.482	2.485	2.397(4)
M_2-C_9	2.143	2.122	2.102(6)	2.129	2.114	2.11(2)
M_2-C_{10}	2.123	2.122	2.098(5)	2.116	2.117	2.10(2)
M_2-C_{11}	2.143	2.122	2.101(5)	2.132	2.117	2.06(2)
M_2-C_{12}	2.123	2.122	2.099(6)	2.113	2.114	2.06(2)
C_5-C_6	1.408	1.408	1.388(9)	1.425	1.425	1.40(3)
C_5-C_{13}	1.525	1.521	1.510(10)	1.529	1.524	1.57(3)
C_6-C_{15}	1.517	1.521	1.500(10)	1.518	1.523	1.53(3)
C_{13}-C_{14}	1.545	1.556	1.480(10)	1.544	1.554	1.46(4)
C_7-C_{14}	1.525	1.521	1.520(10)	1.528	1.523	1.50(3)
C_7-C_8	1.408	1.408	1.401(8)	1.425	1.425	1.44(3)
C_8-C_{16}	1.517	1.521	1.510(10)	1.519	1.524	1.54(3)
C_{15}-C_{16}	1.545	1.556	1.450(10)	1.546	1.554	1.48(3)
C_9-C_{10}	1.408	1.408	1.395(9)	1.425	1.425	1.42(3)
C_9-C_{17}	1.525	1.521	1.510(10)	1.528	1.523	1.42(3)
C_{10}-C_{19}	1.517	1.521	1.500(10)	1.519	1.524	1.45(3)
C_{17}-C_{18}	1.545	1.556	1.500(10)	1.546	1.554	1.50(4)
C_{11}-C_{12}	1.517	1.521	1.520(10)	1.529	1.524	1.56(3)
C_{11}-C_{12}	1.408	1.408	1.389(9)	1.425	1.425	1.46(4)
C_{12}-C_{20}	1.525	1.521	1.502(9)	1.518	1.523	1.60(3)
C_{19}-C_{20}	1.545	1.556	1.480(10)	1.544	1.554	1.51(3)
C_5-H_{21}	1.087	1.087	1.07(4)	1.088	1.088	–
C_6-H_{22}	1.087	1.087	1.09(8)	1.088	1.088	–

Table 2
Continued

	M=Rh			M=Ir		
Bond Length	D_2	D_{2h}	Experiment[a]	C_2	C_{2v}	Experiment[b]
C_{13}-H_{29}	1.099	1.091	1.07(3)	1.098	1.097	–
C_{13}-H_{30}	1.093	1.097	1.06(4)	1.094	1.092	–
C_{14}-H_{31}	1.093	1.091	1.05(3)	1.093	1.092	–
C_{14}-H_{32}	1.093	1.097	1.05(4)	1.093	1.097	–
C_7-H_{23}	1.087	1.087	1.07(7)	1.087	1.088	–
C_8-H_{24}	1.087	1.087	1.06(4)	1.089	1.088	–
C_{15}-H_{33}	1.093	1.091	1.07(2)	1.093	1.091	–
C_{15}-H_{34}	1.099	1.097	1.09(6)	1.099	1.097	–
C_{16}-H_{35}	1.093	1.091	1.06(3)	1.092	1.091	–
C_{16}-H_{36}	1.093	1.097	1.07(6)	1.093	1.097	–
C_9-H_{25}	1.087	1.087	1.07(5)	1.087	1.088	–
C_{10}-H_{26}	1.087	1.087	1.09(8)	1.089	1.088	–
C_{19}-H_{41}	1.093	1.097	1.06(3)	1.093	1.097	–
C_{19}-H_{42}	1.093	1.091	1.05(5)	1.099	1.091	–
C_{20}-H_{43}	1.099	1.097	1.10(3)	1.092	1.097	–
C_{20}-H_{44}	1.093	1.091	1.07(4)	1.093	1.091	–
C_{11}-H_{27}	1.087	1.087	1.10(7)	1.088	1.088	–
C_{12}-H_{28}	1.087	1.087	1.07(4)	1.088	1.088	–
C_{17}-H_{37}	1.093	1.097	1.09(3)	1.094	1.097	–
C_{17}-H_{38}	1.093	1.091	1.12(5)	1.098	1.092	–
C_{18}-H_{39}	1.099	1.097	1.09(2)	1.093	1.097	–
C_{18}-H_{40}	1.093	1.091	1.08(5)	1.093	1.092	–

[a] [44]

[b] [47]

Table 3. Bond angles (^{o}) in [Rh(μ-Cl)(COD)]$_2$ and [Ir(μ-Cl)(COD)]$_2$ complexes compared with X-ray crystallography data

	M=Rh			M=Ir		
Bond Angles	D_2	D_{2h}	Experiment[a]	C_2	C_{2v}	Experiment[b]
Cl_3-M_1-Cl_4	86.2	86.2	85.83(4)	84.6	84.6	84.2(2)
Cl_3-M_1-C_5	94.0	92.4	92.5(2)	96.2	94.5	95.0(5)
Cl_3-M_1-C_6	91.2	92.4	92.2(2)	90.6	91.5	91.6(5)
Cl_3-M_1-C_7	163.0	160.6	160.4(2)	158.3	155.8	155.9(5)
Cl_3-M_1-C_8	158.4	160.6	160.9(2)	162.2	164.7	164.6(6)
Cl_4-M_1-C_5	163.0	160.6	161.2(2)	166.9	164.7	164.6(5)
Cl_4-M_1-C_6	158.4	160.6	160.1(2)	153.8	155.8	154.9(5)
Cl_4-M_1-C_7	94.0	92.4	92.8(2)	92.9	91.5	90.7(5)
Cl_4-M_1-C_8	91.2	92.4	93.6(2)	93.1	94.5	95.9(5)
C_5-M_1-C_6	38.5	38.8	38.6(3)	39.2	39.3	–
C_5-M_1-C_7	90.7	95.2	94.8(2)	91.0	95.3	–
C_5-M_1-C_8	82.4	82.5	81.9(2)	82.1	82.3	–
C_6-M_1-C_7	82.4	82.5	82.4(3)	82.2	82.3	–
C_6-M_1-C_8	98.8	95.2	94.6(2)	98.9	95.3	–
C_7-M_1-C_8	38.5	38.8	38.6(2)	39.2	39.3	–
Cl_3-M_2-Cl_4	86.2	86.2	85.66(5)	84.6	84.6	84.1(2)
Cl_3-M_2-C_9	163.0	160.6	163.0(2)	162.2	164.7	164.0(5)
Cl_3-M_2-C_{10}	158.4	160.6	158.2(2)	158.3	155.8	156.6(6)
Cl_3-M_2-C_{11}	94.0	92.4	92.4(2)	96.2	94.5	95.2(5)
Cl_3-M_2-C_{12}	91.2	92.4	93.0(2)	90.6	91.5	94.3(5)
Cl_4-M_2-C_9	94.0	92.4	93.4(2)	93.1	94.5	93.5(6)
Cl_4-M_2-C_{10}	91.2	92.4	93.3(2)	92.9	91.5	91.7(6)
Cl_4-M_2-C_{11}	163.0	160.6	163.6(2)	166.9	164.7	164.0(5)
Cl_4-M_2-C_{12}	158.4	160.6	157.7(2)	153.8	155.8	156.6(6)
C_9-M_2-C_{10}	38.5	38.8	38.8(2)	39.2	39.3	–
C_9-M_2-C_{12}	90.7	95.2	93.2(2)	91.0	95.3	–
C_9-M_2-C_{11}	82.4	82.5	81.5(2)	82.2	82.3	–
C_{10}-M_2-C_{12}	82.1	82.5	82.5(2)	82.1	82.3	–
C_{10}-M_2-C_{11}	98.8	95.2	96.0(2)	98.9	95.3	–
C_{11}-M_2-C_{12}	38.5	38.8	38.6(2)	39.2	39.3	–
M_1-Cl_3-M_2	93.8	93.8	94.08(5)	73.9	74.0	74.5(1)

Table 3
Continued

	M=Rh			M=Ir		
Bond Angles	D_2	D_{2h}	Experiment[a]	C_2	C_{2v}	Experiment[b]
M_1-Cl_4-M_2	93.8	93.8	93.32(4)	73.9	74.0	74.7(1)
M_1-C_5-C_6	70.0	70.6	70.5(4)	69.7	70.2	–
M_1-C_5-C_{13}	112.7	113.8	112.8(5)	113.5	114.3	–
M_1-C_5-H_{21}	105.5	105.5	109(5)	108.8	108.8	–
C_6-C_5-C_{13}	123.9	123.5	123.5(7)	123.2	123.1	124.0(2)
C_6-C_5-H_{21}	116.8	116.8	120(5)	116.3	116.4	–
C_6-C_5-H_{21}	115.8	117.0	112(5)	115.2	114.6	–
M_1-C_6-C_5	71.5	70.6	71.0(4)	71.1	70.4	–
M_1-C_6-C_{15}	110.0	113.8	112.4(5)	110.9	114.3	–
M_1-C_6-H_{22}	105.9	105.5	98(4)	108.4	108.1	–
C_5-C_6-C_{15}	125.8	123.5	125.1(7)	125.7	123.6	124.0(2)
C_5-C_6-H_{22}	116.8	117.0	115(4)	116.4	116.4	–
C_{15}-C_6-H_{22}	114.4	115.3	118(4)	113.8	114.5	–
C_6-C_{15}-C_{16}	113.0	114.1	116.0(6)	112.7	113.8	114.0(2)
C_6-C_{15}-H_{33}	110.4	108.2	109.0(10)	110.5	108.1	–
C_6-C_{15}-H_{34}	107.2	108.9	108(4)	106.8	109.0	–
C_{16}-C_{15}-H_{33}	110.7	109.1	109.0(10)	110.9	109.1	–
C_{16}-C_{15}-H_{34}	109.0	110.0	106(3)	109.0	110.3	–
H_{33}-C_{15}-H_{34}	106.3	106.2	109(3)	106.6	106.2	–
C_{15}-C_{16}-C_8	111.9	114.1	114.8(6)	111.5	113.8	114.0(2)
C_{15}-C_{16}-H_{35}	109.3	109.1	109.0(10)	109.5	109.1	–
C_{15}-C_{16}-H_{36}	110.6	110.0	118(4)	110.7	110.3	–
C_8-C_{16}-H_{35}	109.2	108.2	109.0(10)	109.3	108.1	–
C_8-C_{16}-H_{36}	109.6	108.9	97(5)	109.6	109.0	–
H_{35}-C_{16}-H_{36}	106.1	106.2	109(2)	106.1	106.2	–
M_1-C_8-C_{16}	112.7	113.8	112.1(4)	113.5	114.3	–
M_1-C_7-C_8	70.0	70.6	71.4(3)	69.9	70.4	–
M_1-C_7-H_{23}	105.5	105.5	100(4)	108.1	108.1	–
C_{16}-C_7-C_8	123.9	123.5	124.3(6)	123.5	123.6	126.0(2)
C_{16}-C_7-H_{23}	115.8	115.3	111(4)	115.1	114.5	–
C_8-C_7-H_{23}	116.8	117.0	123(4)	116.3	116.4	–
M_1-C_8-C_7	71.5	70.6	70.0(3)	70.9	70.2	–
M_1-C_8-C_{14}	110.0	113.8	111.5(5)	111.4	114.3	–
M_1-C_8-H_{24}	105.9	105.5	107(5)	108.9	108.8	–

Table 3
Continued

	M=Rh			M=Ir		
Bond Angles	D_2	D_{2h}	Experiment[a]	C_2	C_{2v}	Experiment[b]
C_7-C_8-C_{14}	125.8	123.5	123.7(6)	125.0	123.1	117.0(2)
C_7-C_8-H_{24}	116.8	117.0	123(5)	116.4	116.4	–
C_{14}-C_8-H_{24}	114.4	115.3	110(5)	114.1	114.6	–
C_8-C_{14}-C_{13}	113.0	114.1	116.5(7)	112.7	113.9	112.0(2)
C_8-C_{14}-H_{31}	110.4	108.2	109.0(10)	110.4	108.1	–
C_8-C_{14}-H_{32}	107.2	108.9	111(3)	107.1	109.1	–
C_{13}-C_{14}-H_{31}	110.7	109.1	109(2)	110.8	109.1	–
C_{13}-C_{14}-H_{32}	109.0	110.0	102(4)	109.0	110.3	–
H_{31}-C_{14}-H_{32}	106.3	106.2	109(3)	106.5	106.1	–
C_5-C_{13}-C_{14}	111.9	114.1	115.5(7)	111.8	113.9	115.0(2)
C_5-C_{13}-H_{29}	109.6	108.2	109(2)	109.5	108.1	–
C_5-C_{13}-H_{30}	109.2	108.9	105(3)	109.2	109.1	–
C_{14}-C_{13}-H_{29}	110.6	109.1	109.0(10)	110.7	109.1	–
C_{14}-C_{13}-H_{30}	109.3	110.0	109(3)	109.4	110.3	–
H_{29}-C_{13}-H_{30}	106.1	106.2	109(3)	106.0	106.1	–
M_2-C_9-C_{10}	70.0	70.6	70.5(3)	69.9	70.2	–
M_2-C_9-C_{17}	112.8	113.8	113.8(4)	113.5	114.3	–
M_2-C_9-H_{25}	105.5	105.5	105(5)	108.1	108.1	–
C_{10}-C_9-C_{17}	124.2	123.5	123.6(6)	123.5	123.6	125.0(2)
C_{10}-C_9-H_{25}	116.7	117.0	108(5)	116.3	116.4	–
C_{17}-C_9-H_{25}	115.6	115.3	123(5)	115.1	114.5	–
M_2-C_{10}-C_9	71.5	70.6	70.8(3)	70.9	70.2	–
M_2-C_{10}-C_{19}	110.0	113.8	112.0(4)	111.4	114.3	–
M_2-C_{10}-H_{26}	105.9	105.5	107(4)	108.9	108.8	–
C_9-C_{10}-C_{19}	125.8	123.5	124.8(7)	125.0	123.1	–
C_9-C_{10}-H_{26}	116.8	117.0	119(4)	116.4	116.4	–
C_{19}-C_{10}-H_{26}	114.4	115.3	112(4)	114.1	114.6	–
C_{10}-C_{19}-C_{20}	113.0	114.1	115.3(6)	112.7	113.9	115.0(2)
C_{10}-C_{19}-H_{41}	110.4	108.9	109.0(10)	110.4	109.1	–
C_{10}-C_{19}-H_{42}	107.2	108.2	132(3)	107.1	108.1	–
C_{20}-C_{19}-H_{41}	110.7	110.0	109.0(10)	110.8	110.3	–
C_{20}-C_{19}-H_{42}	109.0	109.1	78(3)	109.0	109.1	–
H_{41}-C_{19}-H_{42}	106.3	106.2	109(4)	106.5	106.1	–
C_{19}-C_{20}-C_{12}	111.9	114.1	113.9(6)	111.8	113.9	113.0(2)
C_{19}-C_{20}-H_{43}	109.3	110.0	109.0(10)	109.4	110.3	–

Table 3
Continued

	M=Rh			M=Ir		
Bond Angles	D_2	D_{2h}	Experiment[a]	C_2	C_{2v}	Experiment[b]
C_{19}-C_{20}-H_{44}	110.6	109.1	117(4)	110.7	109.1	–
C_{12}-C_{20}-H_{43}	109.2	108.9	109.0(10)	109.2	109.1	–
C_{12}-C_{20}-H_{44}	109.6	108.2	99(5)	109.5	108.1	–
H_{43}-C_{20}-H_{44}	106.1	106.2	109(2)	106.0	106.1	–
M_2-C_{12}-C_{20}	112.7	113.8	113.1(4)	113.5	114.3	–
M_2-C_{12}-C_{11}	70.0	70.6	70.6(3)	69.7	70.2	–
M_2-C_{12}-H_{28}	105.5	105.5	98(4)	108.8	108.8	–
C_{20}-C_{12}-C_{11}	123.9	123.5	123.7(6)	123.2	123.1	121.0(2)
C_{20}-C_{12}-H_{28}	115.8	115.3	116(4)	115.2	114.6	–
C_{11}-C_{12}-H_{28}	116.8	117.0	118(4)	116.3	116.4	–
M_2-C_{11}-C_{12}	71.5	70.6	70.8(3)	71.1	70.4	–
M_2-C_{11}-C_{18}	110.0	113.8	112.4(4)	110.9	114.3	–
M_2-C_{11}-H_{27}	105.9	105.5	110(5)	108.4	108.1	–
C_{12}-C_{11}-C_{18}	125.8	123.5	125.5(5)	125.7	123.6	124.0(2)
C_{12}-C_{11}-H_{27}	116.8	116.8	126(5)	116.4	116.4	–
C_{18}-C_{11}-H_{27}	114.4	117.0	105(5)	113.8	114.5	–
C_{11}-C_{18}-C_{17}	113.0	114.1	115.0(6)	112.7	113.8	112.0(2)
C_{11}-C_{18}-H_{39}	107.2	108.9	109.0(10)	106.8	109.0	–
C_{11}-C_{18}-H_{40}	110.4	108.2	118(4)	110.5	108.1	–
C_{17}-C_{18}-H_{39}	109.1	110.0	109.0(10)	109.0	110.3	–
C_{17}-C_{18}-H_{40}	110.7	109.1	96(4)	110.9	109.1	–
H_{39}-C_{18}-H_{40}	106.3	106.2	109(2)	106.6	106.2	–
C_9-C_{17}-C_{18}	111.9	114.1	114.0(6)	111.5	113.8	116.0(2)
C_9-C_{17}-H_{37}	109.6	108.9	109.0(10)	109.6	109.0	–
C_9-C_{17}-H_{38}	109.2	108.2	105(3)	109.3	108.1	–
C_{18}-C_{17}-H_{37}	110.6	110.0	109.0(10)	110.7	110.3	–
C_{18}-C_{17}-H_{38}	109.3	109.1	111(3)	109.5	109.1	–
H_{37}-C_{17}-H_{38}	106.1	106.2	109(3)	106.1	106.2	–

[a] [44]

[b] [47]

Table 4. Experimental and theoretical ^{1}H NMR chemical shift values (ppm) for the two complexes

[Rh(μ-Cl)(COD)]$_2$						[Ir(μ-Cl)(COD)]$_2$					
Expt.	D_{2h}		D_2		Assignment[a]	Expt.	C_{2v}		C_2		Assignment[a]
	Gas	Solution	Gas	Solution			Gas	Solution	Gas	Solution	
1.73	1.87	1.97	1.55	1.64	$H_{30}, H_{32}, H_{34}, H_{36}, H_{38}, H_{40}, H_{42}, H_{44}$	1.51	2.04	2.11	1.62	1.7	$H_{30}, H_{32}, H_{34}, H_{36}, H_{38}, H_{40}, H_{42}, H_{44}$
			2.38	2.45			2.15	2.22	1.70	1.76	
2.46	2.52	2.58	1.93	1.99	$H_{29}, H_{31}, H_{33}, H_{35}, H_{37}, H_{39}, H_{41}, H_{43}$				2.45	2.51	
			3.04	3.07					2.53	2.59	
4.20	3.76	3.76	3.53	3.54	$H_{21}, H_{22}, H_{23}, H_{24}, H_{25}, H_{26}, H_{27}, H_{28}$	2.25	2.54	2.57	2.09	2.13	$H_{29}, H_{31}, H_{33}, H_{35}, H_{37}, H_{39}, H_{41}, H_{43}$
			3.74	3.74			2.61	2.7	2.81	2.2	
									2.98	2.82	
									-	3.07	
						4.21	3.64	3.62	3.64	3.65	$H_{21}, H_{22}, H_{23}, H_{24}, H_{25}, H_{26}, H_{27}, H_{28}$
							3.69	3.73	3.71	3.82	
									3.79	-	

[a] Refer to Scheme 9b for hydrogen atoms numbering.

3.2.2. Theoretical insight into Complex Catalytic Activities

Adequate knowledge about the fundamental properties, such as orbital hybridization, frontier orbital energies, ionization potentials and others is essential in designing an effective catalytic system. These valuable information needed to better predict the catalytic properties of the investigated complexes can efficiently be estimated via theoretical calculation. During this work, quite a number of essential chemical properties have been computed to provide reasonable comprehension of the catalytic behavior of the titled complexes.

The orbital hybridization obtained from the Natural Bond Order (NBO) analysis for the coordinated and free COD rings are given in Table 5. For the sake of clarity only the hybridizations of the atoms associated to the C_5=C_6 unit are presented. Carbon atoms in both C_2 and C_{2v} configurations in the free COD were predicted to exhibit almost the same population nature that reflects the sp^2 hybridization. However, upon coordination with the more electropositive metal, the olefinic carbon atoms exhibit a greater *p* character as reflected in their hybridization values (see Table 5). The average hybridization values for the olefinic carbon atoms in the coordinated COD of the Rh and Ir complexes are $sp^{2.3}$ to $sp^{2.4}$ respectively. This shows that the olefinic carbon atoms are moving towards sp^3 hybridization upon coordination. The relatively greater *p* character obtained for C_5 or C_6 of the Ir complex compared to Rh can be attributed to the higher electropositive nature of the Ir metal center as reported by Pauling [1]. This is translated into a slightly longer C=C bond length recorded for COD in Ir complex (see Table 2) and a higher stability as well.

Selected parameters that attest to complex reactivity were computed and the results obtained are presented in Table 6. The absolute electronegativity and absolute hardness

parameters are worthy of considering in any catalytic system. They give insight into the metal-ligand bond polarity [44]. The absolute hardness is essential in catalyst development as soft ligands prefer to go with soft metals while hard ones go with hard metals [1]. The ionization potential (IP) and electron affinity (EA) on the other hand depict the acidity and basicity of molecule respectively [54]. The ionization potential and absolute hardness were predicted to be greater for a higher symmetry complex. The higher IP value obtained for higher symmetry corresponding to the crystalline phase predicts them to be less basic compared to the respective lower symmetry conformations. On the other hand, the C_{2v} configuration of the iridium complex shows a lower electron affinity than the lower C_2 symmetry, while that of the two Rh complex configurations are predicted to be nearly equal. The lower electron affinity value points out that C_{2v} form is more acidic. The values presented in Table 6 affirm that higher symmetry configurations of both complexes are slightly harder than their respective lower symmetry. According to the principle, the higher value obtained for them is an indication that hard ligands will be more compatible with them than lower symmetry configurations, when used as catalyst precursor. On the other hand, electron donating ligands will be coordinating more effectively to the metal center in the D_{2h}-Rh than the C_{2v}-Ir complexes. In the context of HOMO-LUMO of complex, the HOMO is related to ionization potential since its responsibility is electron donation while the LUMO on the other hand whose role is electron acceptance is related to electron affinity [54]. It is important to note that the chemical reactivity of a complex depends on HOMO-LUMO energy gap and the closer this gap, the more reactive the molecule is expected to be. Thus the lower energy difference between the HOMO and LUMO levels predicted for Ir complex as depicted in

Figure 2 explains its more reactive nature compared to the Rh complex. More importantly, the LUMO and LUMO+1 associated to the Ir complex are predicted to be more delocalized across the complex, unlike the case of the corresponding Rh complex. A close energy gap between the HOMO of a ligand which is a σ-donors and LUMO of the metal facilitates more efficient orbital overlap and thus a stronger coordination bond. In the same sense, the LUMO of a ligand should be close to HOMO of the metal for easier back-donation from the occupied d_{π} orbital of the metal.

Table 5. Natural bond orbital analysis for 1,5-cyclooctadiene and complexes

Molecule	Orbital	Bond Polarization (%)	Hybridization	Average
Cyclooctadiene (C_2)	C_1-C_2	C_1, 49.89; C_2, 50.11	C_1, $sp^{1.51}$; C_2, $sp^{1.49}$	
	C_1-C_2	C_1, 50.68; C_2, 49.32	C_1, p; C_2, p	
	C_1-C_8	C_1, 49.02; C_8,50.98	C_1, $sp^{2.00}$; C_8, $sp^{2.47}$	C_1, $sp^{2.08}$
	C_1-H_9	C_1, 59.52; H_9, 40.48	C_1, $sp^{2.72}$; H_9, s	C_2, $sp^{2.09}$
	C_2-C_3	C_2, 49.05; C_3, 50.95	C_2, $sp^{1.98}$; C_3, $sp^{2.40}$	
	C_2-H_{10}	C_2, 59.46; H_{10}, 40.54	C_2, $sp^{2.80}$; H_{10}, s	
Cyclooctadiene (C_{2v})	C_1-C_2	C_1, 50.00; C_2, 50.00	C_1, $sp^{1.54}$; C_2, $sp^{1.54}$	
	C_1-C_2	C1, 50.00; C2, 50.00	C_1, p; C_2, p	
	C_1-C_8	C_1, 48.86; C_8, 51.14	C_1, $sp^{2.06}$; C_8, $sp^{2.39}$	C_1, $sp^{2.06}$
	C_1-H_9	C_1, 59.70; H_9, 40.30	C_1, $sp^{2.58}$; H_9, s	C_2, $sp^{2.06}$
	C_2-C_3	C_2, 48.86; C_3, 51.14	C_2, $sp^{2.06}$; C_3, $sp^{2.39}$	
	C_2-H_{10}	C_2, 59.70; H_{10}, 40.30	C_2, $sp^{2.58}$; H_{10}, s	
$[Rh(\mu\text{-}Cl)(COD)]_2$ (D_2)	C_5-C_6	C_5, 50.02; C_6, 49.98	C_5, $sp^{2.00}$; C_6, $sp^{1.98}$	
	C_5-C_{13}	C_5, 49.90; C_{13}, 50.10	C_5, $sp^{2.22}$; C_{13}, $sp^{2.54}$	
	C_5-H_{21}	C_5, 61.23; H_{21}, 38.77	C_5, $sp^{2.69}$; H_{21}, s	C_5, $sp^{2.30}$
	C_6-C_{15}	C_6, 49.96; C_{15}, 50.04	C_6, $sp^{2.18}$; C_{15}, $sp^{2.48}$	C_6, $sp^{2.31}$
	C_6-H_{22}	C_6, 61.27; H_{22}, 38.73	C_6, $sp^{2.76}$; H_{22}, s	
$[Rh(\mu\text{-}Cl)(COD)]_2$ (D_{2h})	C_5-C_6	C_5, 50.00; C_6, 50.00	C_5, $sp^{2.03}$; C_6, $sp^{2.03}$	
	C_5-C_{13}	C_5, 49.85; C_{13}, 50.15	C_5, $sp^{2.22}$; C_{13}, $sp^{2.48}$	
	C_5-H_{21}	C_5, 61.26; H_{21}, 38.74	C_5, $sp^{2.72}$; H_{21}, s	C_5, $sp^{2.32}$
	C_6-C_{15}	C_6, 49.85; C_{15}, 50.15	C_6, $sp^{2.22}$; C_{15}, $sp^{2.48}$	C_6, $sp^{2.32}$
	C_6-H_{22}	C_6, 61.26; H_{22}, 38.74	C_6, $sp^{2.72}$; H_{22}, s	
$[Ir(\mu\text{-}Cl)(COD)]_2$ (C_2)	C_5-C_6	C_5, 49.96; C_6, 50.04	C_5, $sp^{2.16}$; C_6, $sp^{2.10}$	
	C_5-C_{13}	C_5, 50.07; C_{13}, 49.93	C_5, $sp^{2.26}$; C_{13}, $sp^{2.55}$	
	C_5-H_{21}	C_5,61.16; H_{21}, 38.84	C_5, $sp^{2.74}$; H_{21}, s	C_5, $sp^{2.39}$
	C_6-C_{15}	C_6, 49.95; C_{15}, 50.05	C_6, $sp^{2.22}$; C_{15}, $sp^{2.47}$	C_6, $sp^{2.38}$
	C_6-H_{22}	C_6, 61.17; H_{22}, 38.83	C_6, $sp^{2.81}$; H_{22}, s	
$[Ir(\mu\text{-}Cl)(COD)]_2$ (C_{2v})	C_5-C_6	C_5, 49.96; C_6, 50.04	C_5, $sp^{2.17}$; C_6, $sp^{2.15}$	
	C_5-C_{13}	C_5, 50.06; C_{13}, 49.94	C_5, $sp^{2.25}$; C_{13}, $sp^{2.49}$	
	C_5-H_{21}	C_5,61.15; H_{21}, 38.85	C_5, $sp^{2.78}$; H_{21}, s	C_5, $sp^{2.40}$
	C_6-C_{15}	C_6, 49.88; C_{15}, 50.12	C_6, $sp^{2.26}$; C_{15}, $sp^{2.47}$	C_6, $sp^{2.40}$
	C_6-H_{22}	C_6 61.13; H_{22}, 38.87	C_6, $sp^{2.78}$; H_{22}, s	

Table 6. B3LYP/6-311++G(d,p) calculated ionization potential (IP), electron affinity (EA), absolute hardness (η) and electronegativity (χ) in ev

$[Rh(\mu\text{-}Cl)(COD)]_2$					$[Ir(\mu\text{-}Cl)(COD)]_2$				
Configuration	IP	EA	η	χ	Configuration	IP	EA	η	χ
D_2	6.83	0.43	3.20	3.63	C_2	6.60	0.74	2.93	3.67
D_{2h}	6.89	0.44	3.22	3.67	C_{2v}	6.64	0.54	3.05	3.59

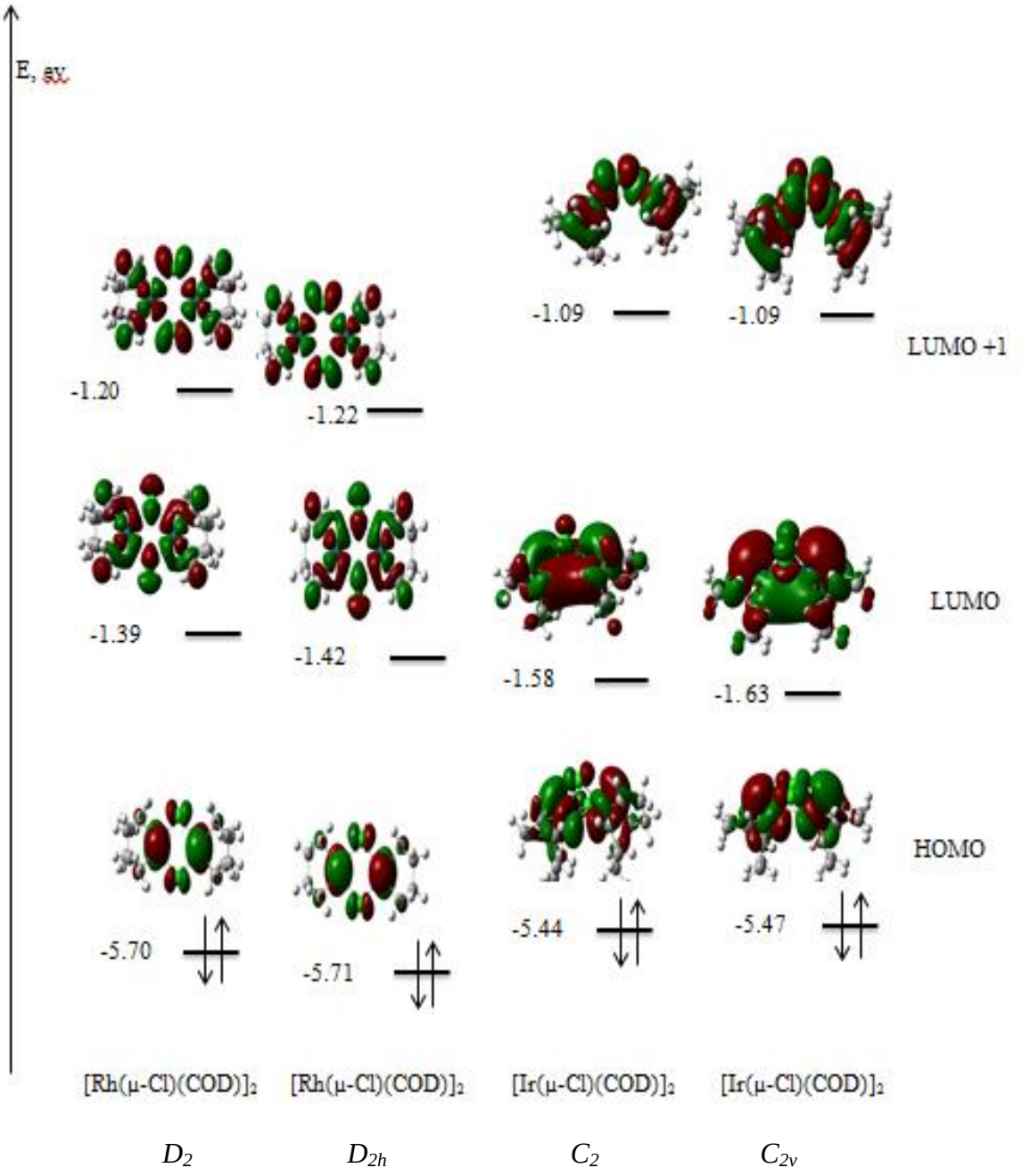

Figure 2. Frontier orbitals for the complexes

3.2.3. Vibrational Spectra

Vibrational infrared and Raman spectroscopies are valuable tools being used to investigate the nature of the metal-olefin interaction in several metal complexes [13, 48, 49, 55]. Careful inspections of the fundamental modes associated with the olefinic carbon and hydrogen atoms in 1,5-cyclooctadienes provide useful information about the coordination aspects. On the other hand, molecular symmetry plays a significant role in properly assigning the infrared and Raman spectra to the corresponding vibrational modes. The vibrational spectra of the two chloro-bridged complexes are shown in Figures 3-6. For a more comprehensive comparison, the experimental, calculated high-symmetry and calculated low symmetry IR and Raman spectra are shown. Although the calculated spectra represent the gas phase, they show very good agreement with the experimental ones. The theoretical high-symmetry spectra in both complexes are closer in their pattern and peak positions to the experimental ones. For some calculated peaks in the low-symmetry spectra, the corresponding ones can still be observed in experimental spectra, thus providing evidence to the non-strict higher symmetry structures of the two complexes.

Unlike similar works reported previously [13, 48, 55] the overall complex symmetry, and not just that for COD, has been followed to provide comprehensive and meaningful assignments of the fundamental modes. The structure of $[Rh(\mu\text{-}Cl)(COD)]_2$ and $[Ir(\mu\text{-}Cl)(COD)]_2$ were reported to adopt D_{2h} and C_{2v} symmetries, respectively, in the solid state [44, 47], although these symmetries are not strictly enforced within the unit cell as revealed from the experimentally determined structures (see Table 2 and 3). The [Rh(μ-

Cl)(COD)]$_2$ complex in the solid state adopts near D_{2h} symmetry with 123 vibrational modes which can be described by the following irreducible representation:

$$\Gamma irr = 17\ A_g + 14\ A_u + 16\ B_{1g} + 15\ B_{2g} + 14\ B_{3g} + 15\ B_{1u} + 16\ B_{2u} + 16\ B_{3u} \quad (1)$$

While for the [Ir(μ-Cl)(COD)]$_2$ complex, the same number of fundamentals with near C_{2v} symmetry being adopted and described by the following irreducible representation:

$$\Gamma irr = 33\ A_1 + 30\ A_2 + 30\ B_1 + 31\ B_2 \quad (2)$$

Adequate assignments were made based on the higher symmetry structures in the two complexes. This was carried out on the basis of calculated infrared band and Raman line intensities, and Gauss-View graphical animations [56] as presented in Tables 7 and 8. Scaling factors of 0.985, 0.973 and 0.961 were used for frequencies range of $\nu < 1800$ cm^{-1}, 1800 cm^{-1} $< \nu <$ 2800 cm^{-1} , and $\nu >$ 2800 cm^{-1}, respectively [57].

Tables 7 and 8 show that, the calculated harmonic frequencies are in very good agreement with the corresponding experimental ones and account for the vibrational shifts due to the metal-diolefinic coordination. In a few cases, the infrared bands and/or Raman lines are assigned to the low-symmetry structures. For instance in the region just below 1200 cm^{-1} in the [Rh(μ-Cl)(COD)]$_2$ spectrum, only one IR active mode is predicted at 1190 cm^{-1} and is assigned to the CH_2 twisting. In the experimental spectrum, however, two low- and medium-intensity band can be observed. As one of them (1175 cm^{-1}) is assigned to CH_2 twisting, the other one (1151 cm^{-1}), should be assigned to CH in-plane waging of low-symmetry structure (D_2). In the same sense, the experimental

Raman line 1075 cm^{-1} could only be matched with 1082 cm^{-1} predicted for the CH_2 rocking mode of D_2 symmetry. Similar cases are seen in $[Ir(\mu\text{-}Cl)(COD)]_2$ spectrum. For the higher symmetry (C_{2v}), there is only one IR active mode predicted at 1338 cm^{-1} for CH_2 waging and this could be assigned to the medium-intensity experimental band of 1321 cm^{-1}. However, the other low-intensity band (1297 cm-1) in this region goes with 1317 cm^{-1} predicted for CH_2 waging mode of C_2 symmetry. Furthermore, the experimental Raman line 499 cm^{-1} could only be assigned to 494 cm^{-1} predicted for ring deformation of C_2 symmetry. In addition, the other infrared bands and/or Raman lines that could be assigned to the respective lower symmetry of the complexes are italicized in vibrational assignment Tables 7 and 8. A thorough analysis of the vibrational spectra of the solid-packed forms of both complexes brought evidences of the presence of a trace of D_2 and C_2 along with the predominant D_{2h} and C_{2v} configurations of the two complexes respectively. Like the higher symmetry, COD maintains C_2 symmetry in the respective lower symmetry configuration of the two complexes. On the other hand, the assignment of infrared bands and Raman lines to vibrational modes predicted from calculation for the predominant D_{2h} configuration of $[Rh(\mu\text{-}Cl)(COD)]_2$ obeys the rule of point of inversion. As depicted in Table 7, two sets of calculated frequencies can be seen having the same value with one of the sets being Raman active while the other are infrared active. Raman lines 2935 cm^{-1}, 2910 cm^{-1}, 2875 cm^{-1}, 1446 $cm^{-1}$and 1370cm^{-1} can be assigned to Raman active vibrational modes predicted at 2965 cm^{-1}(ν_2), 2943 cm^{-1} (ν_{95}), 2897 cm^{-1}(ν_3), 1468 cm^{-1}(ν_{36}), 1384 cm^{-1}(ν_{67}) respectively. At the same time the infrared bands with same values as the Raman lines can be assigned to the other set.

Generally, C-H stretching frequencies have shown to exercise minimal shifts upon COD coordination, unlike C-H bending modes where the frequency shift could reach up to 12% compared to the free COD ring. More detailed spectral shift analyses of selected vibrational modes are presented in Figures 7 and 8. Upon coordination, the frequencies associated with the C=C stretching and C-H in-plane wagging modes are expected to shift to lower values as C=C moves towards sp3 hybridization. These two vibrational modes have been denoted as band I and band II and correlated to be total ($\pi+\sigma$) metal-olefin interaction [49, 56]. Table 9 shows greater total ($\pi+\sigma$) metal-olefin interaction for $[Ir(\mu\text{-}Cl)(COD)]_2$ as the sum of its percent shifts is higher. On the other hand, the frequencies associated with C-H rocking and ring bending mode would shift to greater values upon coordination. The C-H rocking moves the hydrogen into and out of π electron density section while the metal constrains the ring bending mode [49, 56]. These two modes are important in evaluating π components in the total interaction. Hence, the higher percent shifts obtained for Ir complex in both modes as presented in Figure 7 shows a greater π component than Rh complex. Another vibrational mode that is also important for π components evaluation is metal-carbon stretching mode which moves olefinic carbon atom into and out of π-electron density section. Table 10 shows the list of these frequencies with higher values being recorded for Ir complex. This further buttresses greater π components in total metal-olefinic interaction for Ir than Rh complex. The trend of π components in the interaction for both complexes is in line with the total ($\pi+\sigma$) metal-olefin interaction. Other vibrational modes worthy of considering are those associated with CH_2. Though the CH_2 is not directly linked with the metal centre but the pattern of frequency shift upon coordination as depicted in Figure 8 is similar to CH. The

frequencies of CH_2 wagging and twisting modes are red shifted just like that of CH wagging and C=C stretching vibrations which are the determinant of total ($\pi+\sigma$) metal-olefin interaction. In the same sense, the blue shift in frequency recorded for the rocking mode is in line with that of CH which is being used as a measure for π components in the total interaction. Interestingly, percent shift in CH_2 vibrational modes is consistent with that of CH as greater values are recorded for $[Ir(\mu\text{-}Cl)(COD)]_2$. Hence, we can say that the extent metal-olefin interaction can also be reflected from the change in frequencies associated with diolefin CH_2 vibrational modes upon coordination. In general, greater interaction obtained for iridium complex might be due to the slightly lower electronegative nature of Ir metal than Rh, which enables it to populate the orbital of carbon in C=C with more electrons than Rh and thus resulting into longer bond lengths which eventually lowers the vibrational frequencies.

Table 7. Vibrational assignment of $[Rh(\mu\text{-}Cl)(COD)]_2$ complex compared with 1,5-cyclooctadiene

	$[Rh(\mu\text{-}Cl)(COD)]_2$						1,5-Cyclooctadiene			
	Experiment		Calc. (D_{2h})		Calc. (D_2)		Experiment			
Description	IR	Raman	Frequency		Frequency		IR		Raman	
A_g, A										
ν_1 CH str.		2976 w	3017	(0,37)	3017	(0,44)	3005	s	3008	s
ν_2 CH_2 str.		2935 m	2965	(0,30)	2963	(0,16)			2956	w
ν_3 CH_2 str.		2875 s	2897	(0,100)	2928	(0,65)	2881	vs	2884	vs
ν_4 CH_2 def.			1498	(0,1)	1510	(0,3)				
ν_5 C=C str.		1468 m	1488	(0,17)	1495	(0,19)	1657	w	1659	s
ν_6 CH_2 wag			1287	(0,13)	1313	(0,0)			1273	m
ν_7 CH in-plane wag			1229	(0,6)	1199	(0,5)	1265	w		
ν_8 CH_2 twist		1175 w	1189	(0,1)	1172	(0,0)	1168	w	1164	vw
ν_9 C-C str.		1004 w	1007	(0,2)	1002	(0,1)	1002	w	999	w (sh)
ν_{10} CH rock		880 m	890	(0,9)	883	(0,11)	824	w	824	w (sh)
ν_{11} CH rock		776 s	780	(0,4)	847	(0,1)	705	m	708	m
ν_{12} CH_2 rock			737	(0,17)	696	(0,3)			748	vw
ν_{13} Ring bend		476 vs	471	(0,38)	461	(0,33)			269	s
ν_{14} C-Rh str.		351 s	342	(0,22)	348	(0,26)				
ν_{15} Ring puck		247 m (sh)	253	(0,15)	284	(0,8)				
ν_{16} Ring puck		*169 m*	229	(0,5)	241	(0,12)				
ν_{17} Skeletal str.		104 vs	96	(0,74)	95	(0,100)				
A_u, A										
ν_{18}CH str.		*2990 m*	3001	(0,0)	3000	(0,1)				
ν_{19} CH_2 str.		*2935 m*	2943	(0,0)	2934	(0,12)				
ν_{20} CH_2 str.		*2875 s*	2883	(0,0)	2876	(0,74)			2852	w (sh)

Table 7.
Continued

	[Rh(μ-Cl)(COD)]$_2$								1,5-Cyclooctadiene			
	Experiment				Calc. (D_{2h})		Calc. (D_2)		Experiment			
Description	IR		Raman		Frequency		Frequency		IR		Raman	
ν_{21} CH_2 def.			*1429*	*m*	1454	(0,0)	1461	(0,6)			1452	w (sh)
ν_{22} CH wag					1385	(0,0)	1387	(0,0)			1407	w
ν_{23} CH_2 wag			*1334*	*vw (sh)*	1330	(0,0)	1342	(0,2)			1315	w
ν_{24} CH_2 twist					1256	(0,0)	1250	(0,18)				
ν_{25} CH_2 rock			*1075*	*vw*	1069	(0,0)	1082	(0,2)			1083	w
ν_{26} CH twist			*993*	*w (sh)*	998	(0,0)	999	(0,2)			970	w
ν_{27} CH rock					979	(0,0)	972	(0,0)			988	vw (sh)
ν_{28} Ring def.					767	(0,0)	770	(0,24)			731	vw (sh)
ν_{29} Ring def.			*513*	*s*	496	(0,0)	508	(0,10)			237	s
ν_{30} Ring def.			*385*	*s*	384	(0,0)	388	(0,6)				
ν_{31} Ring bend					33	(0,0)	43	(0,5)				
			169	*m*	i		173	(0,11)				
B_{1g}, B_1												
ν_{32} CH str.					3014	(0,1)	3014	(0,1)				
ν_{33} CH_2 str.	*2936*	*s*			2943	(0,0)	2933	(2,0)				
ν_{34} CH_2 str.			*2875*	*s*	2881	(0,18)	2875	(34,26)	2828	s		
ν_{35} C=C str.	*1468*	*m*	*1468*	*m*	1480	(0,0)	1489	(3,4)			1634	vw (sh)
ν_{36} CH_2 def.	*1448*	*m*	1446	m	1468	(0,10)	1457	(11,7)	1448	w	1445	vw (sh)
ν_{37} CH_2 wag			1334	vw (sh)	1339	(0,0)	1345	(0,0)	1357	w	1349	w
ν_{38} CH_2 twist			*1237*	*m*	1255	(0,1)	1240	(1,0)			1252	vw (sh)
ν_{39} CH in-plane wag	*1151*	*w*	1211	w	1211	(0,6)	1188	(4,4)			1222	vw
ν_{40} CH_2 rock	*993*	*m*			990	(0,0)	1003	(9,0)				

Table 7.
Continued

	[Rh(μ-Cl)(COD)]$_2$								1,5-Cyclooctadiene			
	Experiment				Calc. (D_{2h})		Calc. (D_2)		Experiment			
Description	IR		Raman		Frequency		Frequency		IR		Raman	
ν_{41} CH rock					851	(0,1)	893	(0,0)	903	vw		
ν_{42} CH rock					810	(0,0)	800	(0,0)	753	m	757	vw
ν_{43} Ring bend					653	(0,1)	689	(0,0)	465	vw	463	w
ν_{44} C-Rh str.			385	s	374	(0,11)	363	(0,13)				
ν_{45} Ring puck					230	(0,2)	230	(0,2)				
ν_{46} Ring def.			137	m	136	(0,1)	133	(0,3)			103	m
ν_{47} CH_2 rock			*196*	*w*	120	(0,1)	190	(0,1)				
B_{1u}, B_1												
ν_{48} CH str.			*3004*	*m*	3001	(8,0)	3000	(9,1)				
ν_{49} CH_2 str.	2936	s	*2935*	*m*	2963	(50,0)	2956	(61,3)	2961	s (sh)		
ν_{50} CH_2 str.	2872	s	*2910*	*m*	2899	(7,0)	2923	(14,4)	2935	s		
ν_{51} CH_2 def.					1476	(4,0)	1479	(1,0)	1484	m	1486	w
ν_{52} CH wag	1368	w	*1370*	*w*	1384	(1,0)	1384	(1,0)	1398	w		
ν_{53} CH_2 wag	1299	m			1299	(1,0)	1319	(0,2)	1318	w		
ν_{54} CH_2 twist	1210	w			1216	(5,0)	1231	(3,2)	1234	w	1238	vw (sh)
ν_{55} C-C str.	*1077*	*w*			1101	(1,0)	1080	(1,0)			1047	vw (sh)
ν_{56} CH rock	959	s			977	(14,0)	976	(13,0)	966	w		
ν_{57} C-C str.	870	m			876	(3,0)	865	(9,1)			872	vw
ν_{58} CH_2 rock	816	m			812	(1,0)	813	(1,0)	797	w	801	s
ν_{59} Ring def.	*580*	*vw*			607	(0,0)	574	(0,0)			571	vw
ν_{60} Ring def.	486	w			509	(3,0)	484	(6,0)			494	w
ν_{61} Ring def.			*254*	*m*	249	(1,0)	253	(1,0)				

Table 7.
Continued

	[Rh(μ-Cl)(COD)]$_2$								1,5-Cyclooctadiene			
	Experiment			Calc. (D_{2h})		Calc. (D_2)			Experiment			
Description	IR		Raman		Frequency		Frequency		IR		Raman	
ν_{62} Ring bend					94	(0,0)	95	(0,0)				
					-14	(1,0)	17	(1,6)				
B_{2g}, B_2												
ν_{63} CH str.					3001	(0,0)	3000	(0,0)			2992	m (sh)
ν_{64} CH_2 str.					2963	(0,3)	2956	(3,6)	2961	s (sh)		
$\nu_{65}$$CH_2$ str.					2899	(0,3)	2923	(9,2)	2935	s		
ν_{66} CH_2 def.					1476	(0,2)	1479	(2,0)	1484	m	1486	w
ν_{67} CH wag			1370	w	1384	(0,1)	1384	(0,1)	1398	w		
ν_{68} CH_2 wag			1299	w	1299	(0,2)	1319	(5,1)	1318	w		
ν_{69} CH_2 twist					1216	(0,0)	1231	(1,0)	1234	w	1238	vw (sh)
ν_{70} C-C Str.			*1075*	*vw*	1101	(0,0)	1080	(0,0)			1047	vw (sh)
ν_{71} CH rock			960	w	976	(0,7)	976	(0,8)	966	w		
ν_{72} C-C str.			872	vw (sh)	876	(0,0)	893	(1,0)			872	vw
ν_{73} CH_2 rock					812	(0,0)	814	(9,0)	797	w	801	s
ν_{74} Ring bend			582	w	607	(0,2)	575	(0,8)			571	vw
ν_{75} Ring def.			513	s	509	(0,14)	485	(1,15)			494	w
ν_{76} Ring def.			254	m	247	(0,2)	250	(0,2)				
ν_{77} Ring bend					65	(0,22)	69	(0,28)				
B_{2u}, B_2												
ν_{78} CH str.					3014	(14,0)	3015	(24,0)				
ν_{79} CH_2 str.	2911	s			2943	(7,0)	2933	(3,12)			2917	s

Table 7.
Continued

	[Rh(μ-Cl)(COD)]$_2$								1,5-Cyclooctadiene			
	Experiment				Calc. (D_{2h})		Calc. (D_2)		Experiment			
Description	IR		Raman		Frequency		Frequency		IR		Raman	
ν_{80} CH_2 str.	2828	s			2881	(25,0)	2875	(34,19)	2828	s		
ν_{81} C=C str.	1468	m			1481	(6,0)	1489	(4,1)			1634	vw (sh)
ν_{82} CH_2 def.	1448	w	*1429*	*m*	1468	(0,0)	1457	(0,3)	1448	w	1445	vw (sh)
ν_{83} CH_2 wag	1325	m			1339	(6,0)	1345	(9,0)	1357	w	1349	w
ν_{84} CH_2 twist	*1227*	*w*			1255	(1,0)	1240	(0,1)			1252	vw (sh)
ν_{85} CH in-plane wag	1210	w	*1154*	*vw*	1212	(0,0)	1188	(1,0)			1222	vw
ν_{86} CH_2 rock					990	(1,0)	1003	(1,2)				
ν_{87} CH rock					851	(1,0)	865	(0,0)	903	vw		
ν_{88} CH rock	*794*	*w*			811	(2,0)	802	(0,1)	753	m	757	vw
ν_{89} ring bend					654	(0,0)	690	(0,0)	465	vw	463	w
ν_{90} C-Rh str.					376	(3,0)	365	(4,0)				
ν_{91} Skeletal movement					236	(6,0)	238	(10,0)				
ν_{92} CH_2 rock					126	(0,0)	187	(1,1)			103	m
ν_{93} Ring bend					76	(1,0)	81	(2,3)				
ν_{94} CH str.			3004	m	3001	(0,13)	3000	(0,15)			2992	m (sh)
ν_{95} CH_2 str.			2910	m	2943	(0,8)	2934	(0,1)			2917	s
ν_{96} CH_2 str.	*2872*	*s*			2883	(0,1)	2875	(61,7)			2852	w (sh)
ν_{97} CH_2 def.			1429	m	1454	(0,2)	1461	(0,4)			1452	w (sh)
ν_{98} CH wag			1370	w	1385	(0,3)	1387	(0,2)			1407	w
ν_{99} CH_2 wag			1324	vw	1330	(0,0)	1342	(1,0)			1315	w

Table 7.
Continued

	[Rh(μ-Cl)(COD)]$_2$								1,5-Cyclooctadiene			
	Experiment				Calc. (D_{2h})		Calc. (D_2)		Experiment			
Description	IR		Raman		Frequency		Frequency		IR		Raman	
ν_{100} CH_2 twist			1237	m	1256	(0,1)	1250	(0,2)				
ν_{101} CH_2 rock					1069	(0,0)	1082	(3,0)			1083	w
ν_{102} CH rock			993	w (sh)	999	(0,0)	1000	(1,0)			970	w
ν_{103} C-C str.			977	w	979	(0,2)	972	(0,2)			988	vw (sh)
ν_{104} Ring def.					767	(0,0)	769	(8,0)			731	vw (sh)
ν_{105} Ring def.	*512*	*vw*			496	(0,3)	508	(0,1)			237	s
ν_{106} Ring def.			394	s	384	(0,11)	388	(0,10)				
ν_{107} Ring bend			*161*	*w*	78	(0,17)	170	(0,3)				
					-146	(0,4)	80	(0,20)				
B_{3u}, B_3												
ν_{108} CH str.	2994	s			3017	(9,0)	3017	(16,1)	3005	s	3008	s
ν_{109} CH_2 str.					2965	(1,0)	2963	(10,3)			2956	w
ν_{110} CH_2 str.	2872	s			2897	(100,0)	2928	(100,5)	2881	vs	2884	vs
ν_{111} CH_2 def.					1498	(4,0)	1510	(6,0)				
ν_{112} C=C str.					1489	(1,0)	1495	(1,0)	1657	w	1659	s
ν_{113} CH_2 wag					1287	(1,0)	1313	(0,0)			1273	m
ν_{114} CH in-plane wag	1227	w			1228	(0,0)	1199	(3,0)	1265	w		
ν_{115} CH_2 twist	1172	w			1189	(7,0)	1172	(4,0)	1168	w	1164	vw
ν_{116} C-C str.	993	m			1007	(1,0)	1002	(1,2)	1002	w	999	w (sh)
ν_{117} CH rock	*880*	*m*			888	(2,0)	881	(3,0)	824	w	824	w (sh)
ν_{118} CH rock	775	w			779	(4,0)	846	(4,0)	705	m	708	m
ν_{119} CH_2 rock	688	vw	*694*	*vw*	737	(0,0)	695	(0,0)			748	vw

Table 7.
Continued

	[Rh(μ-Cl)(COD)]$_2$								1,5-Cyclooctadiene	
	Experiment		Calc. (D_{2h})		Calc. (D_2)		Experiment			
Description	IR		Raman		Frequency		Frequency		IR	Raman
ν_{120} Ring bend	486	w			471	(2,0)	461	(4,4)		269 s
ν_{121} C-Rh str.					340	(1,0)	346	(0,0)		
ν_{122} Ring puck					274	(28,0)	292	(20,1)		
ν_{123} Ring puck			*247*	*m (sh)*	226	(5,0)	252	(35,1)		

Table 8. Vibrational assignment of [Ir(μ-Cl)(COD)]$_2$ complex compared with 1,5-cyclooctadiene

	[Ir(μ-Cl)(COD)]$_2$								1,5-Cyclooctadiene			
	Experiment				Calc. (C_{2v})		Calc. (C_2)		Experiment			
Description	IR		Raman		Frequency		Frequency		IR		Raman	
A_1, A												
ν_1 CH str.			2980	s	3004	(1,57)	3005	(2,54)	3005	s	3008	s
ν_2 CH str.					2987	(17,10)	2989	(7,8)			2992	m
ν_3 CH_2 str.			*2964*	*s*	2963	(8,10)	2960	(11,3)			2956	w
ν_4 CH_2 str.	2934	s			2959	(25,4)	2954	(31,11)	2961	s (sh)		
ν_5 CH_2 str.	2908	s	2913	m	2902	(49,69)	2926	(46,93)	2935	s		
ν_6 CH_2 str.			2880	s	2900	(11, 100)	2919	(5,5)	2881	vs	2884	vs
ν_7 CH_2 def.					1497	(8,2)	1501	(7,1)				
ν_8 CH_2 def.			*1478*	*w*	1477	(4,3)	1480	(5,3)	1484	m	1486	w
ν_9 C=C str.			1448	s	1463	(0,21)	1465	(1,8)	1657	w	1659	s
ν_{10} CH wag	1363	w			1378	(1,2)	1379	(0,2)	1398	w		
ν_{11} CH_2 wag					1300	(0,2)	1316	(0,2)	1318	w		
ν_{12} CH_2 wag			1297	w	1287	(0,16)	1310	(0,0)			1273	m
ν_{13} CH in-plane-wag	1230	w	1232	w	1226	(2,8)	1225	(1,2)	1265	w		
ν_{14} CH_2 twist					1215	(2,0)	1196	(0,2)				
ν_{15} CH_2 twist	1174	m (sh)	1181	w	1189	(2,1)	1173	(2,1)	1234	w	1238	vw (sh)
ν_{16} C-C str.					1103	(0,0)	1081	(0,1)			1047	vw (sh)
ν_{17} C-C str.	1000	m	1001	w	1004	(3,5)	1010	(5,5)	1002	w	999	w (sh)
ν_{18} CH wag	971	m	970	w	999	(10,7)	993	(3,2)				
ν_{19} CH rock			915	m	934	(0,11)	927	(0,9)	824	w	824	w (sh)
ν_{20} CH_2 rock	869	m	*903*	*w (sh)*	877	(3,0)	900	(0,0)	797	w	801	s

Table 8.
Continued

	[Ir(μ-Cl)(COD)]$_2$								1,5-Cyclooctadiene			
	Experiment				Calc. (C_{2v})		Calc. (C_2)		Experiment			
Description	IR		Raman		Frequency		Frequency		IR		Raman	
ν_{21} CH_2 rock	806	w	*830*	*w*	812	(1,1)	832	(0,1)	903	vw		
ν_{22} CH_2 rock			785	s	790	(3,10)	802	(0,1)			748	vw
ν_{23} CH_2 rock					733	(0,31)	695	(0,0)				
ν_{24} Ring def	*603*	*vw*	601	m	625	(0,11)	596	(1,17)			571	vw
ν_{25} Ring bend	530	m	534	vs	526	(4,63)	528	(1,64)			269	s
ν_{26} Ring def			511	vs	517	(1,72)	506	(3,26)				
ν_{27} Ir-C str.			337	s	329	(1,68)	335	(1,56)				
ν_{28} Skeletal			301	s	276	(5,28)	279	(5,21)				
ν_{29} Ring def			246	w	257	(3,16)	262	(0,17)				
ν_{30} Ring puck					225	(1,2)	255	(6,8)				
ν_{31} Skeletal move.			177	s (sh)	153	(0,33)	185	(0,2)				
ν_{32} skeletal str.			102	vs	84	(0,51)	85	(0,45)				
ν_{33} Skeletal move.					20	(0,88)	20	(0,58)				
A_2, A												
ν_{34} CH str.					2999	(0,0)	3002	(1,1)				
ν_{35} CH str.			*2980*	*s*	2985	(0,13)	2984	(8,12)				
ν_{36} CH_2 str.			*2935*	*w*	2942	(0,3)	2934	(6,15)				
ν_{37} CH_2 str.			*2913*	*m*	2937	(0,3)	2929	(3,8)			2917	s
ν_{38} CH_2 str.	*2877*	*s*			2887	(0,4)	2881	(42,51)			2852	w (sh)
ν_{39} CH_2 str.			2830	m	2884	(0,20)	2878	(1, 100)	2828	s		

Table 8.
Continued

	[Ir(μ-Cl)(COD)]$_2$								1,5-Cyclooctadiene			
	Experiment				Calc. (C_{2v})		Calc. (C_2)		Experiment			
Description	IR		Raman		Frequency		Frequency		IR		Raman	
ν_{40} CH_2 def.					1473	(0,4)	1468	(3,6)	1448	w	1445	vw (sh)
ν_{41} CH_2 def.					1454	(0,2)	1459	(0,9)			1452	w (sh)
ν_{42} C=C str.	*1425*	*m*	1430	m	1448	(0,7)	1446	(3,11)			1634	vw (sh)
ν_{43} CH wag	*1363*	*w*	1362	w	1377	(0,2)	1378	(1,1)			1407	w
ν_{44} CH_2 wag			*1321*	*vw*	1338	(0,0)	1343	(0,1)	1357	w	1349	w
ν_{45} CH_2 wag					1329	(0,0)	1338	(0,3)			1315	w
ν_{46} CH_2 twist	*1230*	*w*			1257	(0,1)	1247	(1,20)			1222	vw
ν_{47} CH_2 twist					1256	(0,0)	1239	(0,2)	1168	w	1164	vw
ν_{48} CH in-plane wag	*1174*	*m (sh)*	*1181*	*w*	1203	(0,7)	1184	(2,4)			1252	vw (sh)
ν_{49} CH_2 rock			*1082*	*vw*	1068	(0,0)	1079	(0,3)			1083	w
ν_{50} CH_2 rock					1021	(0,0)	1025	(2,1)			970	w
ν_{51} CH rock					999	(0,1)	997	(4,8)				
ν_{52} C-C str.					980	(0,1)	971	(0,3)			988	vw (sh)
ν_{53} CH rock	*869*	*m*			867	(0,0)	867	(7,1)	753	vw	757	vw
ν_{54} CH rock					822	(0,0)	843	(1,1)				
ν_{55} Ring def	*783*	*w*	*785*	*s*	770	(0,0)	775	(3,35)			731	vw (sh)
ν_{56} Ring bend	*694*	*vw*	*~ 696*	*vw (br)*	674	(0,0)	690	(0,6)	465	vw	463	w
ν_{57} Ring def.			*499*	*m*	513	(0,3)	494	(2,39)			237	s
ν_{58} Ir-C str.	*413*	*w*	412	vs	410	(0,23)	407	(0,8)				
ν_{59} Ring def.					397	(0,4)	399	(0,22)			103	m
ν_{60} skeletal move.					186	(0,1)	190	(0,3)				

Table 8.
Continued

	[Ir(μ-Cl)(COD)]$_2$								1,5-Cyclooctadiene			
	Experiment				Calc. (C_{2v})		Calc. (C_2)		Experiment			
Description	IR		Raman		Frequency		Frequency		IR		Raman	
ν_{61} Ring def.			*161*	*vs*	121	(0,0)	152	(0,31)				
ν_{62} Ring def.					108	(0,0)	112	(0,0)				
ν_{63} Ring def.					38	(0,21)	49	(0,13)				
					i		167	(0,3)				
B_1, B												
ν_{64} CH str.	2975	s			3000	(36,1)	3002	(50,1)	3005	s	3008	s
ν_{65} CH str.					2986	(2,17)	2984	(5,9)			2992	m
ν_{66} CH_2 str.					2942	(5,3)	2934	(4,4)				
ν_{67} CH_2 str.			2935	w	2937	(3,2)	2928	(15,5)			2917	s
ν_{68} CH_2 str.	2877	s			2887	(14,7)	2881	(25,24)			2852	w (sh)
ν_{69} CH_2 str.	2828	s			2884	(27,5)	2878	(100,2)	2828	s		
ν_{70} CH_2 def.	1471	m	1478	w	1476	(6,3)	1479	(1,1)	1484	m	1486	w
ν_{71} CH_2 def.					1456	(0,2)	1453	(0,3)			1452	w (sh)
ν_{72} C=C str.	1425	m	*1430*	*m*	1449	(2,1)	1445	(2,1)			1634	vw (sh)
ν_{73} CH wag			*1362*	*w*	1378	(0,3)	1381	(0,2)			1407	w
ν_{74} CH_2 wag	1321	m	1321	vw	1338	(9,0)	1341	(8,0)	1357	w	1349	w
ν_{75} CH_2 wag					1329	(0,0)	1337	(6,1)			1315	w
ν_{76} CH_2 twist					1258	(3,0)	1246	(8,1)			1222	vw
ν_{77} CH_2 twist					1257	(1,2)	1239	(2,0)	1168	w	1164	vw
ν_{78} CH in-plane-wag	*1155*	*m*	1210	vw	1204	(0,2)	1185	(6,1)			1252	vw (sh)

Table 8.
Continued

	[Ir(μ-Cl)(COD)]$_2$								1,5-Cyclooctadiene			
	Experiment				Calc. (C_{2v})		Calc. (C_2)		Experiment			
Description	IR		Raman		Frequency		Frequency		IR		Raman	
ν_{79} CH_2 rock	1072	w	1082	vw	1070	(0,0)	1079	(6,0)			1083	w
ν_{80} CH rock?					1024	(0,0)	1027	(0,2)			970	w
ν_{81}CH rock					1001	(5,0)	996	(4,2)				
ν_{82} C-C str.					981	(0,2)	971	(1,1)			988	vw (sh)
ν_{83} CH rock					875	(0,0)	867	(2,0)	753	vw	757	vw
ν_{84} CH rock	830	m	830	w	824	(6,0)	842	(6,1)				
ν_{85} Ring def					771	(0,0)	774	(4,0)			731	vw (sh)
ν_{86} Ring bend	694	vw	~ 696	vw (br)	674	(0,1)	690	(0,0)	465	vw	463	w
ν_{87} Ring def					514	(0,3)	493	(7,1)			237	s
ν_{88} Ir-C str.	413	w			412	(8,5)	404	(2,6)				
ν_{89} Ring def					398	(0,6)	401	(9,5)			103	m
ν_{90} Skeletal move.			266	m	261	(13,15)	262	(17,14)				
ν_{91} Skeletal move.			145	m	145	(0,5)	162	(0,17)				
ν_{92} Ring def.					121	(0,0)	142	(0,4)				
ν_{93} Skeletal move.					50	(0,0)	42	(0,12)				
					i	(0,4)	178	(0,1)				
B_2, B												
ν_{94} CH str.	*2975*	*s*			3003	(9,3)	3005	(12,3)				
ν_{95} CH str.					2986	(9,3)	2989	(6,7)				
ν_{96} CH_2 str.			2964	s	2962	(13,34)	2960	(2,23)			2956	w

Table 8.
Continued

	[Ir(μ-Cl)(COD)]$_2$								1,5-Cyclooctadiene			
	Experiment				Calc. (C_{2v})		Calc. (C_2)		Experiment			
Description	IR		Raman		Frequency		Frequency		IR		Raman	
ν_{97} CH_2 str.	*2934*	*s*			2958	(24,5)	2954	(52,2)	2961	s (sh)		
ν_{98} CH_2 str.	*2908*	*s*			2901	(17,12)	2926	(77,3)	2935	s		
ν_{99} CH_2 str.	2877	s			2899	(100, 11)	2920	(22,2)	2881	vs	2884	vs
ν_{100} CH_2 def.					1493	(3,1)	1500	(4,3)				
ν_{101} CH_2 def.	*1471*	*m*			1475	(2,0)	1465	(9,4)	1448	w	1445	vw (sh)
ν_{102} C=C str.	1445	m			1462	(3,3)	1464	(4,1)	1657	w	1659	s
ν_{103} CH wag					1377	(0,1)	1376	(0,1)	1398	w		
ν_{104} CH_2 wag	*1297*	*w*			1298	(0,0)	1317	(7,1)	1318	w		
ν_{105} CH_2 wag					1285	(7,1)	1310	(2,0)			1273	m
ν_{106} CH in-plane wag					1224	(2,1)	1223	(6,0)	1265	w		
ν_{107} CH_2 twist	1205	m			1214	(6,0)	1195	(2,4)				
ν_{108} CH_2 twist	1155	m	1168	w	1187	(14,2)	1171	(10,0)	1234	w	1238	vw (sh)
ν_{109} C-C str.	*1072*	*w*			1102	(0,0)	1080	(1,0)			1047	vw (sh)
ν_{110} C-C str.	*1000*	*m*	*1001*	*w*	1003	(3,2)	1009	(11,0)	1002	w	999	w (sh)
ν_{111} CH rock	*971*	*m*	*970*	*w*	993	(17,2)	989	(17,2)				
ν_{112} CH rock	902	s	903	w (sh)	924	(26,2)	919	(29,2)	824	w	824	w (sh)
ν_{113} C-C str.					876	(1,0)	905	(1,0)	797	w	801	s
$\nu_{114}CH_2$ rock					811	(0,0)	834	(7,0)	903	vw		
ν_{115} CH rock	783	w			789	(3,0)	801	(5,0)			748	vw
ν_{116} CH_2 rock					733	(0,0)	694	(0,0)				

Table 8.
Continued

	[Ir(μ-Cl)(COD)]$_2$						1,5-Cyclooctadiene	
	Experiment		Calc. (C_{2v})		Calc. (C_2)		Experiment	
Description	IR	Raman	Frequency		Frequency		IR	Raman
ν_{117} Ring def.	603 vw		622	(0,0)	593	(0,1)		571 vw
ν_{118} Ring bend	*530 m*		519	(3,7)	524	(9,5)		
ν_{119} Ring bend	501 w		515	(12,1)	503	(8,4)		269 s
ν_{120} Ir-C str.			326	(2,2)	332	(3,1)		
ν_{121} Ring def.			250	(4,1)	261	(0,4)		
ν_{122} Ring puck			229	(1,9)	250	(5,4)		
ν_{123} Skeletal str.			203	(8,4)	210	(12,0)		
ν_{124} Ring def.			54	(0,17)	52	(0,15)		

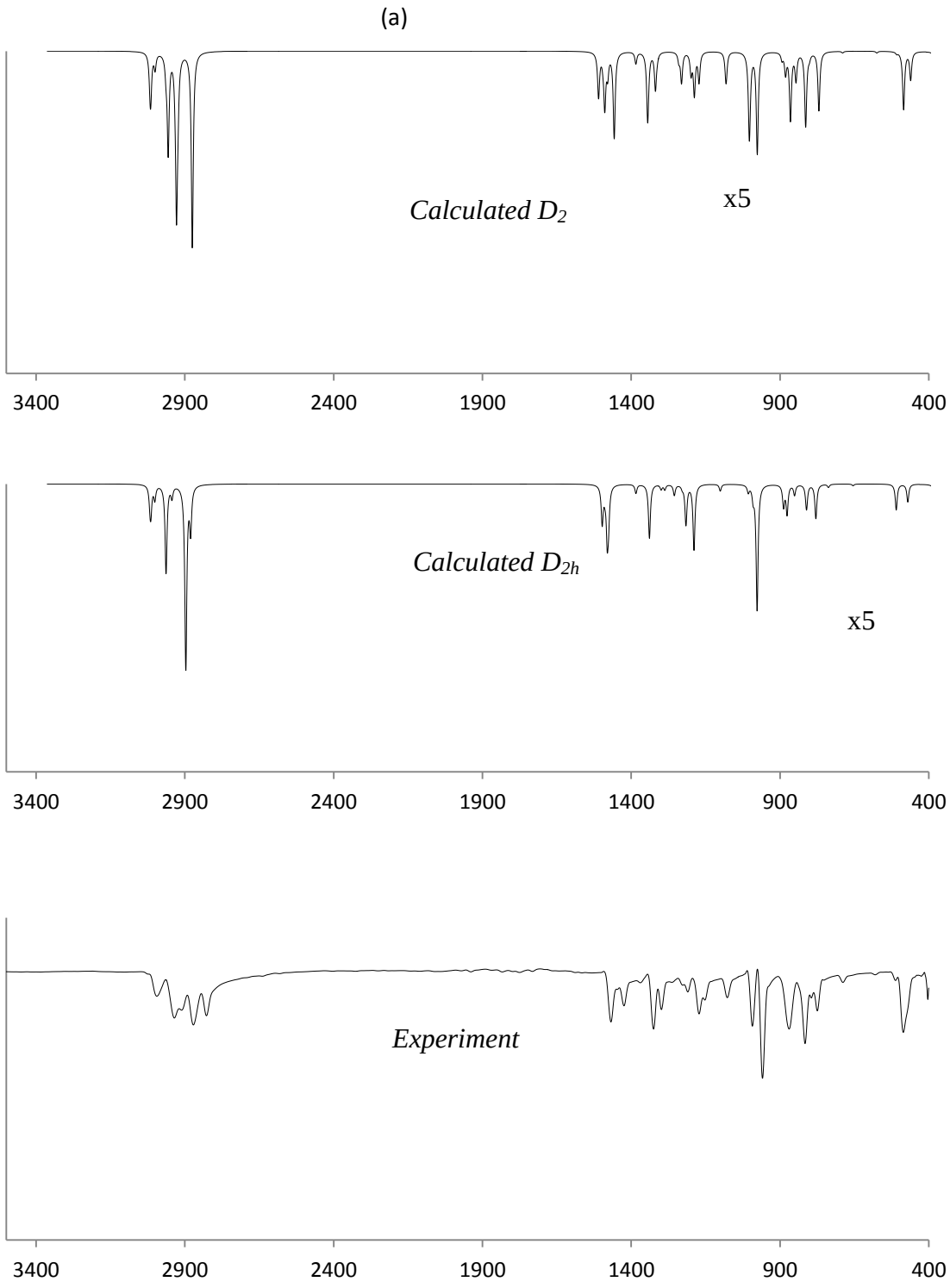

Figure 3a. Experiment and calculated (using the DFT-B3LYP-D3/6-311++G(d,p)/SDD/ level of theory) mid IR of the $[Rh(\mu\text{-}Cl)(COD)]_2$ spectra

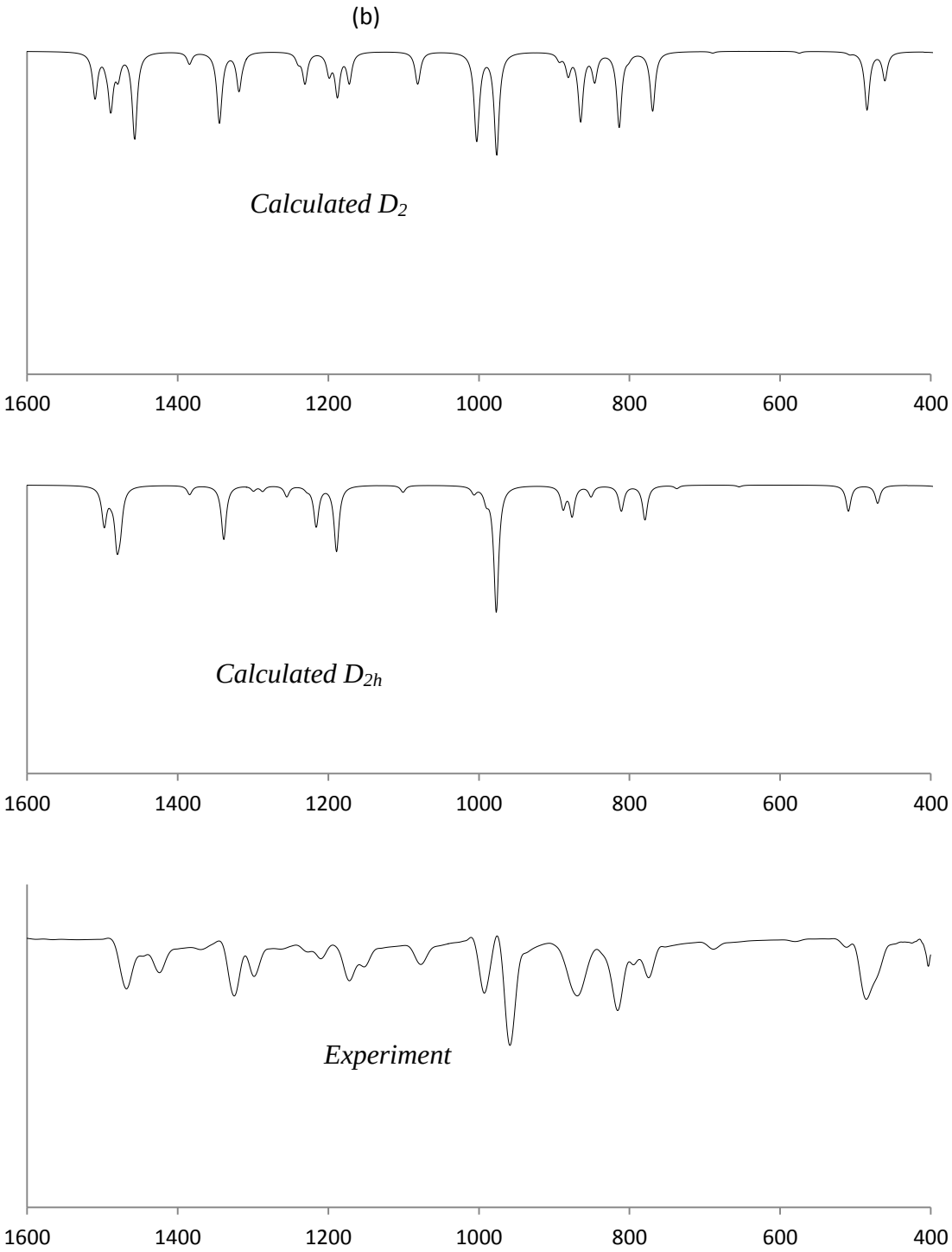

Figure 3b. Expanded mid IR spectra for $[Rh(\mu\text{-}Cl)(COD)]_2$

(a)

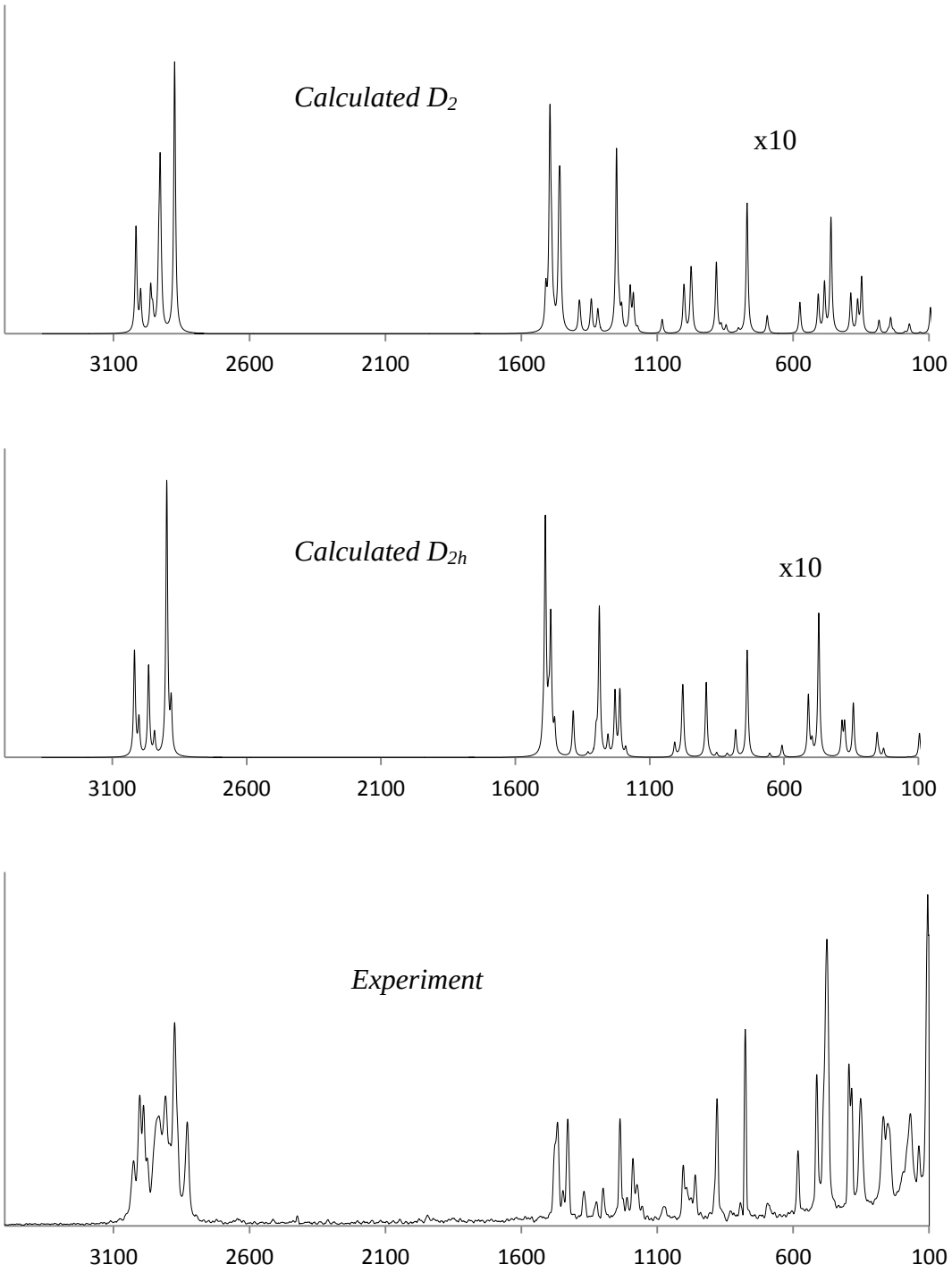

Figure 4a. Experiment and calculated (using the DFT-B3LYP-D3/6-311++G(d,p)/SDD level of theory) Raman of the $[Rh(\mu\text{-}Cl)(COD)]_2$ spectra

(b)

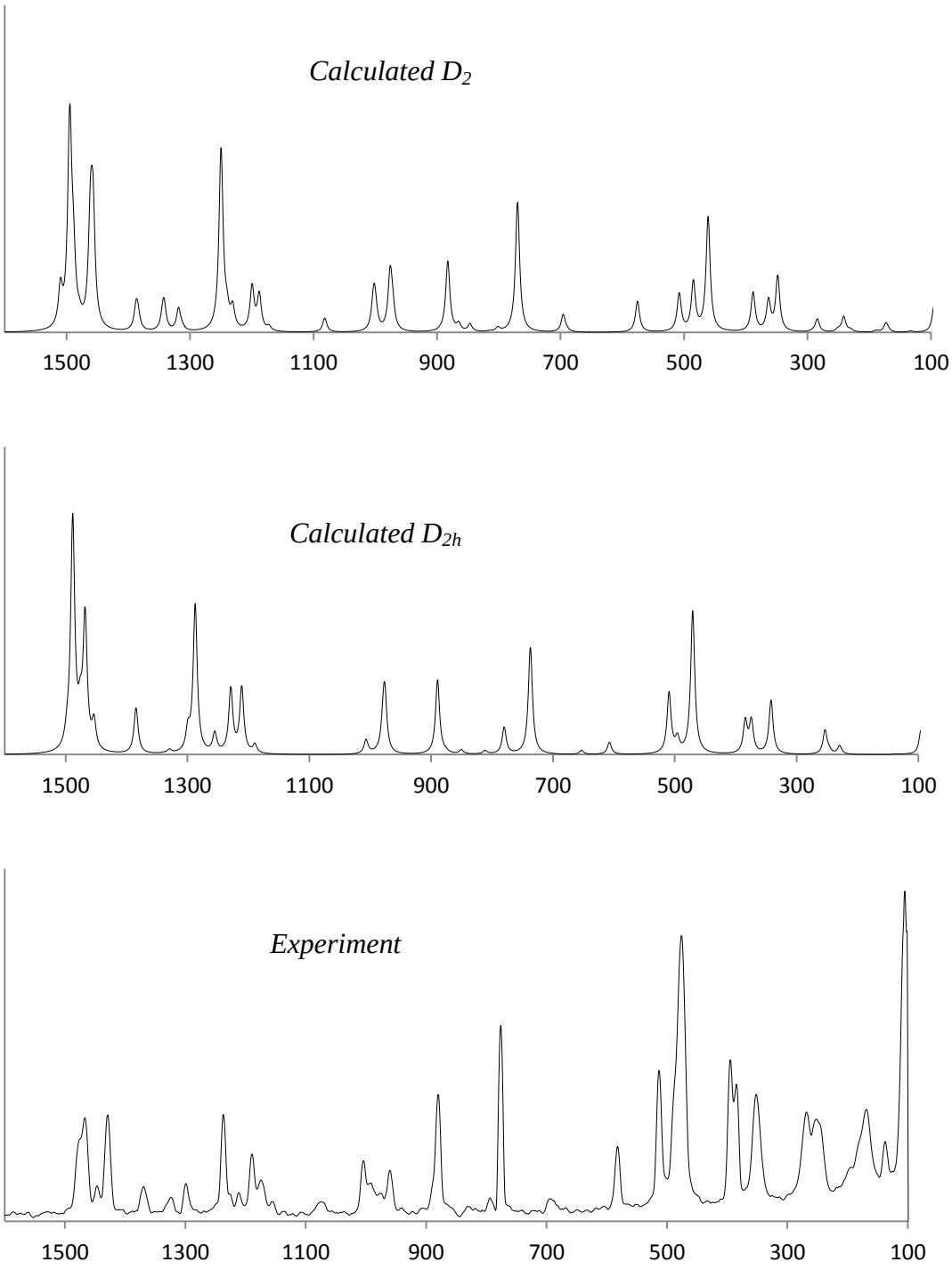

Figure 4b. Expanded Raman spectra for $[Rh(\mu\text{-}Cl)(COD)]_2$

(a)

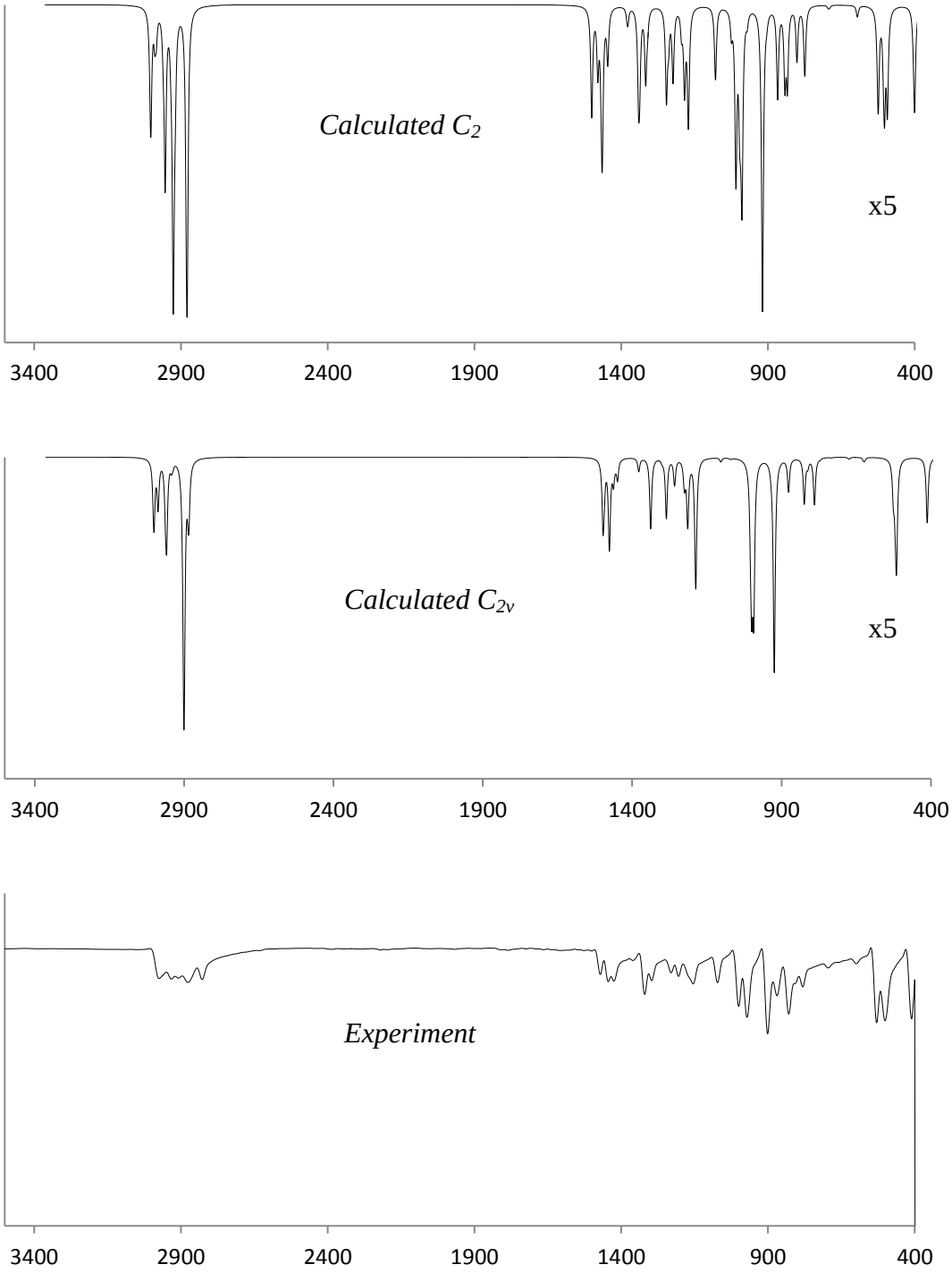

Figure 5a. Experiment and calculated (using the DFT-B3LYP-D3/6-311++G(d,p)/SDD level of theory) mid IR of the $[Ir(\mu\text{-}Cl)(COD)]_2$ spectra

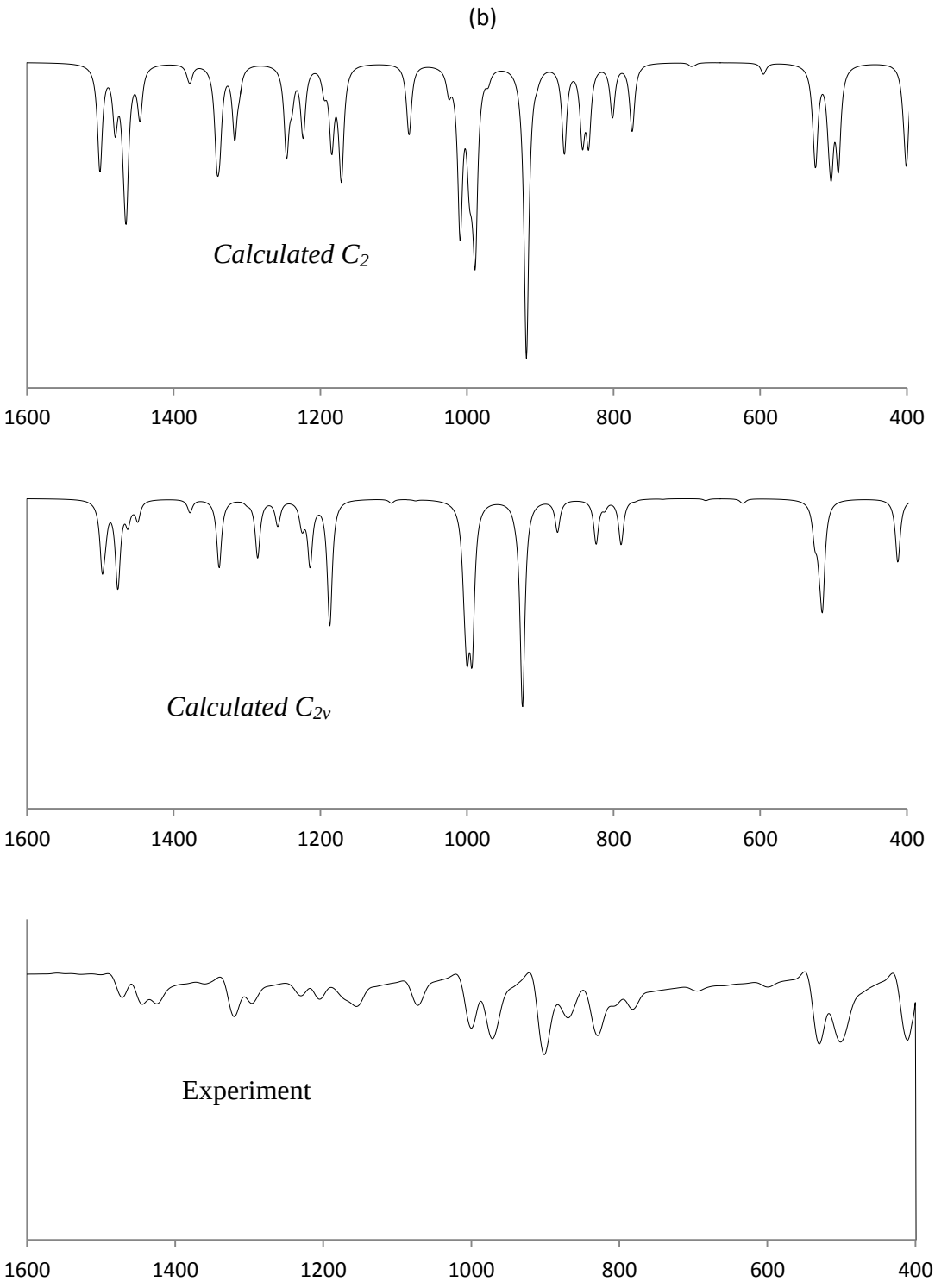

Figure 5b. Expanded mid IR spectra for $[Ir(\mu\text{-}Cl)(COD)]_2$

(a)

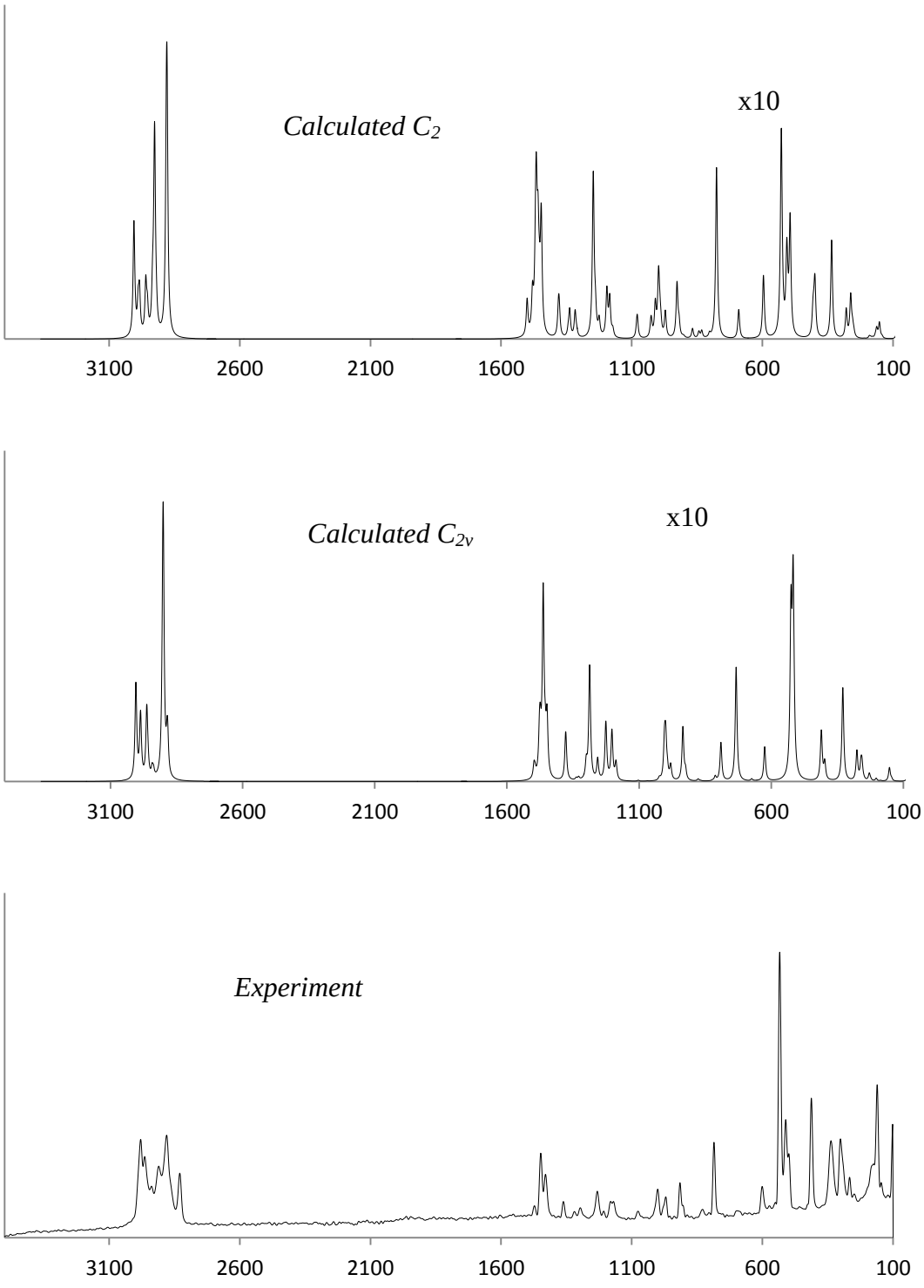

Figure 6a. Experiment and calculated (using the DFT-B3LYP-D3/6-311++G(d,p)/SDD level of theory) Raman of the $[Ir(\mu\text{-}Cl)(COD)]_2$ spectra

(b)

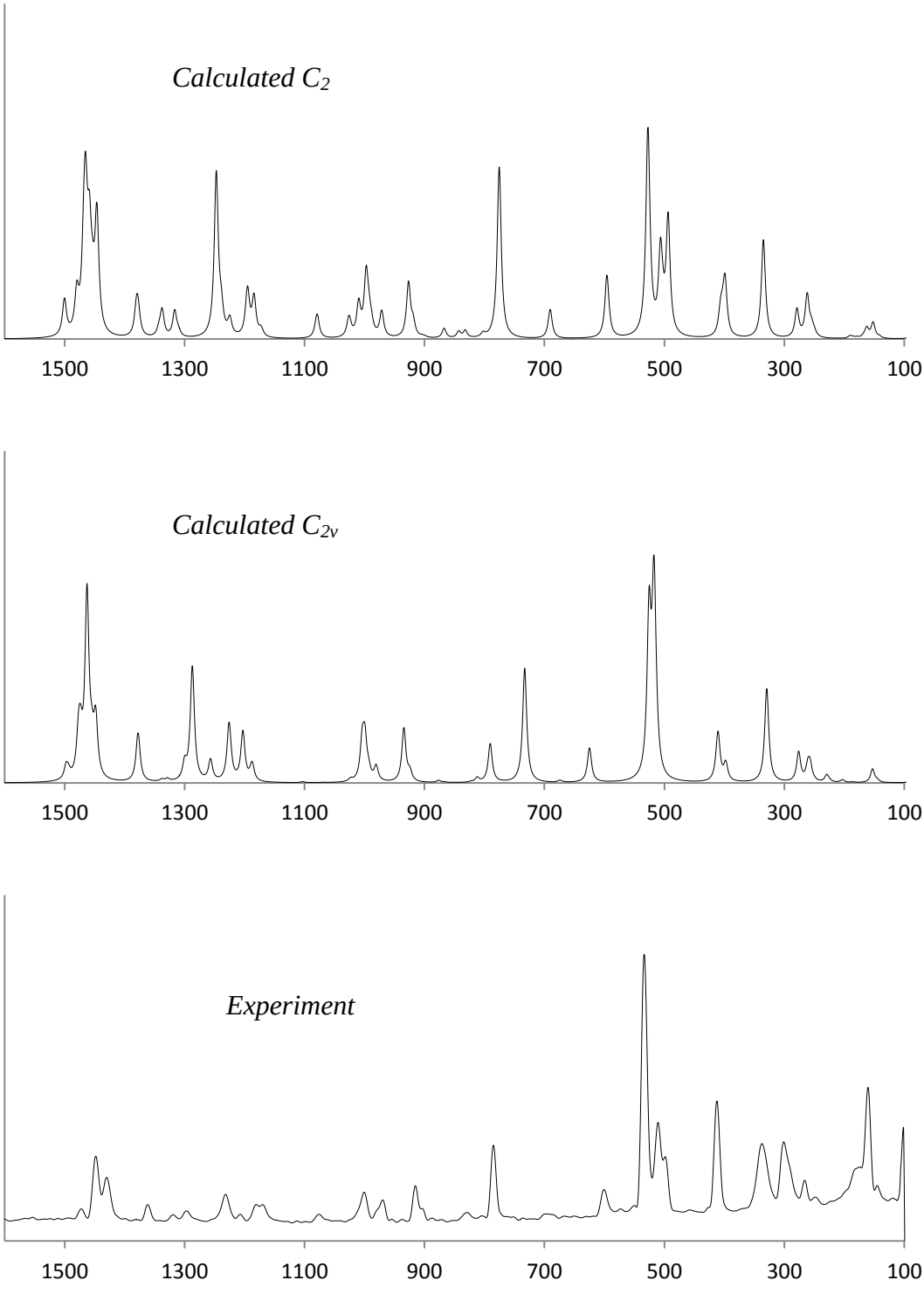

Figure 6b. Expanded Raman spectra for $[Ir(\mu\text{-}Cl)(COD)]_2$

Table 9. Percent shift in band I and II of the two complexes

		$[Rh(\mu\text{-}Cl)(COD)]_2$		COD	$[Ir(\mu\text{-}Cl)(COD)]_2$	
Band	Vibrational mode	Freq. (cm^{-1})	Percent shift (%)	Freq. (cm^{-1})	Freq. (cm^{-1})	Percent shift (%)
I	C=C stretching	1468	11.5	1659	1448	12.7
II	In-plane C-H wagging	1227	3.0	1265	1230	2.8

Table 10. Frequencies associated with metal-carbon bond in cm^{-1}

$[Rh(\mu\text{-}Cl)(COD)]_2$		$[Ir(\mu\text{-}Cl)(COD)]_2$	
IR	Raman	IR	Raman
376[b]	385[a]	413[a]	412[a]
340[b]	351[a]	326[b]	337[a]

[a] Experimental value [b] Theoretical value

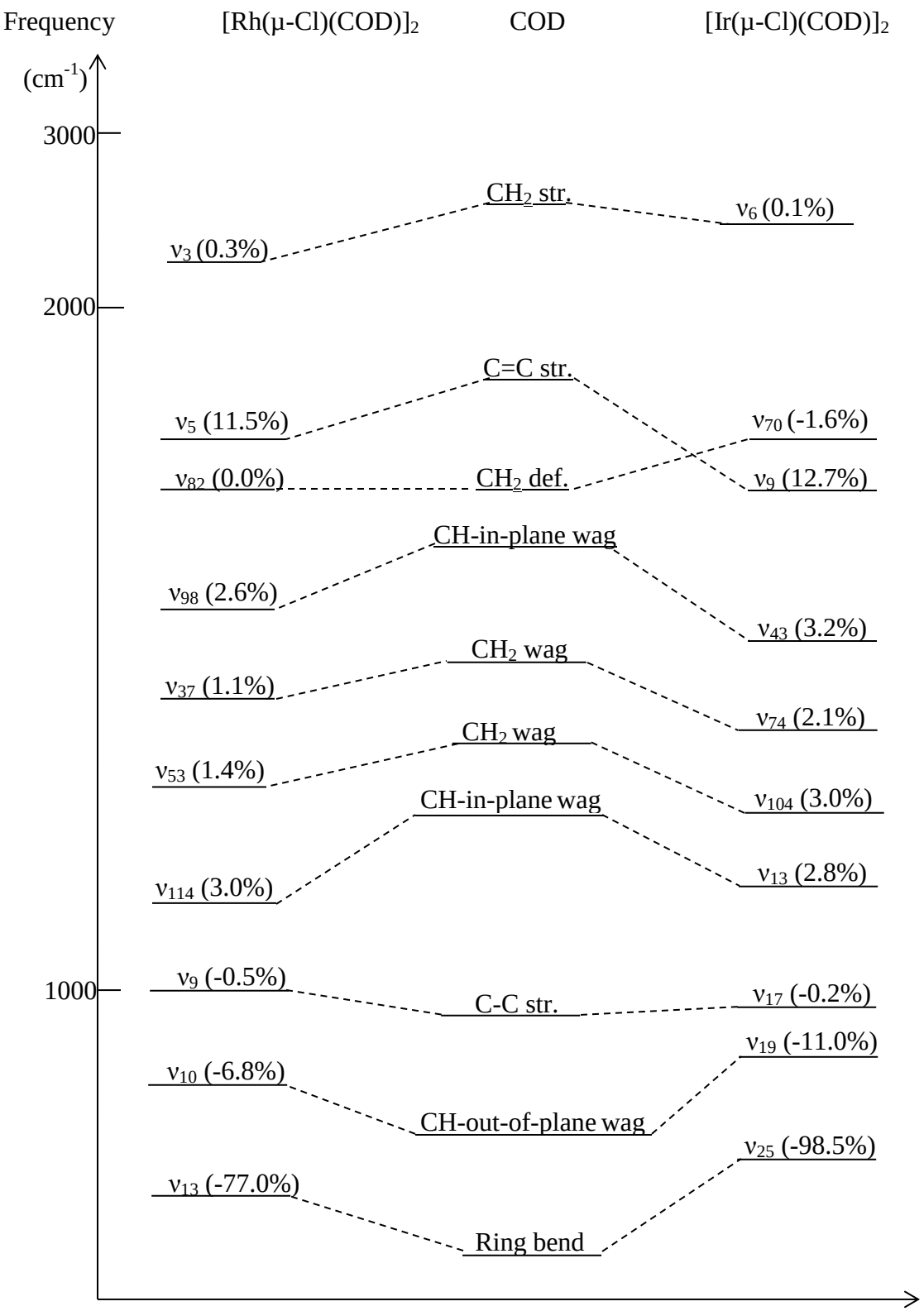

Figure 7. Correlation diagram for shift in frequencies for both complexes

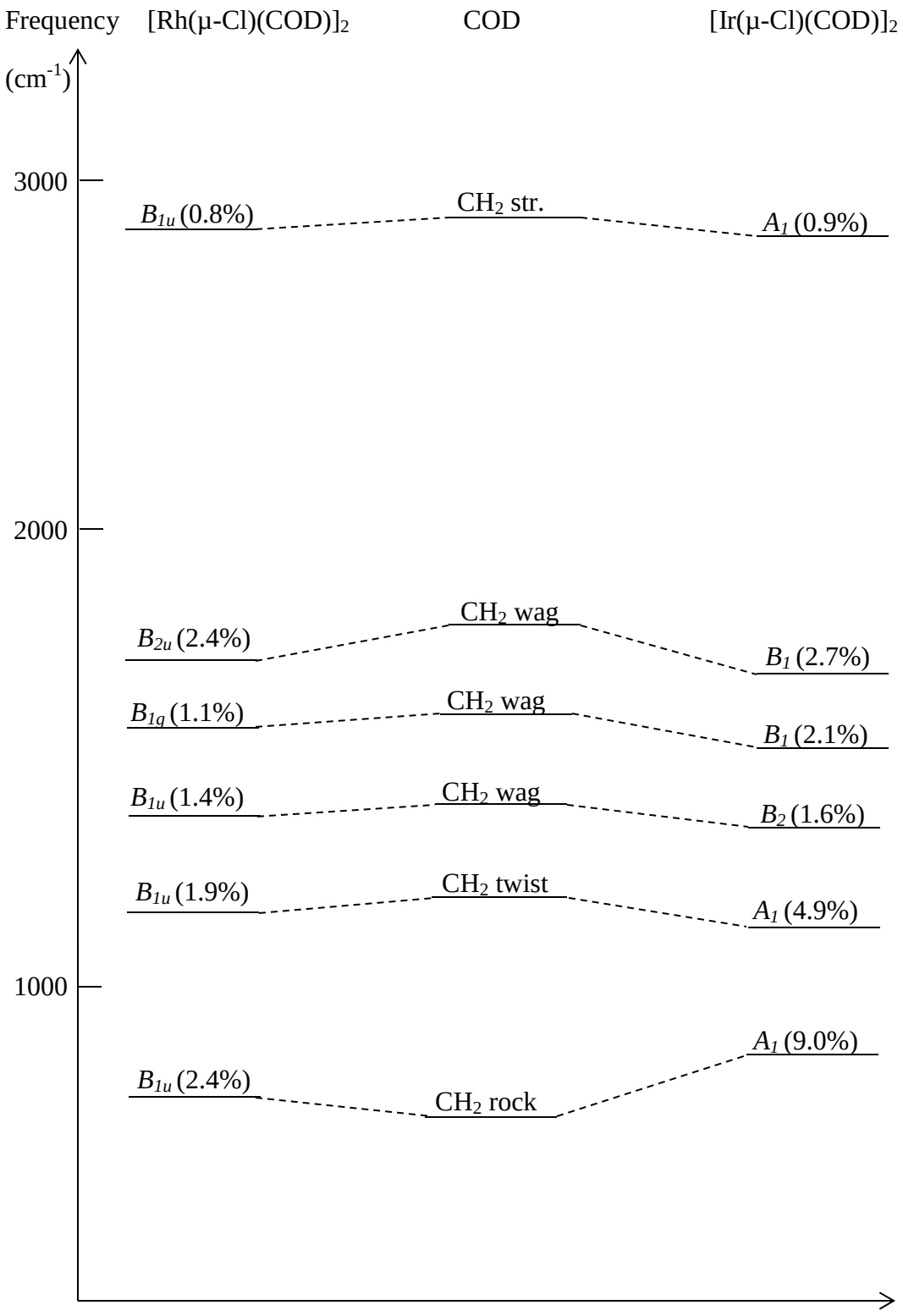

Figure 8. Correlation diagram showing the frequency shift of CH_2 vibrational modes due to coordination in both complexes

3.3. Conclusion

Lower symmetry D_2 and C_2 have been theoretically found for $[Rh(\mu\text{-}Cl)(COD)]_2$ and $[Ir(\mu\text{-}Cl)(COD)]_2$ in addition to their experimentally reported configurations. The single-molecule vapor-phase density functional theory (DFT) calculation shows that the respective lower symmetry of both complexes are more stable than their corresponding higher symmetry. In the same sense, spectroscopic analysis study reveals the presence of the trace of lower symmetry along with the dominant higher symmetry in the solid phase of the two complexes. Investigation into the complex reactivity with respect to electronic properties via NBO analysis affirms iridium complex to be more reactive. In the case of vibrational study, extent of destruction of olefinic character of 1,5-cyclooctadiene upon coordination was found to accounts for the total ($\pi+\sigma$) metal-olefin interaction as well as π components of the interaction with overall frequencies shifts showing greater interaction for iridium complex.

CHAPTER 4

VIBRATIONAL AND THEORETICAL ASSESSMENT OF SOME BRIDGING LIGAND ON THE STRUCTURE-REACTIVITY PROPERTIES $[IR(\mu\text{-}L)(COD)]_2$ AND $[RH(\mu\text{-}L)(COD)]_2$ COMPLEXES

4.1. Introduction

The outcome of the work presented in the previous Chapter shows that computational and vibrational techniques can be very useful tools to evaluate the metal-olefin interaction in $[Ir(\mu\text{-}L)(COD)]_2$ and $[Rh(\mu\text{-}L)(COD)]_2$ complexes. This has motivated us to explore other bridging ligands (namely $–NH_2$ and $–OCH_3$) to better understand the structure-reactivity relationship and compare predictively using DFT calculations the effect of these ligands.

The vital role played by metal-olefin complexes in organometallic chemistry cannot be underestimated. Olefin is a model of an organic unsaturated ligand [59], and metal-olefin complexes have been shown to be useful precursors for a number of chemical transformations in research and industry such as hydrogenation, hydroformylation, hydrocarbonlyation, isomerization as well as metathesis [1, 60, 61]. Moreover, the ability to tune the catalytic properties of a metal complex toward a desired reaction is based on some thermodynamic factors that govern metal-olefin interaction [60, 61]. The strength of the interactions in several complexes has been assessed through Dewar-Chatt-Duncanson (DCD) model of metal-olefin bonding [59, 61–63] as well as vibrational infrared and Raman spectroscopies [13, 55, 64]. In DCD model, the metal-olefin bond interaction is treated as a two-ways exchange of electrons between the metal and the

olefin unit. The sigma (σ) interaction involves electron donation from highest the occupied molecular orbital (HOMO) of the olefin to the lowest unoccupied molecular orbital (LUMO) of the metal. However, the π back-bonding interaction results from the electron donation from an occupied metal d_π orbital to a vacant antibonding (π^*) olefin orbital [1, 60]. As a result, the interaction devastates the olefinic character of the ligand as it reduces the C=C bond order and the hybridization tends towards sp^3 [59, 60, 64]. Furthermore, the change in vibrational energies associated with the C=C stretching mode of olefinic ligand upon coordination could be explored to understand the nature of metal-olefin interaction (via vibrational spectroscopy). The magnitude of the vibrational shift is related to the extent of metal-olefin interaction. Such a shift was found to be associated with the coupling of C=C stretching mode with in-plane olefinic C-H wagging mode, while the extent of their joint frequency shifts reveal the total (σ+π) metal-olefin interaction [13, 65]. When considering the vibrational modes associated with the magnitude of the electron density region the π component of the total interaction could be in particular explored. For example the metal-olefin tilting mode associated with movement of the olefinic carbon atoms into and out of the electron density region may be used to evaluate the π constituent of the metal-olefin bond [13]. Another important mode is the out-of-plane olefinic C-H waging mode, in which the olefinic hydrogen moves into and out of the electron density region. Its energy is directly related to the magnitude of the electron density in the π constituent and as such, the change in energy reflects the strength of the π component [13]. Additionally, we have shown in the previous Chapter that the CH_2 bending modes (namely wagging, twisting and rocking) could be means to assess the total metal-1,5-cyclooctadiene interaction. Upon complexation, frequency

associated with C=C stretching is expected to shift to lower value while those of olefinic C-H wagging and ring-bending modes shift otherwise and thus signifying the extent of π bonding [13]. For CH_2 bending modes in COD rings waging and twisting frequencies are red-shifted while that of rocking are blue-shifted. DFT calculations could be used to provide reliable and conclusive assignments of these modes and help to overcome the extensive challenge of mixing of the bending modes in the area below 1000 cm^{-1}.

The nature of bridging atoms in dinuclear complexes influence their electronic properties and metal-metal interactions [66]. Their size directly alters the metal centres closeness while their flexibility plays an important role in the extent of metal–metal interactions [67] which in turn has impact on the metal-olefin coordination. In addition, the electronegativity of the bridging atom controls the focus of the electron density on the metal center which consequently dictates the metal-ligand interaction. Cl, OR, SR and NH_2 are among the radicals that have been reported as efficient bridging ligands in dinuclear Rh and Ir complexes [4, 35, 37, 68]. The parent-amido ($-NH_2$) as a bridging ligand has been found to firmly bridge metals together in different dinuclear assemblies [4, 67]. Furthermore, NH_2 in the [Ir–NH_2–Ir] linkage was established to play significant part in the concerted mechanism adopted by amido complexes in a catalytic hydrogen transfer reaction [4, 69]. In the same sense, chloro- and mexo-bridged complexes have served as precursor catalysts in transfer hydrogenation and other catalytic reactions [3, 70–73]. In the present work, Density functional Theory (DFT) calculations were employed to understand the symmetry and electronic structural reactivity relationship of some bridged dinuclear complexes of Ir and Rh (Scheme 9). Infrared and Raman

spectroscopies were used to understand the metal-olefin interaction and the effect of bridging atoms/group the interaction.

4.2. Results and Discussion

4.2.1. Structural Parameters and Molecular Symmetry

Molecular symmetry is an important property of any metal complex which dictates its electronic properties, an essential parameter sought for in the design of catalytic system. The symmetry of binuclear complex largely depends on metal centre-bridging ligand arrangement as well as the structure of diolefin ligand component of the complex. A planar centre which is one of characteristics of D_{2h} and C_{2h} configurations demands 180^o dihedral angle between the coordination planes defined by L-M_1-L and L-M_2-L (see Scheme 10). However, for C_{2v} an angle, lower than 180^o is needed. The structures of different dinuclear rhodium and iridium complexes are presented in Figure 9. Both amido-bridged dinuclear complexes of the two metals are of C_{2v} symmetry while their methoxo-bridged have C_{2h} symmetry. For the chloro-bridged dinuclear complexes, their structures have been extensively discussed in previous Chapter. The methoxo-bridged dinuclear complexes of both metals with C_{2h} symmetry have dihedral angle to be 180^o (see Table 11). However, $[Ir(\mu\text{-}NH_2)(COD)]_2$ and $[Ir(\mu\text{-}Cl)(COD)]_2$ which are of C_{2v} symmetry have their dihedral angle folded at 118.1^o and is 108.8^o respectively as shown in Table 11. The lower value recorded for the chloro-bridged complex is an indication of greater interaction resulting from its high electronegative nature. On the other hand, the symmetry has influence on the distance between the two metals at the centre. The folded configurations are of shorter distance than the planar ones (Table 11).

The extent of the back-bonding can be inferred by examining the variation in the M-C and C=C bond lengths as well as analyzing the natural bond orbital (NBO) values using the Dewar-Chatt-Duncanson (DCD) model [59]. For this study, bond lengths of C=C and

M-C were calculated from the fully optimized metal complex structures and the results are presented in Table 11. Upon coordination, the π-character of the olefinic C=C bond becomes less significant in the iridium complexes compared to the corresponding rhodium ones. Furthermore, π-character of the C=C bonds are slightly more influenced by the chloro- and methoxo- bridge than by the amido-bridge. The greater change noticed in C=C bond length in iridium complexes could be attributed to the more electropositive nature of Ir metal over Rh which gives it ability to back-donate electrons to olefinic carbons more efficiently. In the case of bridging ligands however, inductive effect plays a significant role in availing metal electrons towards the COD olefin units. This inductive effect is electronegativity and distance dependent. Although the Cl atom is more electronegative than OCH_3 and NH_2, its bigger size than either O or N atom results in a longer M-$L_{bridging}$ distance compared to either OCH_3 or NH_2 (Table 11). Moreover, the calculated bond order of the C=C with respect to bridging ligands was predicted in the order of $NH_2 > Cl \approx OCH_3$ (Table 12). Recalling that the C=C bond length is inversely related to bond order, the calculated trend is consistent with the C=C bond length variation and provides insight on the extent of metal-olefin interaction. For instance, the longer olefin C=C bond length observed for iridium complexes is an indication of greater the metal-olefin interaction. It is worthy of mentioning that both metal-olefin (M-C) and C=C bond distances maintain the similar trend. Hence, the shorter M-C bond length in iridium complexes signals stronger π back-bonding phenomenon that results in stronger binding of diolefin ligands towards the iridium metal. For the bridging ligands, the π back-bonding effect is noticed to be in the order of $NH_2 < Cl < OCH_3$. Generally, bridging ligands are believed to have a significant effect on the metal-olefin interaction in

the order of interaction being NH_2 < Cl < OCH_3 for such dinuclear complexes. On the other hand, the greater interaction predicted for the three iridium complexes over the rhodium counterparts could be attributed to the more electropositive nature of the Ir metal.

Table 12 shows that upon coordination, *p*-orbital of olefinic carbons are being populated by electrons from the metal which makes them move more towards sp^3. The greater *p*-character recorded for olefinic carbons in iridium complexes is due to lower electronegative nature of iridium metal than rhodium [1]. It is worthy of noting that electronegative nature of the bridging ligands plays significant role in making metal electrons available to the olefinic carbon. The more electronegative the bridging ligand is, the more it draws electrons from metal towards itself and the less it makes metal electrons available for the C=C carbon. Using Sanderson's formulation [74, 75], group electronegativity (χ_G) in Pauling unit could be obtained as 2.42, 2.44 and 3.16 for NH_2, OCH_3 and Cl, respectively. The χ_G values are found consistent with predicted hybridization for olefinic carbons in the iridium complexes. However, in the case of rhodium, the trend is interrupted by inductive effect exercised by the bridging ligands, and as such, the amido-bridged dinuclear complex exhibits the least *p*-character while the chloro had the highest.

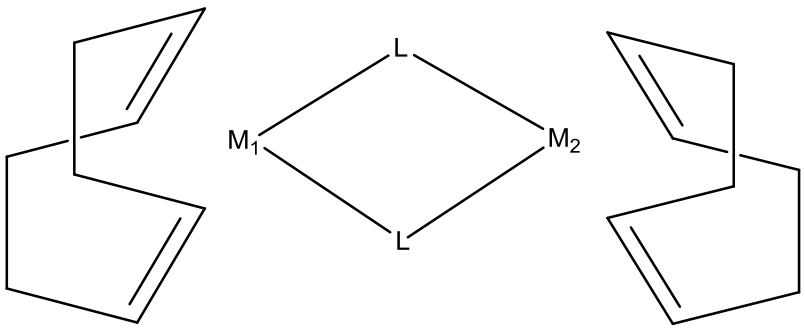

M = Ir or Rh, L= NH_2, OCH_3 or Cl

Scheme 10. Molecular structure template for $[M(\mu\text{-}Cl)(COD)]_2$ complexes.

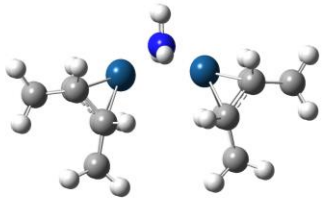	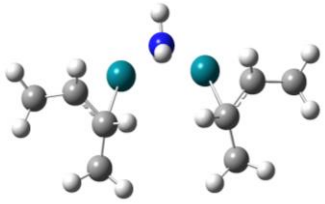
$[Ir(\mu\text{-}NH_2)(COD)]_2$ (C_{2v})	$[Rh(\mu\text{-}NH_2)(COD)]_2$ (C_{2v})
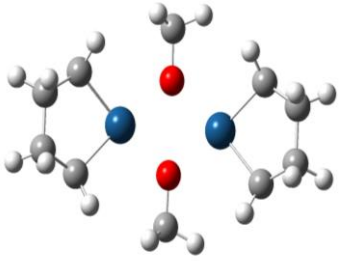	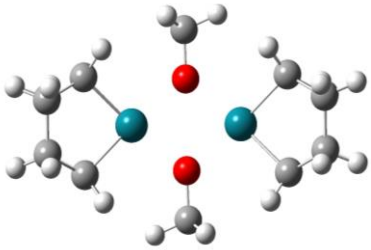
$[Ir(\mu\text{-}OMe)(COD)]_2$ (C_{2h})	$[Rh(\mu\text{-}OMe)(COD)]_2$ (C_{2h})

Figure 9. Structures of amido- and methoxo-bridged dinuclear complexes of iridium and rhodium

Table 11. Selected geometrical parameters in the complexes

Complex	Symmetry	Bond Length (Å)				Folding Angle (°)[f]
		C=C	M-C	M-$L_{Bridging}$	M-M	
Cyclooctadiene		1.335				
[Ir(μ-NH_2)(COD)]$_2$	C_{2v}	1.420 (1.406)[a]	2.127 (2.118)[a]	2.131 (2.081)[a]	2.870 (2.815)[a]	118.1 (119.2)[a]
[Rh(NH_2)(COD)]$_2$	C_{2v}	1.404 (1.397)[b]	2.132 (2.126)[b]	2.114 (2.099)[b]	2.815 (2.863)[b]	116.7 (126.8)[b]
[Ir(μ-OMe)(COD)]$_2$	C_{2h}	1.425	2.113	2.114	3.355	180
[Rh(μ-OMe)(COD)]$_2$	C_{2h}	1.411 (1.406)[c]	2.115 (2.097)[c]	2.101 (2.063)[c]	3.296 (3.231)[c]	180 (180)[c]
[Ir(μ-Cl)(COD)]$_2$	C_{2v}	1.425 (1.400)[d]	2.117 (2.110)[d]	2.485 (2.399)[d]	2.990 (2.910)[d]	108.8 (109.5)[d]
[Rh(μ-Cl)(COD)]$_2$	D_{2h}	1.408 (1.388)[e]	2.122 (2.108)[e]	2.465 (2.400)[e]	3.601 (3.498)[e]	180 (169.8)[e]

[a] [4]

[b] [76]

[c] [77]

[d] [47]

[e] [44]

[f] Dihedral angle between the coordination planes defined by L-M_1-L and L-M_2-L (Scheme 10)

Table 12. Hybridization of olefinic carbons of free and coordinated cyclooctadine

Complex	Average Hybridization		Bond order
	C_5	C_6	
Cyclooctadiene	$sp^{2.06}$	$sp^{2.06}$	1.926
$[Ir(\mu\text{-}NH_2)(COD)]_2$	$sp^{2.43}$	$sp^{2.42}$	1.316
$[Rh(NH_2)(COD)]_2$	$sp^{2.27}$	$sp^{2.26}$	1.402
$[Ir(\mu\text{-}OMe)(COD)]_2$	$sp^{2.42}$	$sp^{2.42}$	1.278
$[Rh(\mu\text{-}OMe)(COD)]_2$	$sp^{2.27}$	$sp^{2.27}$	1.362
$[Ir(\mu\text{-}Cl)(COD)]_2$	$sp^{2.40}$	$sp^{2.40}$	1.282
$[Rh(\mu\text{-}Cl)(COD)]_2$	$sp^{2.32}$	$sp^{2.32}$	1.370

4.2.2. Stability

The stability of a complex can theoretically be inferred from coordination energies as well as binding energies and Frontier molecular orbital. The former parameters reflect the forces holding the atoms together. Practically, binuclear complexes with the same diolefinic ligands but different bridging atoms / groups exhibit different stability towards air and moisture which shows that bridging atoms / groups play an important role in complex stability. To examine the effect of different bridging ligands on the stability of the Rh and Ir complexes, the binding energies and coordination energies were calculated using equations 1 and 2 respectively and the results are presented in Table 13.

$$E_{Binding} = E_{Tot} - (2E_{BL} + E_{COD+Metal}) \quad \text{..... (1)}$$

$$E_{Coordination} = E_{Tot} - 2(E_{Metal} + E_{BL} + E_{COD}) \quad \text{.....(2)}$$

Where $E_{Binding}$ is binding energy, $E_{Coordination}$ is coordination energy, E_{Tot} is electronic energy for the complex, E_{BL} is the electronic energy for the bridging atoms / groups, $E_{COD+Metal}$ is the electronic energy for the metal-COD dimer, E_{Metal} is the electronic energy for the metal and E_{COD} is the electronic energy for the COD.

The values are generally higher for iridium complexes compared to the corresponding rhodium counterparts, except for the chloro-bridged complexes which are of different molecular symmetry. Binding energy is supposed to be planar phenomenon however the folding of Ir_2Cl_2 out of the plane could be responsible for the lower binding energy recorded for $[Ir(\mu\text{-}Cl)COD]_2$ with respect to Rh complex. The order of binding energies with respect to the bridging ligand was predicted to be $NH_2 < OCH_3 < Cl$. In contrary, the order for coordination energies was calculated as $OCH_3 < NH_2 < Cl$. Similar to the

results found for binding energies, iridium complexes were predicted to maintain greater coordination energies than their analogous rhodium complexes, that further affirms their higher stability compared to the corresponding Rh complexes. The further stability noticed in the chloro-bridged complexes compared to amido or methoxo bridged complexes could be due to higher electronegativity value of the Cl. As a result, Cl withdraws electrons from the metal more effectively and hence causes a more significant interaction. In the case of Ir, more electrons are even available for Cl to withdraw and hence higher binding and coordination energies were predicted.

The relative reactivity of substances can be correlated to the HOMO-LUMO energy gap. The closer an energy gap, the more reactive a substance is expected to be. In the development of new catalytic systems, HOMO-LUMO energy levels are useful and given a special attention since the complex HOMO is responsible for the π back-bonding where electrons are donated from the d-orbital of the metal to the vacant orbital of the ligand. The results listed in Table 14 shows a clear trend in the effect of the type of bridging ligands. The Cl bridged which is the most electronegative brings the HOMO in each of the metal complexes to the low energy side, while amido pushes it towards the high side. In terms of reactivity parameters, ionization potential (IP) and absolute electronegativity (χ) of the complexes as well as absolute hardness (η) of rhodium complexes presented in Table 15 are consistent with the order of the group electronegativities of the bridging ligands (i.e, $NH_2 < OCH_3 < Cl$), while the electron affinity (EA) does not follow a definite order. Reactivity parameters IP and EA are associated with electron donating and acceptance ability of a complex, respectively and they are useful factors to assess the polarity of a metal-ligand bond [52]. The amido bridged complexes with small η value

(Table 15) are relatively soft and are more polarizable. Their predicted small HOMO-LUMO energy gaps (Table 14) give further affirmation to their softness as suggested by Pearson [51]. It is worthy of noting that the order HOMO energies ($Cl < OCH_3 < NH_2$) of complexes understudy is in opposite trend compared to IP and χ, which further asserts that ionization potential is related to HOMO and is associated with electron donation capability [54, 79]. On the other hand the small HOMO-LUMO energy gap noticed for the amido-bridged complexes indicates their higher reactivity as well as explaining the extra air sensitivity of the rhodium and iridium amido-bridged dinuclear complexes [4].

Table 13. Binding and coordination energies for the complexes in kcal/mol

Complex	Binding Energy	Coordination Energy
$[Ir(\mu\text{-}NH_2)(COD)]_2$	215	401
$[Rh(NH_2)(COD)]_2$	193	340
$[Ir(\mu\text{-}OMe)(COD)]_2$	220	388
$[Rh(\mu\text{-}OMe)(COD)]_2$	198	332
$[Ir(\mu\text{-}Cl)(COD)]_2$	227	412
$[Rh(\mu\text{-}Cl)(COD)]_2$	229	363

Table 14. HOMO-LUMO energy levels for the complexes in ev

Complex	HOMO	LUMO	ΔE
$[Ir(\mu\text{-}NH_2)(COD)]_2$	-4.69	-1.15	3.54
$[Rh(NH_2)(COD)]_2$	-4.68	-0.96	3.72
$[Ir(\mu\text{-}OMe)(COD)]_2$	-5.24	-0.58	4.65
$[Rh(\mu\text{-}OMe)(COD)]_2$	-5.25	-0.98	4.28
$[Ir(\mu\text{-}Cl)(COD)]_2$	-5.48	-1.64	3.84
$[Rh(\mu\text{-}Cl)(COD)]_2$	-5.72	-1.41	4.31

Table 15. B3LYP/6-311++G(d,p) calculated ionization potential (IP), electron affinity (EA), absolute hardness (η) and electronegativity (χ) in ev

Complex	IP	EA	η	χ
$[Ir(\mu\text{-}NH_2)(COD)]_2$	5.85	0.04	2.90	2.94
$[Rh(NH_2)(COD)]_2$	5.78	-0.11	2.94	2.84
$[Ir(\mu\text{-}OMe)(COD)]_2$	6.48	-0.34	3.41	3.07
$[Rh(\mu\text{-}OMe)(COD)]_2$	6.40	0.03	3.18	3.21
$[Ir(\mu\text{-}Cl)(COD)]_2$	6.64	0.54	3.05	3.59
$[Rh(\mu\text{-}Cl)(COD)]_2$	6.89	0.44	3.22	3.67

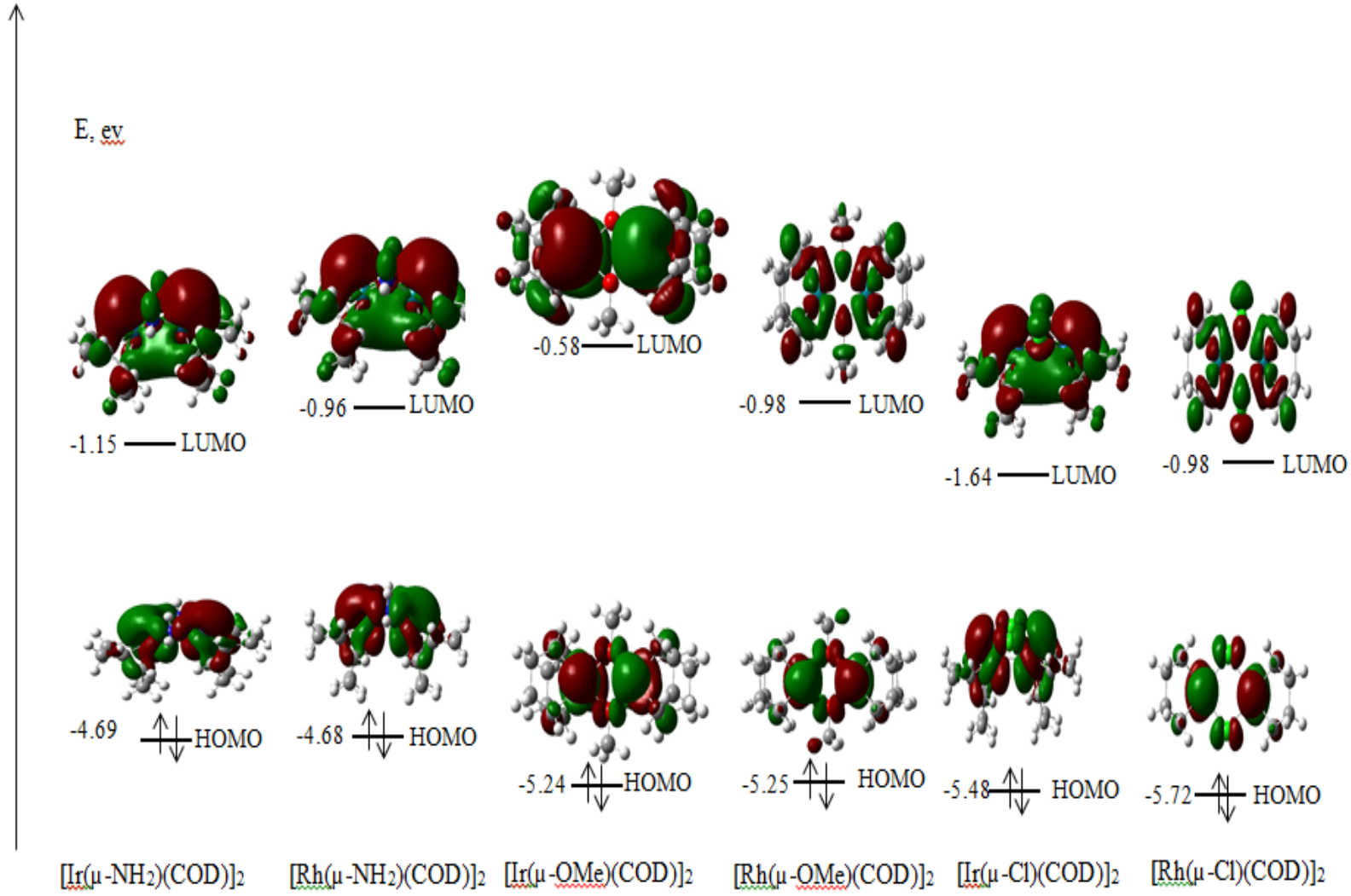

Figure 10. Frontier orbitals for the complexes

4.2.3. Vibrational Spectra

Vibrational spectroscopy is an important tool to investigate metal-olefin interaction. With detailed vibrational assignment, shifts in frequencies associated with certain vibrational modes in 1,5-cyclooctadiene (COD) before and after coordination can easily be identified and used for prediction of the metal-olefin interactions. Vibrational mode associated with C=C stretching and C-H in-plane wagging which have been denoted as band I and band II are being used as a measure for total ($\pi+\sigma$) metal-olefin interaction in complexes [13, 49, 55]. Upon coordination, C=C frequency is expected to shift to lower value as the olefinic carbon hybridization moves toward sp3. The same thing is applicable to C-H in-plane waging mode. As presented in Figure 11 and Figure 13, the total percent change in frequencies associated with these modes are 15.6%, 15.9%,18%, 13.7%, 14.1% and 14.1% for $[Ir(\mu\text{-}NH_2)(COD)]_2$, $[Ir(\mu\text{-}Cl)(COD)]_2$, $[Ir(\mu\text{-}OMe)(COD)]_2$, $[Rh(\mu\text{-}NH_2)(COD)]_2$, $[Rh(\mu\text{-}Cl)(COD)]_2$ and $[Rh(\mu\text{-}OMe)(COD)]_2$ respectively. These results show that the total ($\pi+\sigma$) metal-olefin interaction for iridium complexes with respect to bridging ligands is in the order of $NH_2 < Cl < OCH_3$ while that of rhodium is $NH_2 < Cl = OCH_3$. Although, frequency shifts were recorded for the vibrational modes associated with CH_2 as presented in Figures 12 and Figure 14, but a definite pattern with respect to the bridging ligands could not be rationalized. This could be due to the non-direct link between bridging ligands, metal centre and the CH_2. However, higher percent shift were recorded for iridium complexes than their corresponding rhodium counterparts. The results showed that CH_2 vibrational modes can be used to evaluate extent of interaction of olefin with different metals but it is less significant for examining the effect of bridging ligands on the interaction. On the other hand, to evaluate the π contribution to total metal-

olefin interaction, out-of-plane C-H wagging and ring bending modes are essential. Frequencies associated with these modes shift to greater values upon coordination. The out-of-plane C-H wagging moves the hydrogen into and out of π electron density section while the metal constrains the COD ring bending mode [13, 49]. For these modes, a total of -73.6%, -109.5%, -83.9%, -61.8%, -83.8% and -69.7% was obtained for $[Ir(\mu\text{-}NH_2)(COD)]_2$, $[Ir(\mu\text{-}Cl)(COD)]_2$, $[Ir(\mu\text{-}OMe)(COD)]_2$, $[Rh(\mu\text{-}NH_2)(COD)]_2$, $[Rh(\mu\text{-}Cl)(COD)]_2$ and $[Rh(\mu\text{-}OMe)(COD)]_2$ respectively. Unlike the total (π+σ) metal-olefin interaction, the order of π component of interaction for both metal complexes is NH_2 < OCH_3 < Cl. Furthermore, π component in the total interaction is also evaluated by examining metal-carbon stretching mode which moves olefinic carbon atom into and out of π-electron density section. As shown in Table 16, it can be seen that higher frequency values are being recorded for this mode in Ir complexes. In addition, the order of NH_2 < OCH_3 < Cl is still being maintained for bridging ligands of the dinuclear complexes. This further indicates that the trend for π components in metal-olefinic interaction may not necessary be the same as that of total (π+σ) interaction. However, this trend is consistent with HOMO levels (Table 14) of the complexes as well as their ionization potential and absolute electronegativity (Table 15). Hence, HOMO level and some reactivity parameters (IP and χ) can be used as a measure for π component of the interaction.

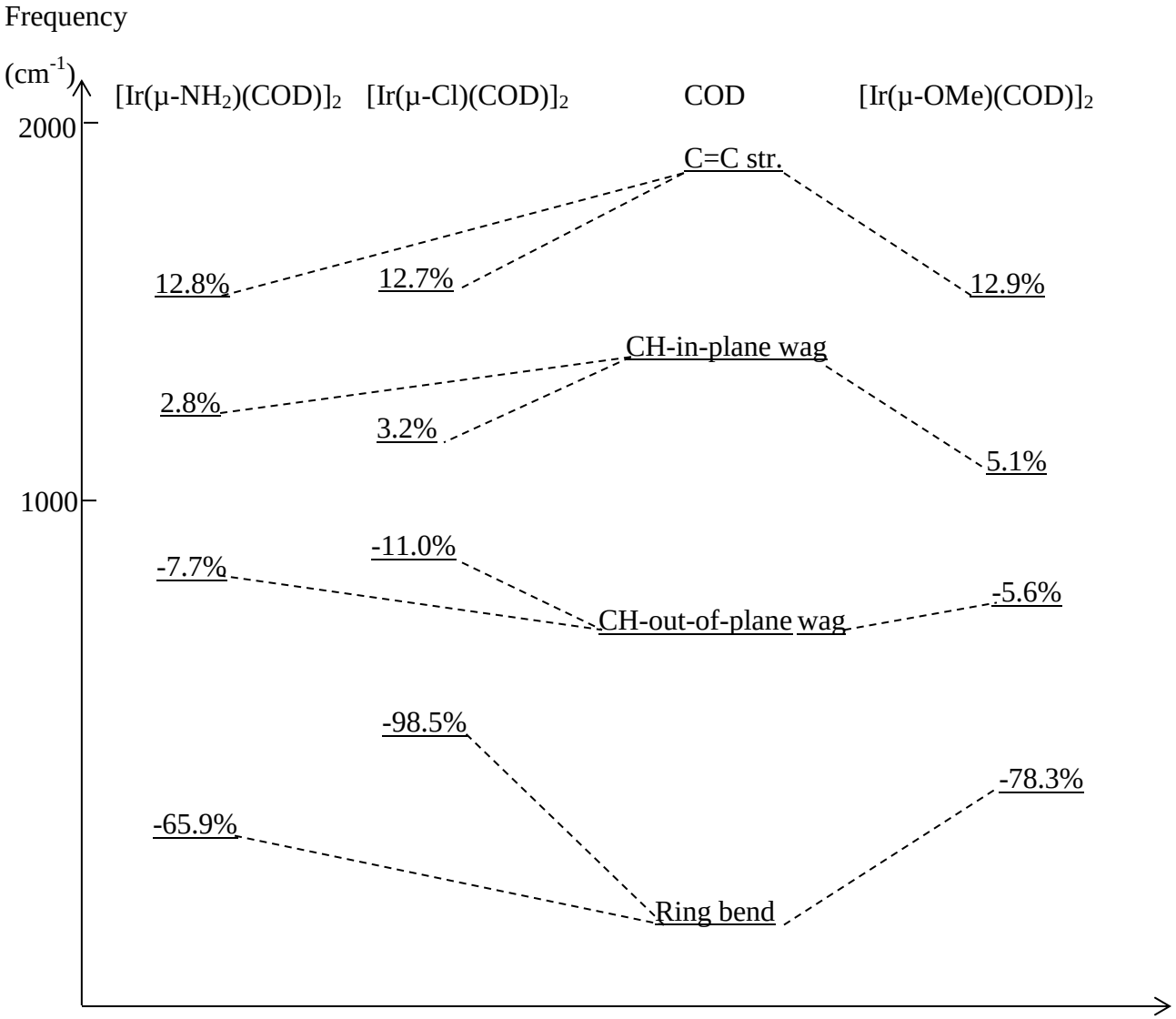

Figure 11. Correlation diagram for frequency shifts in Ir complex

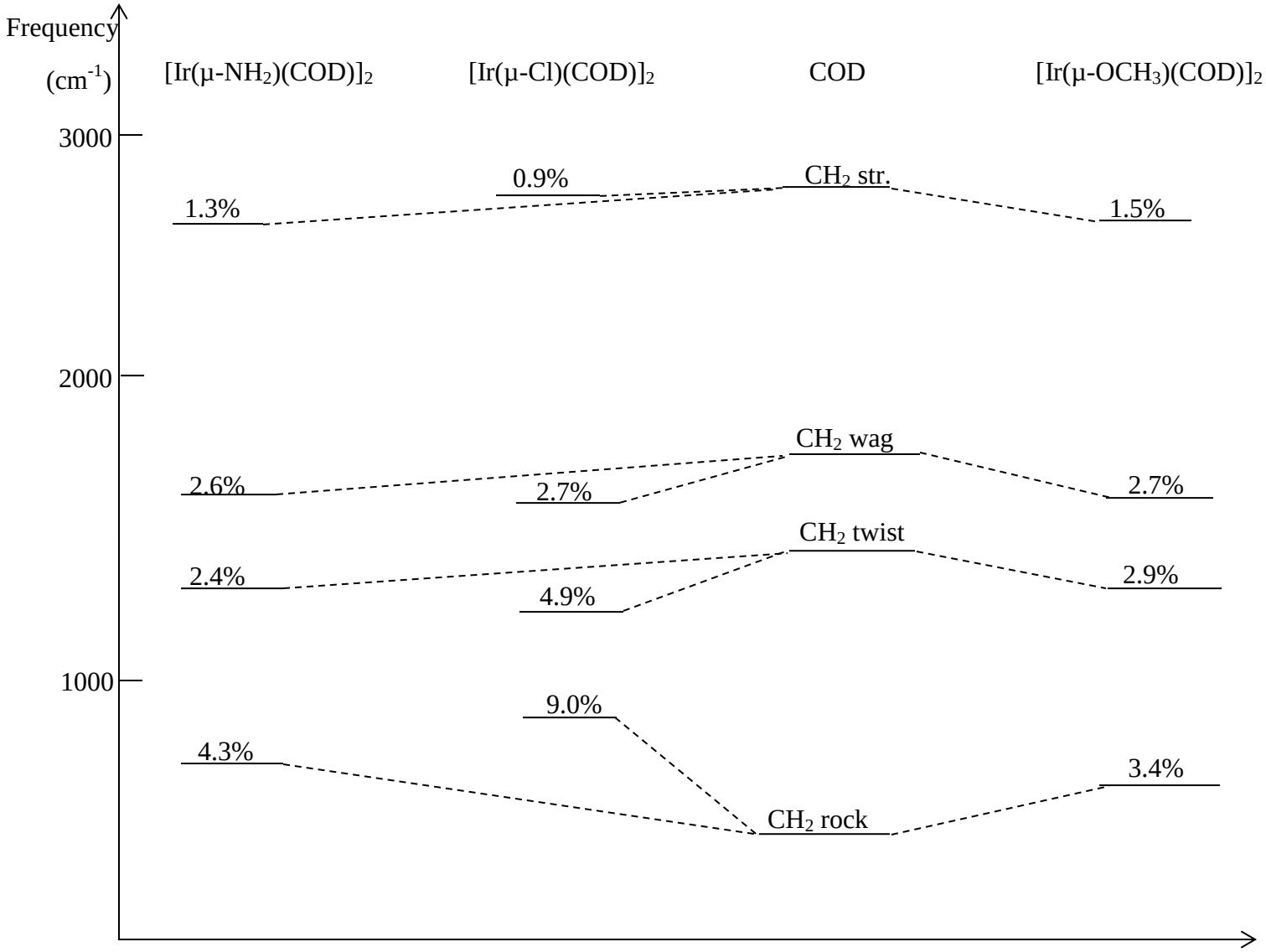

Figure 12. Correlation diagram for CH_2 frequency shifts in Ir complex

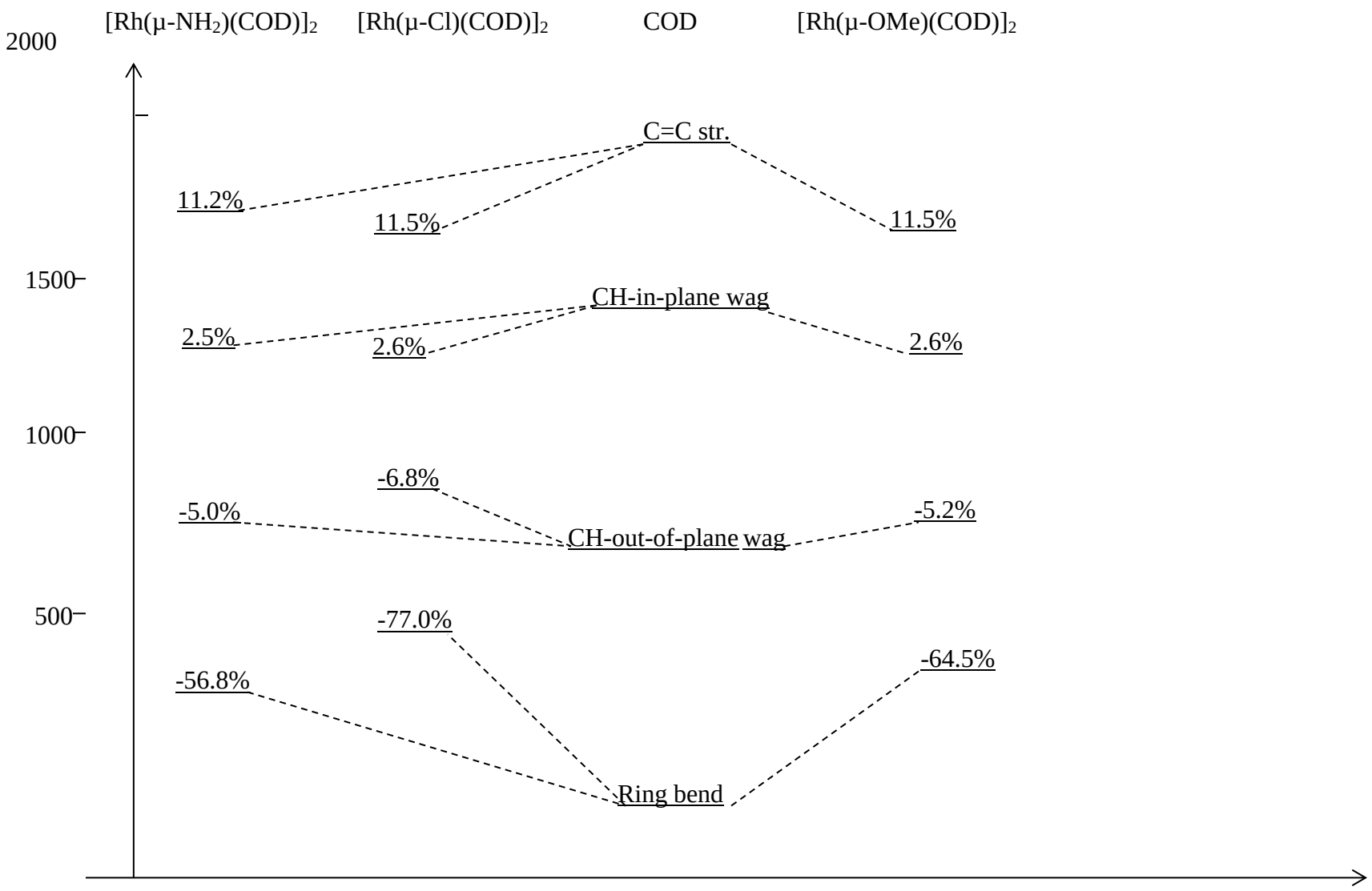

Figure 13. Correlation diagram for frequency shifts in Rh complex

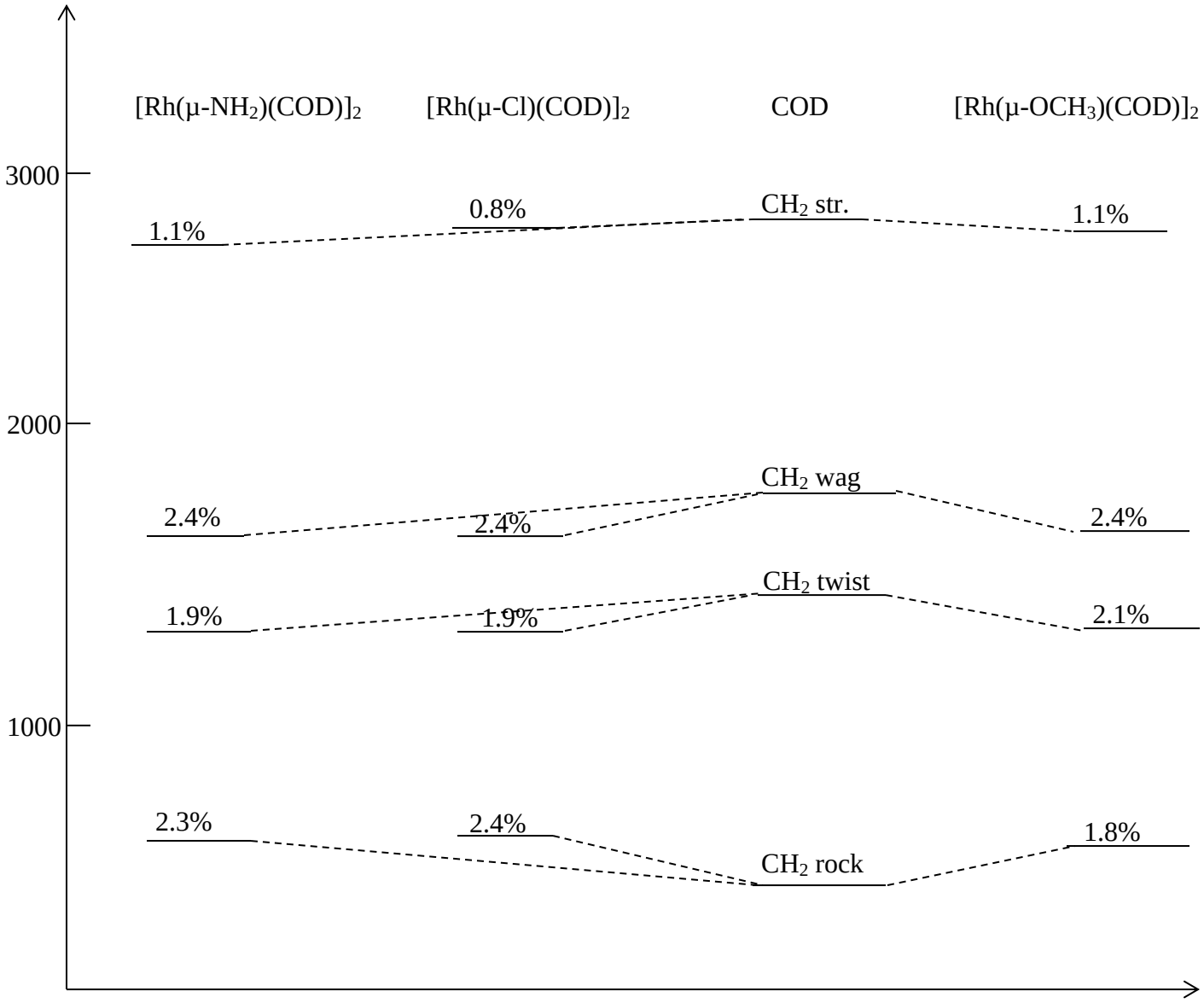

Figure 14. Correlation diagram for CH_2 frequency shifts in Rh complex

Table 16. Frequencies associated with metal-carbon bond in cm^{-1}

$[Ir(\mu\text{-}NH_2)(COD)]_2$		$[Rh(\mu\text{-}NH_2)(COD)]_2$		$[Ir(\mu\text{-}OMe)(COD)]_2$		$[Rh(\mu\text{-}OMe)(COD)]_2$		$[Ir(\mu\text{-}Cl)(COD)]_2$		$[Rh(\mu\text{-}Cl)(COD)]_2$	
IR	Raman	IR	Raman	IR	Raman	IR	Raman	IR	Raman	IR	Raman
407[a]	394[b]	365[b]	375[a]	410[a]	409[a]	410[a]	397[a]	413[a]	412[a]	376[b]	385[a]
314[b]	325[b]	311[b]	351[a]	324[b]	332[a]	322[b]	347[a]	326[b]	337[a]	340[b]	351[a]

[a] Experimental value

[b] Theoretical value

4.3. Conclusion

Evaluation of stability of iridium and rhodium complexes through the examination of calculated binding and coordination energies shows greater stability for iridium complexes over rhodium analogue. The magnitude of binding energy with respect to bridging ligands is in order of NH_2 < OCH_3 < Cl while that of coordination energy is OCH_3 < NH_2 < Cl. Application of Dewar-Chatt-Duncanson (DCD) model to examine the effect of bridging ligands on metal-olefin interaction showed that ligands' inductive effect influenced the interaction. Overall, the metal-olefin interaction was predicted to be in the order of NH_2 < Cl < OCH_3 for the dinuclear complexes. On the issue of hybridization, the *p*-character of olefinic carbons was found to increase upon coordination and the extent of increase depended on the electronegativity of bridging ligands. For the complex reactivity, amido bridged dinuclear complexes of both metals were found to more reactive than other while the complexes ionization potentials and absolute electronegativity were in the order of NH_2 < OCH_3 < Cl. The use of vibrational spectroscopy to evaluate the metal-olefin interaction showed that total ($\pi+\sigma$) metal-olefin interaction followed a trend of NH_2 < Cl < OCH_3 with respect to bridging ligands. However, the π components in the interaction was NH_2 < OCH_3 < Cl which surprisingly coincided with some reactivity parameters.

CHAPTER 5

HYDROGEN TRANSFER REACTION WITH MONODENTATE LIGANDS

5.1. Introduction

Hydrogen transfer reaction is known to be second to molecular hydrogenation in the catalytic reduction of multiple bonds. Quite a number of functional groups had been reduced via transition metal catalyzed transfer hydrogenation using different hydrogen donors [79]. Its wide acceptability as an alternative to the conventional molecular hydrogenation is predicated upon its atom efficiency, environmental friendliness [22, 81] as well as avoidance of risk associated with the use of pressure vessel [25].

It is established that the nature of ligands plays significant role in the catalytic reduction of aldehyde to alcohol via hydrogen transfer reactions. Monodentate phosphines are among ligands commonly used for this type of reaction. Triphenylphosphine and it substituted derivatives have been employed in different transfer hydrogenation catalytic systems [24, 82–84]. Phosphine ligands do influence the properties of the metal centre. Electron donating type like P(*p*-$OMeC_6H_4)_3$ makes the metal electron rich while electron withdrawing type makes it electron deficient. This act influences the activity of catalytic system as well as reaction mechanism. Furthermore, the electron donating ability of phosphines has been employed to promote catalytic activity of complex in hydrogen transfer [24] as well as carbonylation reaction [84]. Also, the ratio of ligands to catalyst complex has significant effect on the catalytic activities of the system. High ratio might involve discoordination step to create vacancy on the centre metal and this eventually results to the lowering of substrate conversion [24, 73].

The success of transfer hydrogenation reaction is predicated upon the right choice of organometallic complexes. Among the complexes, chloro, methoxo and amido bridged dinuclear complexes of iridium and rhodium metals have been reported to be used as precursor catalysts in the ligand based hydrogen transfer reaction [4, 86–89]. On the other hand, the chloro bridged type was used as catalyst in the ligand free transfer hydrogenation of ketones [23]. The property of complex metal centre is being modified by the diolefin coordinating with it. Electron donating type like 1,5-cyclooctadiene (COD) makes the centre electron rich while tetrafluorobenzoba- rrelene (TFBB), an electron withdrawing type makes it electron deficient.

In the field of transfer hydrogenation reaction, classical hydrido and concerted mechanisms are popular mechanisms. The classical hydrido involves metal hydride species formation as well as transfer of hydrogen to the substrate while the concerted mechanism proceeds without involvement of metal but with the formation of six membered transition state [4, 22]. In the hydrido type, the properties of metal centre are influenced by the electronic nature of diolefin and ligand as well as the type of the ligands coordinating with the metal centre [83, 90]. Electron withdrawing types make metal centre electron deficient and as such ease the formation of metal hydride. Likewise, basic ligand in a complex aids insertion reaction while the metal hydride stability plays a significant role in the release of hydrogen to the substrate.

Research works on the reduction of acetophenone to 1-phenylethanol using different catalytic systems with isopropanol as hydrogen donor have been reported [4, 23, 33, 88–91] but there is scarce comprehensive information on the effect of electronic nature of the ligands and diolefin on catalytic activities and mechanistic pathway for transfer

hydrogenation of acetophenone. In this work, the popular dinuclear iridium complexes [{Ir(μ-OMe)(diolef)}$_2$] (diolef=COD (1), TFBB (2)) were employed as catalyst precursors for the hydrogen transfer reduction of acetophenone using 2-propanol as hydrogen source. The study aims at assessing the influence of external *P* and *N*-donor ligands in the outcome of catalytic reaction.

5.2. Results and Discussion

We have studied the transfer hydrogenation of acetophenone using isopropanol as the hydrogen source (Scheme 11) catalyzed by binary systems that composed of iridium dinuclear complexes (Scheme 12) and additional ligands.

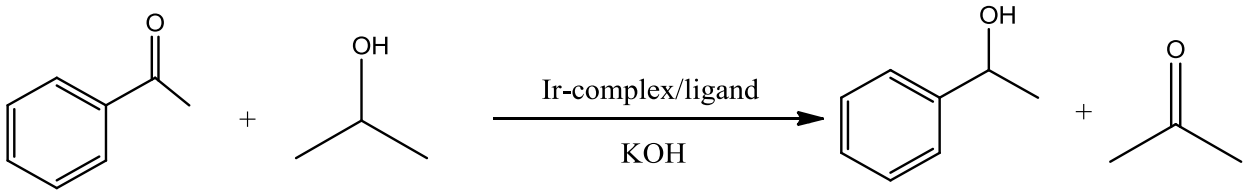

Scheme 11. Hydrogen transfer reaction

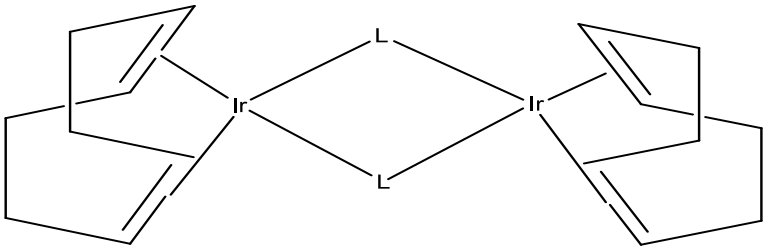

L= OMe- Catalyst 1

L= Cl- Catalyst 2

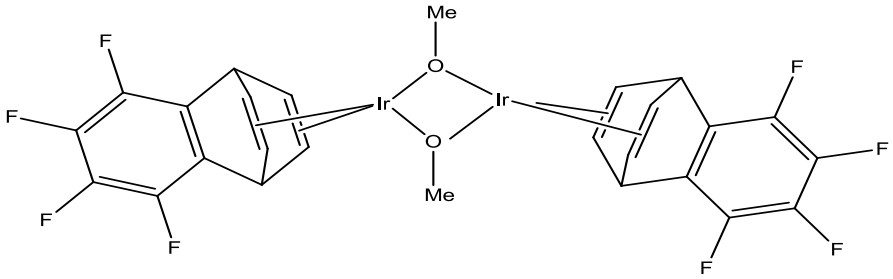

Catalyst 3

Scheme 12. Structure of the Catalysts

5.2.1. Study of the Effect of the Base

We started the study by screening bases since it is an important ingredient in the recipe for hydrogen transfer reaction. It influences the ease of formation of alkoxo $(CH_3)_2CHO^-$ from isopropanol in the course of transfer hydrogenation of acetophenone. The result shown in Table 17 indicates that a more basic base is more beneficial for the reaction. With the catalytic system that comprised $[Ir(\mu\text{-}OMe)(COD)]_2$/ 2 PPh_3, KOH the most basic gave highest conversions (39.8% and 87.6% at 4Hrs and 24Hrs respectively). This shows that with KOH, $(CH_3)_2CHO^-$ are more readily available for the continuity of reaction cycle. Having established KOH as the best base, different systems were set up with monodentate phosphines

Table 17. Screening of bases with $[Ir(\mu\text{-}OMe)(COD)]_2$

Entry	[Ir]/PPh_3	Base	Conversion (%)	
			4Hrs	24Hrs
1	1:2	KOH	39.8	87.6
2	1:2	K^tBuO	28.7	80.9
3	1:2	NaOH	13.4	54.4
4	1:2	Cs_2CO_3	29.7	58.8
5	1:4	KOH	29.1	61.5

.

5.2.2. Hydrogen Transfer Reactions with P-donor Ligands

5.2.2.1. [Ir(μ-OMe)(COD)]$_2$/ 2 PAr$_3$ Catalytic System

For this study, the catalytic activity of a system comprising [Ir(μ-OMe)(COD)]$_2$ (catalyst 1) and phosphine ligands in the ratio of 1 mmol to 2 mmol was tested. In this system, the dinuclear [Ir(μ-OMe)(COD)]$_2$ splits to give [Ir(O^iPr)(COD)PAr$_3$] (16-electron system) as the active catalyst (Scheme 13). Going by the results presented in Figure 15, it could be seen that phosphines with electron releasing group substituents are more beneficial for the acetophenone reduction. In addition, the order of catalytic activity with respect to the ligands is P(*p*-OMeC$_6$H$_4$)$_3$ > P(*p*-MeC$_6$H$_4$)$_3$ > PPh$_3$ > P(*p*-FC$_6$H$_4$)$_3$ > P(Cy)$_3$. This trend is in line with the report by Tencich *et al* [24] for catalytic transfer hydrogenation of ketone and olefins. The low conversion obtained for P(Cy)$_3$ could be attributed to steric hindrance. On the other hand, the increase in catalytic activity of system observed with increased ligand basicity as reflected by the turnover frequency presented in Table 18, signals promotion of insertion reaction which is an important step in inner sphere mechanism for hydrogen transfer. Thus we can assume that [Ir(μ-OMe)(COD)]$_2$/ 2 PAr$_3$ catalytic system would probably follow inner sphere mechanism involving active participation of hydrido complex (see Scheme 18) for the transfer hydrogenation of acetophenone.

.

Table 18. TOF and percent yield for different catalytic systems using P- donor Ligands

Entry	Catalyst	Ligand	TOF[c] (h^{-1})	Yield[d] (%)
1	1	PPh_3	7.8	45
2	1	$P(p\text{-}FC_6H_4)_3$	7.1	42
3	1	$P(p\text{-}OMeC_6H_4)_3$	11.6	56
4[b]	1	PPh_3	3.4	18
5[b]	1	$P(p\text{-}FC_6H_4)_3$	6.8	34
6[b]	1	$P(p\text{-}OMeC_6H_4)_3$	5.6	44
7	2	PPh_3	2.6	27
8	2	$P(p\text{-}FC_6H_4)_3$	0.6	16
9	2	$P(p\text{-}OMeC_6H_4)_3$	4.8	32
10	3	PPh_3	14.7	72
11	3	$P(p\text{-}FC_6H_4)_3$	29.2	74
12	3	$P(p\text{-}OMeC_6H_4)_3$	10.8	70

Reaction conditions: 3 mmol of acetophenone, Ir catalyst (0.03 mmol), ligand (0.06 mmol), KOH (0.09 mmol) and *i*-PrOH (3 mL) at 60 ^oC

[b] Reaction conditions: 3 mmol of acetophenone, Ir catalyst (0.03 mmol), ligand (0.12 mmol), KOH (0.09 mmol) and *i*-PrOH (3 mL) at 60 ^oC

[c] TOF at 1 hour [d] Yield at 5 hours

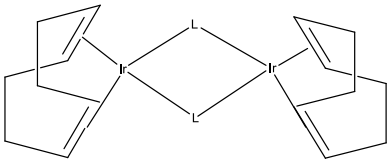

L= OMe- Catalyst 1 L= Cl- Catalyst 2

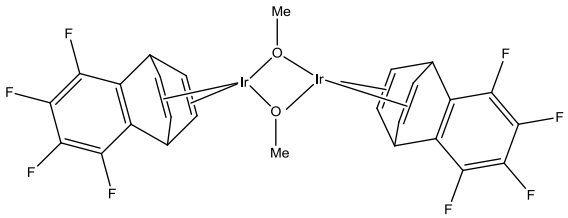

Catalyst 3

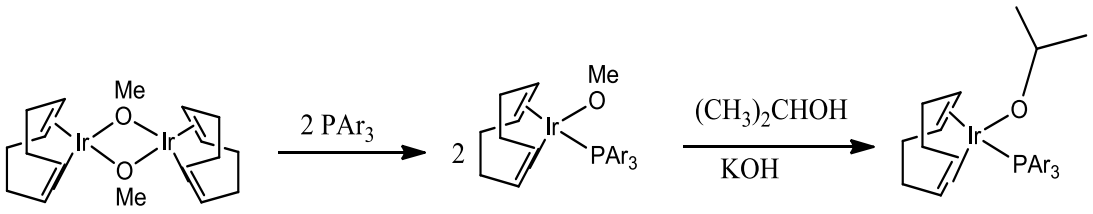

Scheme 13. Formation of active catalyst from $[Ir(\mu\text{-}OMe)(COD)]_2$ / 2 PAr_3 system

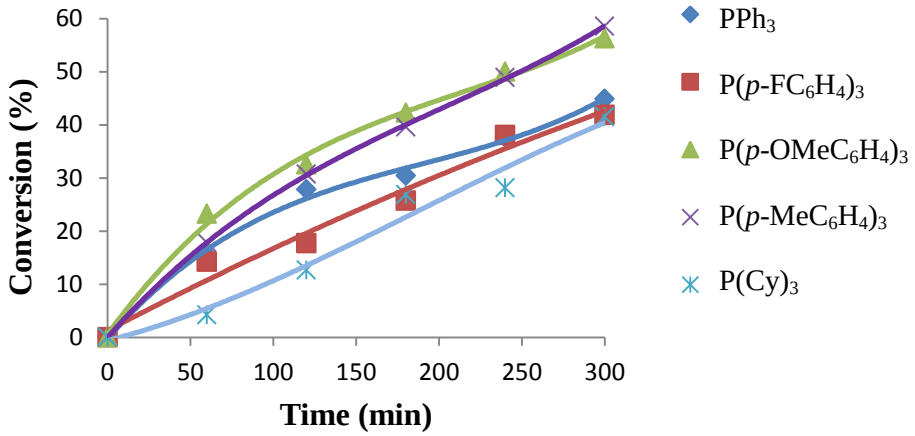

Figure 15. Conversion of acetophenone using [Ir(μ-OMe)(COD)]$_2$/ phosphine ligands system

Reaction conditions: 3 mmol of acetophenone, Ir catalyst (0.03mmol), ligand (0.06 mmol), KOH (0.09 mmol) and *i*-PrOH (3 mL) at 60 ^{o}C

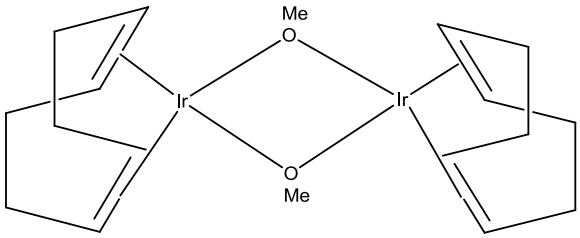

5.2.2.2. Ir(μ-Cl)(COD)]$_2$ (catalyst 2)/ 2 PAr$_3$Catalytic System

This catalytic system was developed to examine the effect of bridging ligand on complex catalytic activity. Like the methoxo-bridged complex, the active catalyst is [Ir(O^iPr)(COD)PAr_3] (see Scheme 14) but its formation in this system is relatively more difficult. The catalytic activity of this system can be inferred from results presented in Figure 16 as well as Table 18. Direct comparison of these results with that of [Ir(μ-OMe)(COD)]$_2$/ 2 PAr_3, indicates that the methoxo-bridge compound is more active than the chloro derivative. The lower activity of the catalyst **2** could be attributed to the difficulty in substituting the Cl on Ir with $(CH_3)_2CHO^-$ because of the Ir-Cl bond strength. Theoretical binding energy calculated for both Ir-Cl and Ir-OMe shows greater strength for the former (see Table 19). However, the trend of activity is consistent with that of methoxo-bridged system with ligands performance order being P(*p*-$OMeC_6H_4)_3$ > PPh_3 > P(*p*-$FC_6H_4)_3$. Since this system shares the same active catalyst with methoxo, it can be assumed it also the mechanism highlighted in Scheme 18.

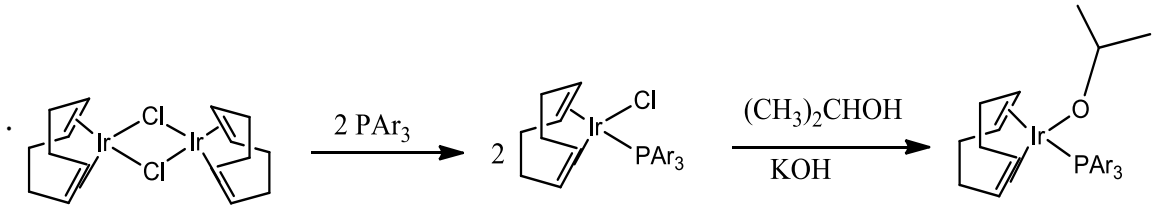

Scheme 14. Formation of active catalyst from $[Ir(\mu\text{-}Cl)(COD)]_2$ / 2 PAr_3 system

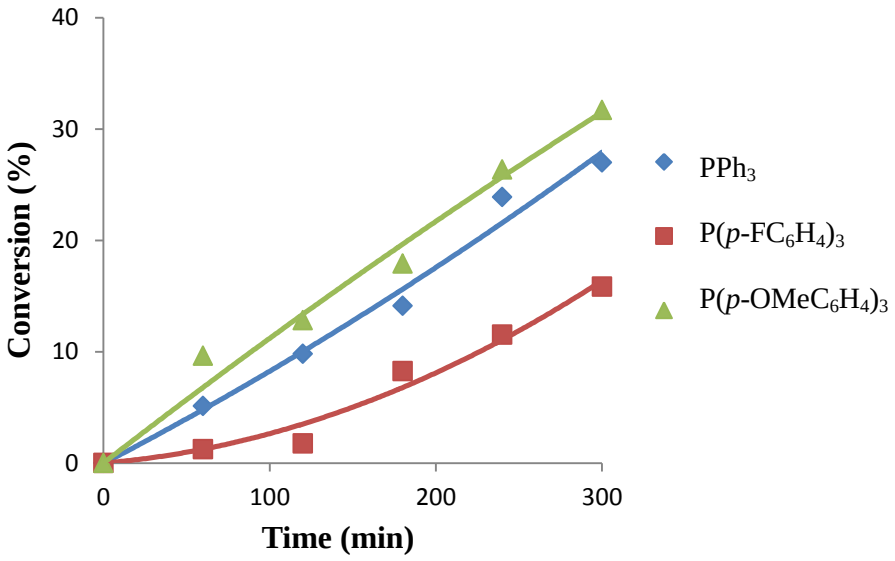

Figure 16. Conversion of acetophenone using [Ir(μ-Cl)(COD)]$_2$/ phosphine ligands system

Reaction conditions: 3 mmol of acetophenone, Ir catalyst (0.03mmol), ligand (0.06 mmol), KOH (0.09 mmol) and *i*-PrOH (3 mL) at 60 ^{o}C

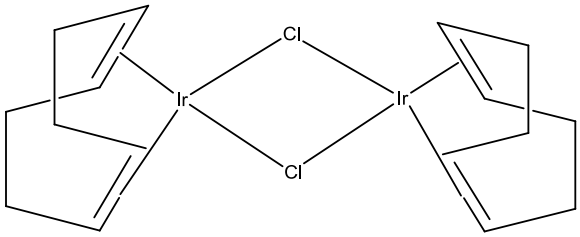

Table 19. Calculated binding energy for methoxo and chloro- bridged complexes

Catalyst	Binding Energy (kcal/mol)
[Ir(OMe)(COD)]	75.4
[Ir(Cl)(COD)]	99.4

5.2.2.3. [Ir(μ-OMe)(TFBB)]$_2$/ 2 PAr$_3$ Catalytic System

Having established the effect of bridging ligand on catalyst perfomance, the work would not be complete without examining the effect of diolefin on catalytic activity. For this purpose, catalyst **3** was used in place of cyclooctadiene complex. The same formulation ratio was used to realize the active catalyst [Ir(O^iPr)(TFBB)PAr$_3$] depicted in Scheme 15 but, the result presented in Figure 17 shows an opposite trend in activity when compared with COD system. The order of conversion is P(*p*-FC$_6$H$_4$)$_3$ > PPh$_3$ > P(*p*-OMeC$_6$H$_4$)$_3$. Interestingly, direct comparison of results of catalyst **1** and **3** presented in Figure 15 and Figure 17 as well as Table 18, clearly shows that the coordination of more electron-withdrawing diolefin, tetrafluorobenzobar-relene (TFBB) to iridium is more beneficial in terms of catalytic activity than that of COD diolefin. On the other hand, the difference in the conversion values obtained for each corresponding ligand in the systems consisting catalyst **1** and **3** suggests that the diolefin remained coordinated with the Ir centre. However, the better performance of TFBB system could be attributed to the easy of formation of metal hydride, which is one of the critical steps involved in hydrogen transfer reaction via a pathway involving participation of hydrido complex [4, 22, 25]. The high electron withdrawing ability of diolefin in [Ir(μ-OMe)(TFBB)]$_2$ / 2 PAr$_3$ system makes Ir metal centre electron deficient, thus favouring easy of coordination of H^- ion with the centre and the overall effect is reflected in the trend of activity observed. This assertion is justified by the lower free energy obtained for the hydride intermediate formation in the reaction mechanism calculation (see Figure 20).

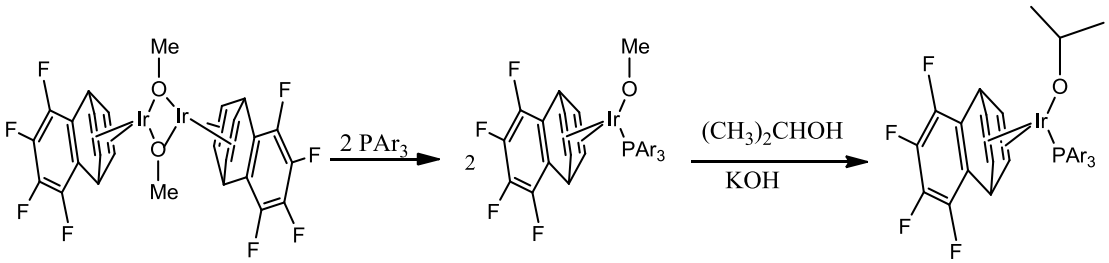

Scheme 15. Formation of active catalyst from $[Ir(\mu\text{-}OMe)(TFBB)]_2$ / 2 PAr_3 system

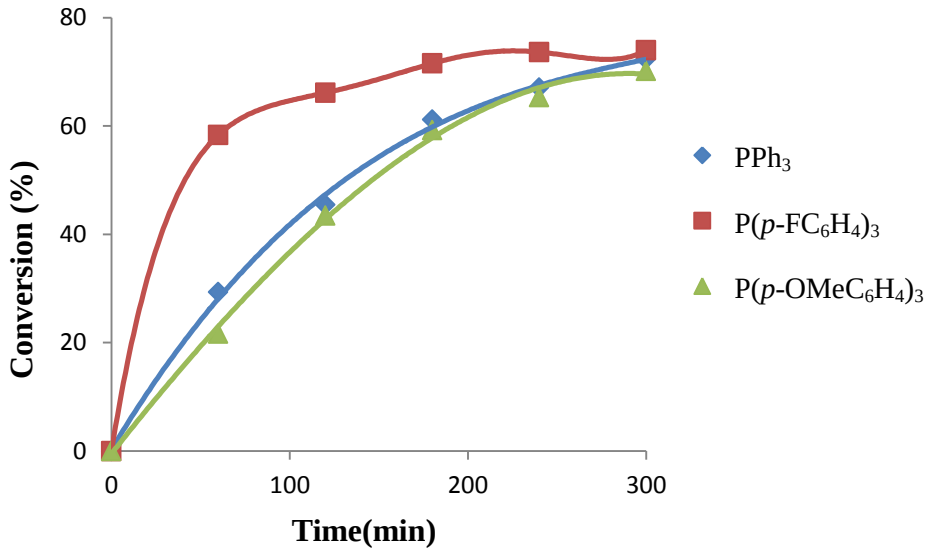

Figure 17. Conversion of acetophenone using [Ir(μ-OMe)(TFBB)]$_2$ catalytic system

Reaction conditions: 3 mmol of acetophenone, Ir catalyst (0.03 mmol), ligand (0.06 mmol), KOH (0.09 mmol) and *i*-PrOH (3 mL) at 60 ^{o}C

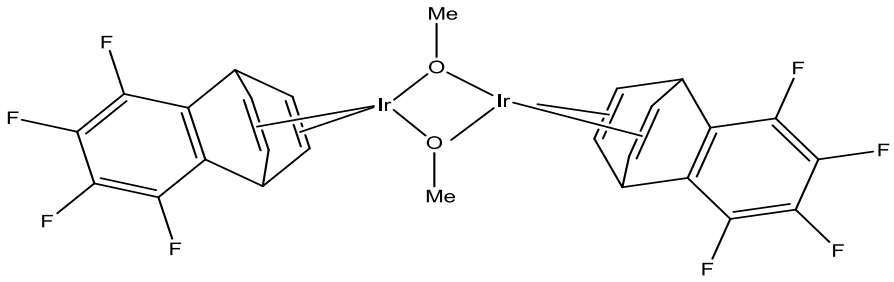

5.2.2.4. [Ir(μ-OMe)(COD)]$_2$/ 4 PAr$_3$Catalytic System

The purpose of developing this system is to examine the effect of saturating the metal centre with ligands. For this objective, 4 mmol of phosphines against 1 mmol of precursor catalyst with respect to substrate were used to make the Ir centre saturated with 18-electrons. This is believed to require an additional step which involves discoordination of a ligand in order to create vacancy at the metal centre (see Scheme16). The need for additional step results in the lowering of catalytic activity of this system (see Figure 18 as well as Table 18) when compared with the system with 2 mmol of phosphines (see Figure 15). The result obtained suggests that the catalytic reaction may follow the usual inner sphere mechanism but with the inclusion of discoordination step as illustrated in Scheme 19. On the other hand, the ease of vacancy creation is a subject of the stability of 18-electron intermediate present in the mechanism. The 18-electron intermediate formed by P(*p*-$FC_6H_4)_3$ is the least stable among its counterparts and as such, the discoordination occurs faster. This is justified by P(*p*-$FC_6H_4)_3$ system having higher TOF at the first hour than either P(*p*-$OMeC_6H_4)_3$ or PPh_3 as illustrated in Table 18.

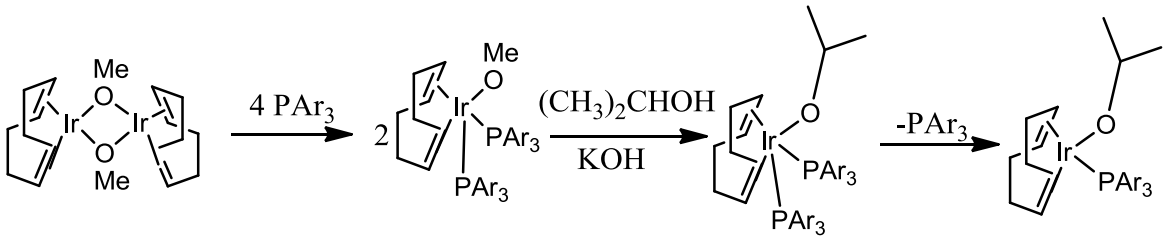

Scheme 16. Formation of active catalyst from $[Ir(\mu\text{-}OMe)(COD)]_2$ / 4 PAr_3 system

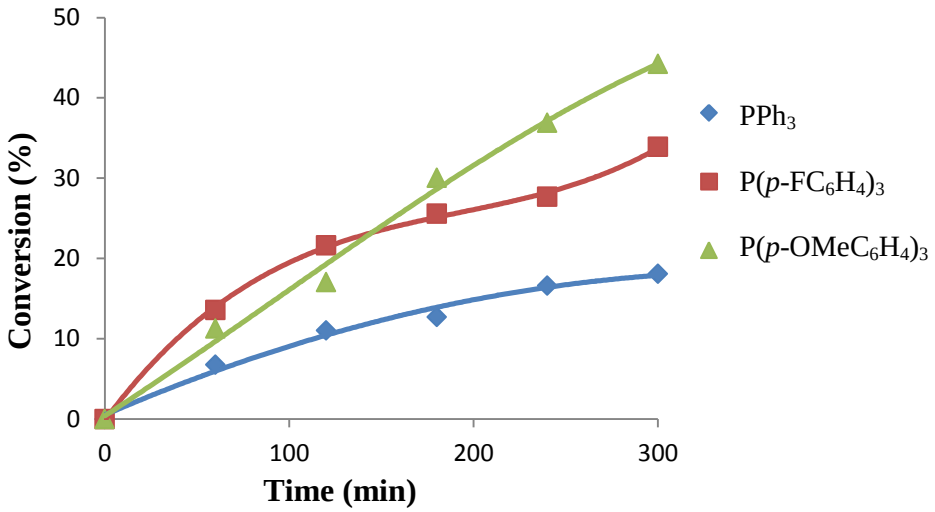

Figure 18. Conversion of acetophenone using 18-electron system of $[Ir(\mu\text{-}OMe)(COD)]_2$

Reaction conditions: 3 mmol of acetophenone, Ir catalyst (0.03 mmol), ligand (0.12 mmol), KOH (0.09 mmol) and *i*-PrOH (3 mL) at 60 ^{o}C

5.2.2.5. Hydrogen Transfer Reactions with N-donor Ligands

Like the phosphine ligands, catalytic activity of pyridine, an N-donor ligand was tested using catalyst **1**. Catalytic systems consisting of 2 (16-electron system) and 4 mmol (18-electron system) of ligand were set up respectively. The 16-electrons system gave [Ir(O^iPr)(TFBB)Py] as the active catalyst (see Scheme 17) while the results presented in Figure 19 shows that the 16-electron system is more catalytically beneficial. This result is in consonant with what was obtained with phosphine ligands. The lower activity recorded for the saturated 18-electron system is due to the need for additional step involving discoordination of one of pyridine in order to create vacancy for substrate entry into the reaction path. This is similar to what happened with phosphine ligands and as such it could be assumed that 16-electron system with pyridine ligand would probably follow stepwise mechanism illustrated in Scheme 18 while the 18-electron follows the one in Scheme 19.

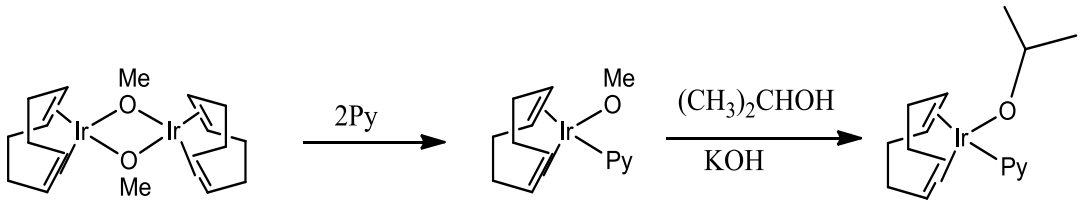

Scheme 17. Formation of active catalyst from $[Ir(\mu\text{-}OMe)(COD)]_2$ / 2 pyridine system

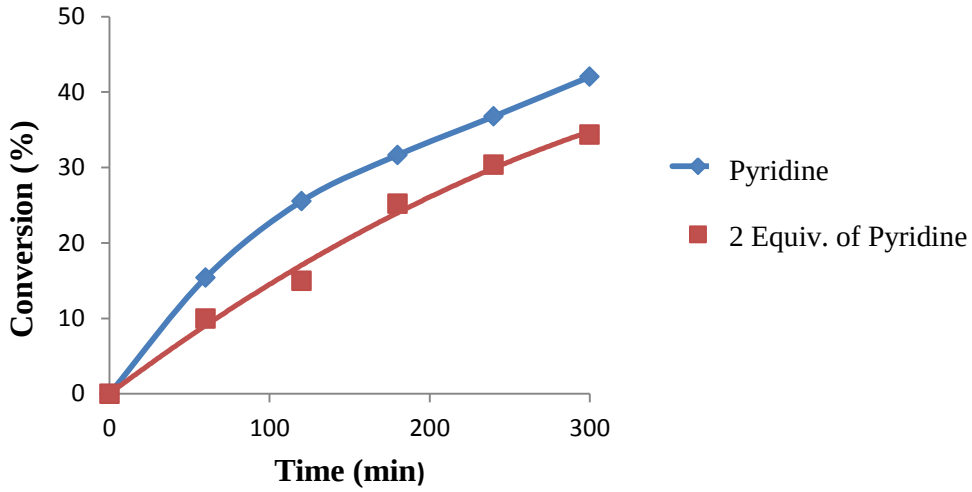

Figure 19. Conversion of acetophenone using $[Ir(\mu\text{-}OMe)(COD)]_2$ with N- donor ligands

Reaction conditions: 3 mmol of acetophenone, Ir catalyst (0.03 mmol), ligand (0.06 mmol), KOH (0.09 mmol) and *i*-PrOH (3 mL) at 60 ^{o}C

Reaction conditions for 2 equiv. of pyridine: 3 mmol of acetophenone, Ir catalyst (0.03 mmol), ligand (0.12 mmol), KOH (0.09 mmol) and *i*-PrOH (3 mL) at 60 ^{o}C

5.2.2.6. Mechanism of Hydrogen Transfer reaction

The proposed mechanisms for the transfer hydrogenation of acetophenone using 16 and 18- electron systems are illustrated in Schemes 18 and 19, respectively. However, the examination of the probable mechanisms was done via theoretical investigation of which the findings are presented in Figure 20. The reaction mechanism was followed by the two established routes in the literature namely classical pathway involving participation of hydrido complex and the Meerwein-Ponndorf-Verley mechanism [22]. Following addition of phosphines, it is assumed that catalyst **1** and **3** would generate [Ir(OMe)(diolefin)PR_3] which in basic media reacts with isopropanol to give [Ir(O^iPr)(diolefin)PR_3] that is believed to be the active catalyst in the reaction. In the case of hydrido route, alkoxo part of the complex undergoes β-elimination to give hydrido intermediate. This is being followed by coordination of substrate acetophenone to the Ir centre, after which it undergoes insertion with the hydrogen. Then the interaction with O^iPr in the system results in the release of the product with the formation of starting catalyst. However, in the case of the direct hydrogen transfer, interaction between the alkoxo part of the complex and the substrate gives an intermediate that interact with O^iPr in the system to give product and starting catalyst [22]. Considering the enthalpies of reaction calculated for the reaction paths in Figure 20, the stepwise mechanism through hydride intermediate is more probable for catalytic systems of catalyst **1** and **3** with P(*p*-$OMeC_6H_4)_3$, P(*p*-$FC_6H_4)_3$ and P($C_6H_5)_3$. The critical steps in this mechanism are the formation of hydrido intermediate as well as coordination of acetophenone to metal centre. For the complex **3**, the diolefin TFBB makes the metal centre electron deficient and this is further enhanced by the coordination of P(*p*-$FC_6H_4)_3$ which contains electron

withdrawing substituent (F). This eventually facilitated the β-elimination and coordination of hydride with the free energy of 4.7 kcal/mol which is lower than that required for either P(*p*-$OMeC_6H_4)_3$ (7.6 Kcal/mol) or P($C_6H_4)_3$ (5.8 Kcal/mol). In the same sense, lower free energy is required for the coordination of acetophenone to hydrido metal centre as well as that for transition state TSDE involving P(*p*-$FC_6H_4)_3$ with complex **3**. On the other hands, P(*p*-$OMeC_6H_4)_3$ with electron donating substituent seems to be more beneficial in the catalytic system with complex **1**. It proceeded with relatively lower free energies in hydrido formation as well as the coordination of substrate to the metal centre. The reaction mechanism also supports the better performance of complex **3** over complex **1** with the corresponding ligands, by having lower free energies in different stages involved in the reaction.

On the issue of catalytic cycle efficiency, the turnover frequency (TOF) which reflects catalyst performance can be calculated via computational studies using energetic span model to account for energy difference between the TOF-determining transition state (TDTS) and the TOF-determining intermediate (TDI) [92]. From Figure 20, **A** complex represent the TDI while the TDTS represents reaction pathway to the transition structure of highest energy denoted as **TSAB**, for catalysts **I** and **III** and **TSCD**. The calculated energy spans are 25.9, 27.5, 25.3 kcal/mol for [Ir(O^iPr)(COD)PR_3] system with PPh_3, P(*p*-$FC_6H_4)_3$ and P(*p*-$OMeC_6H_4)_3$ respectively while 24.9, 24.4 and 24.4 kcal/mol are recorded for corresponding ligand with [Ir(O^iPr)(TFBB)PR_3] system. The calculated energy spans for [Ir(O^iPr)(COD)PR_3] system are in consonant with the TOF obtained for these systems, 7.8, 7.1 and 11.6hr^{-1} respectively (see Table 18) . In the same sense, the TOF (14.7, 29.2 and 10.8hr^{-1} for PPh_3, P(*p*-$FC_6H_4)_3$ and P(*p*-$OMeC_6H_4)_3$ respectively)

recorded in Table 18 for [Ir(O^iPr)(TFBB)PR_3] are also in good agreement with their energy spans. Furthermore, the values obtained for the energy span for the stepwise mechanism can also be correlated to the stability of the hydride intermediates for [Ir(O^iPr)(TFBB)PR_3] system. The relative energy of intermediate **B** as well as **C** is in the same order with the energy span values, thus signifying that the P(*p*-$FC_6H_4)_3$ stabilizes the energy of the hydride while P(*p*-$OMeC_6H_4)_3$ give a less stable intermediate than $P(C_6H_5)_3$.

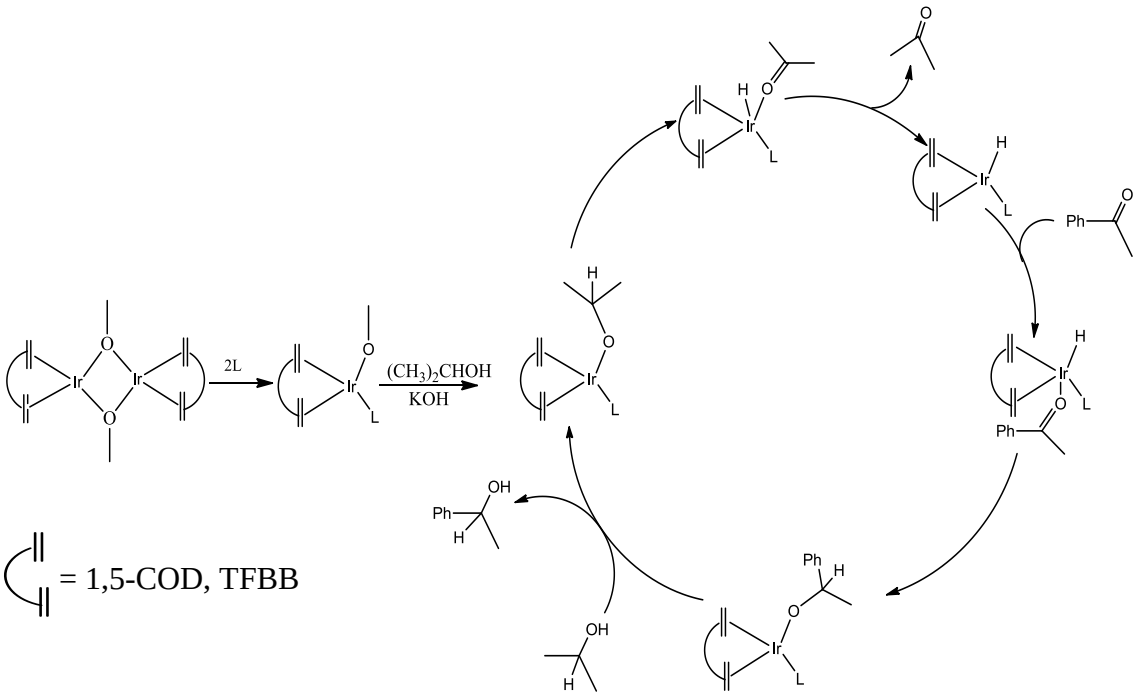

Scheme 18. Proposed mechanism for 16-electron system

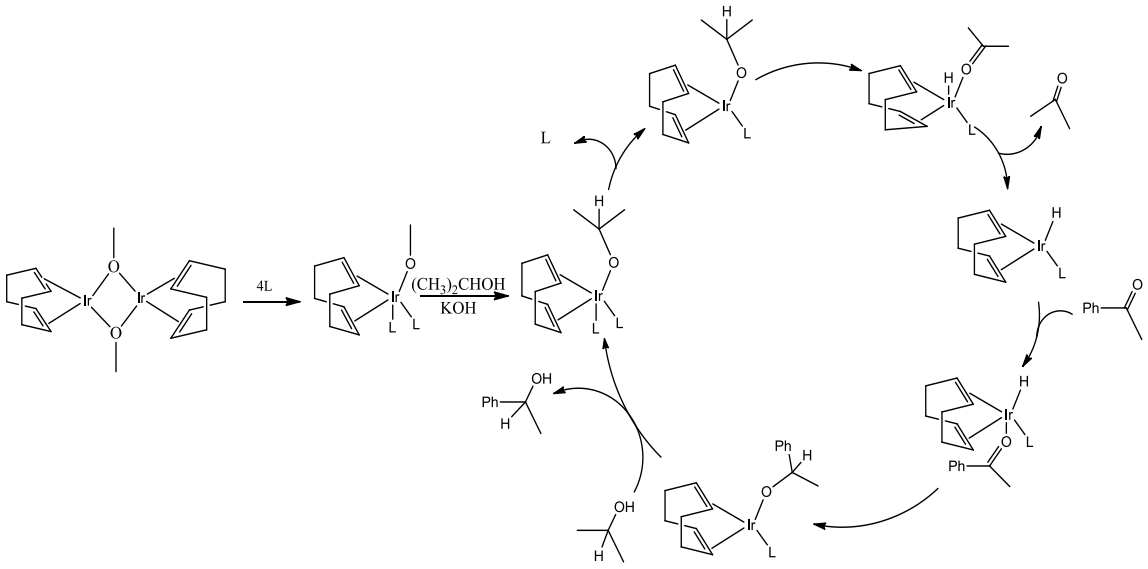

Scheme 19. Proposed mechanism for 18-electron system with monodentate ligands

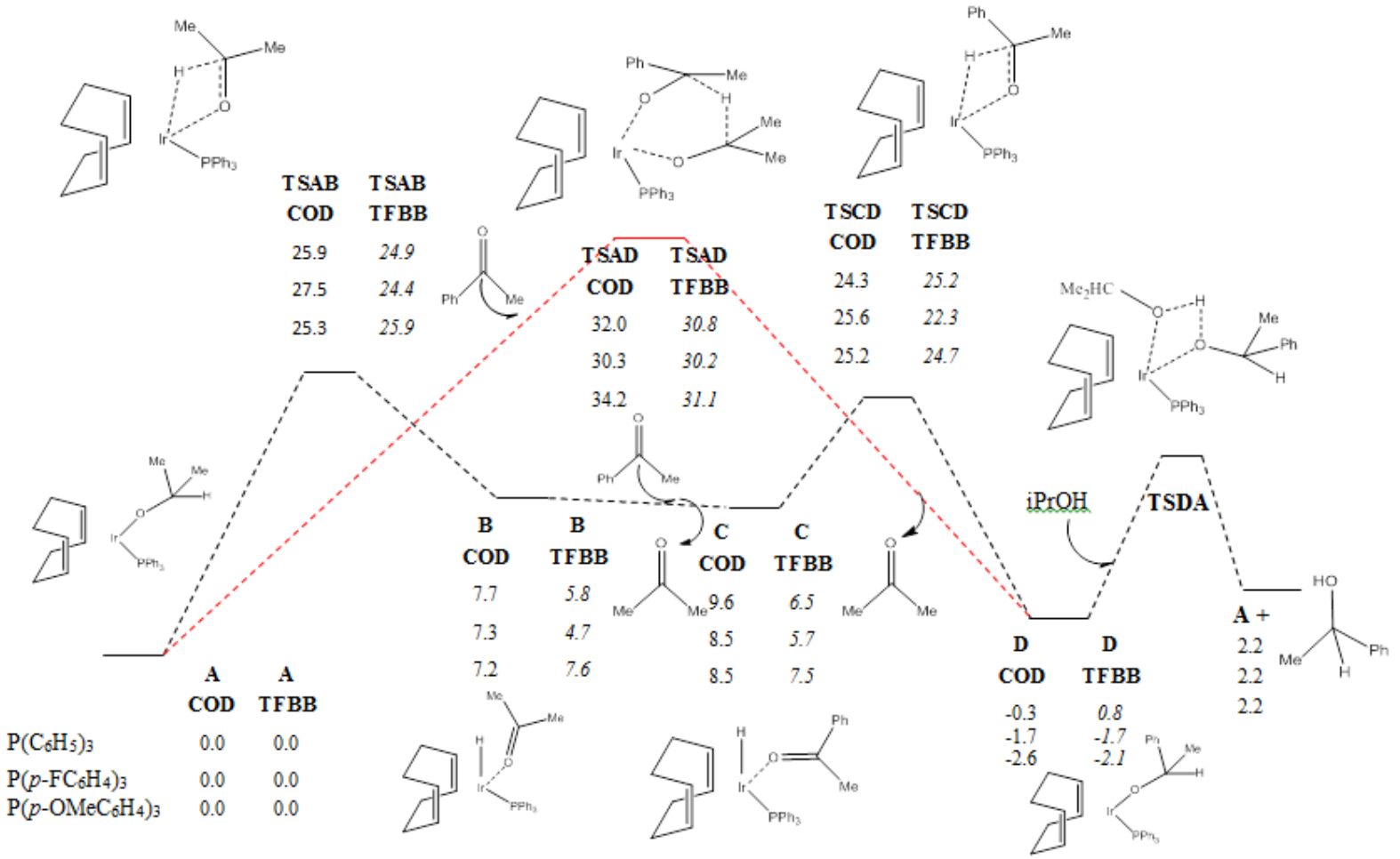

Figure 20. Stepwise mechanism through hydride intermediate calculated at B3LYP/def2svp

5.2.3. Hydrogen Transfer reaction with Rhodium Precursors

The attempt to study catalytic activity of $[Rh(\mu\text{-}OMe)(COD)]_2$ and $[Rh(\mu\text{-}OMe)(TFBB)]_2$ with monodentate phosphines for transfer hydrogenation of acetophenone was not successful because the reaction could not proceed beyond 1 hr before decomposition set in. However, the screening of bases was done using $[Rh(\mu\text{-}OMe)(COD)]_2$ complex with triphenylphosphine (PPh_3) to obtain the result shown in Table 20. In this system, K^tBuO outperformed KOH while NaOH gave the lowest conversion at 1 hr. K^tBuO is also strong base and its brilliant performance could be attributed to smaller size rhodium atom which might have reduced the steric problem that might likely occur with iridium atom of bigger size.

Table 20. Conversion of acetophenone based on basicity of bases

S/N	[Rh]/PPh3	Base	Conversion for 1 hr (%)
1	1:1	KOH	17.70%
2	1:1	K^tBuO	27.50%
3	1:1	NaOH	0.40%

5.3. Conclusion

The study has shown that strong bases are beneficial for transfer hydrogenation of acetophenone. However, the ratio of precursor catalyst to ligand greatly influences the activity of a catalytic system. 16-electron system outperformed the saturated 18-electron system. The need for additional discoordination step in a saturated system with 1:4 moles of catalyst to ligand, causes the reduction in catalytic activity. In the same sense, the nature of dinuclear complex bridging ligand also determines the catalyst performance as a strongly bonded ligand is difficult to be replaced by $(CH_3)_2CHO^-$. Another important factor is the nature of ligand as well as diolefin because they influence the performance of catalytic system. Ligands with electron donating substituents are more beneficial in $[Ir(\mu\text{-}OMe)(COD)]_2$ system while those electron withdrawing substituents are more beneficial in $[Ir(\mu\text{-}OMe)(TFBB)]_2$ system. On the other hand, the difference in the conversion rate of $[Ir(\mu\text{-}OMe)(COD)]_2$ and $[Ir(\mu\text{-}OMe)(TFBB)]_2$ systems with the same set of ligands indicates that diolefin remained coordinated during the course of catalytic reaction while the $[Ir(\mu\text{-}OMe)(TFBB)]_2$ generally performed better. Finally, theoretical calculation reveals that stepwise mechanism through hydride intermediate is the most probable mechanism for the catalytic reaction for both $[Ir(\mu\text{-}OMe)(COD)]_2$ and $[Ir(\mu\text{-}OMe)(TFBB)]_2$ systems.

.

CHAPTER 6

HYDROGEN TRANSFER REACTIONS WITH BIDENTATE LIGANDS

6.1. Introduction

The use of bidentate ancillary ligands has been found beneficial to the catalytic activities of organometallic complexes. These ligands do affect the structure and reactivity of organometallic complexes [93]. Those with soft donor end such as phosphorus have π accepting ability which in turn stabilizes metal centre of low oxidation state [94]. On the other hand, the hard donor end types have σ donating ability which makes the centre more liable to oxidative addition reaction [96]. The activity of metal complex catalysts as well as their stability is being influenced by the steric and electronic nature of the ligands coordinating with the metal centre [98, 99]. More bulky ligands result in the formation of complexes with low dissociation constants indicating low stability [99]. While the substituents at its aromatic ring significantly influences the electronic nature of ligand. This consequently reflects in the catalytic activity of metal complex as the reaction rate is altered [95]. In a broad sense, the steric effect of the ligands is predicated upon the cone angle and bite angle [17, 19, 20, 101]. The formal is limited to monodentate ligands whereas the latter, which is the ligand-metal-ligand angle, is important in understanding the chelating effect of bidentate ligands [17, 20, 96, 100, 102]. Casey and coworker suggested a model for predicting chelating ability of bidentate ligands by introducing the idea of natural bite angle together with flexibility range for diphosphine ligands [102]. This natural bite angle is essentially dependent on ligand backbone which when altered affects the activity of the resulting complexes [96, 104]. However, the flexibility range is limited to bite angles whose excess strain energies of 3kcal/mol are not beyond the

determined natural bite angle [95]. Diphosphines possess significant influence on catalyst reactivity [96, 104]. Their coordination with metal usually saturates the centre, thus necessitating discoordination of one bond to create vacancy on the metal centre. In addition, there is geometrical restriction on metal complex activity as demonstrated by Thorn and Hoffmann in their theoretical calculation [104]. In an attempt to release the migrating group, they established that phosphine ligand inclined to widening the natural bite angle in a way similar to transition. In line with this, it was experimentally found in palladium diphosphine complexes that the migration rates increase with increasing bite angles [105]. However, having rigid backbone can impose a particular geometry which dictates direction of catalytic reaction.

Various types of bidentate phosphines have been used for transfer hydrogenation reaction. Different derivatives of bis(phosphino)ethane with fixed backbone were used with $[Rh(\mu\text{-}Cl)(COD)]_2$ for the reduction of 4-t-butylcyclohexanone by Spogliarich and co-workers [24]. In another report, rhodium(I) complexes of diphosphine ligands were used for systematic study of asymmetric transfer hydrogenation of acrylic acids in order to evaluate the effect of changing the size of metal-diphosphine chelate as well as the flexibility of the backbone [106]. In addition, amine(imine)diphosphine iron complex was found to be an active catalyst precursor for asymmetric transfer hydrogenation of ketones and imines [107]. However, there is scarce information about the effect of bidentate P or N- donor on the catalytic activity of iridium complex. This in turn motivated us to undertake this research endeavor.

6.2. Results and Discussion

6.2.1. $[Ir(\mu\text{-}OMe)(COD)]_2$/ Diphosphine Ligand Catalytic System

The way bidentate ligands affect activity of a catalyst is different from monodentate due to the interplay of both electronic and steric factors. Steric effect is associated with flexibility of backbone as well as bite angle. For this reason we intended to examine the combined effect of these two factors on the transfer hydrogenation of acetophenone using $[Ir(\mu\text{-}OMe)(COD)]_2$ as precursor catalyst. The catalytic experiments were set up using four different diphosphine ligands namely bis(diphenylphosphino)methane (dppm), bis(diphenylphosphino)ethane (dppe), bis(diphenylphosphino)propane (dppp) and bis(diphenylphosphino)butane (dppb). The ligands were in the ratio of two to one molar equivalent to the precursor catalyst and this makes Ir centre saturated with 18 electrons to give $[Ir(O^iPr)(COD)(Ph)_2P(CH_2)nP(Ph)_2]$ (Scheme 20) as the active catalyst. However, there is need for discoordination of one of the Ir-P bonds to create vacancy for the incoming substrate. On the other hand, the freed P following the bond cleavage remained attached to the diphosphine and in return enhances the activity of the intermediate through electron donation towards the Ir centre. From the result presented in Table 21, the activity of the diphosphines tested is in the order of dppp > dppm > dppb > dppe as indicated by both the TOF and yield (entries 1-4). Graphical representation of the result is also presented in Figure 21 for comparison purpose. It is important to note that the performance of this catalytic system depends on many factors which can be summarized into electronic and steric effects. One of the critical factors is the stability of starting 18-electron complex formed from the precursor catalyst. The poor performance of dppe ligand in the set of diphosphines could be attributed to the formation of five membered rigid ring with the metal centre which slowdowns its catalytic activity as previously

reported by Birkholz and co-workers [103]. On the other hand, the preferable geometry for Ir (I) complexes is square planar [1] which demands a bond angle of 90^{o}. Thus the appreciable conversion realized when dppm was used as ligand could be attributed to electronic destabilization resulting from extremely low bite angle (see Table 22). This in turn resulted in low binding energy and lower activation energy as reflected by calculated coordination energy recorded in Table 22 which is in line with Zuidema et al report [108]. Since the reaction is in-situ the dppm catalyst can easily be formed and reformed during the course of reaction and this, could have translated to the appreciable performance observed. The best results obtained in the diphospine's set was for dppp which could be attributed to the favourable electronic properties as indicated in Table 23, as well as the stabilization of the resulting complex where the dppp bite angle is almost 90^{o}; the bond angle needed for square planar geometry [95], [100]. The negative electron affinity (EA) indicates its high acidic nature which helps in the formation of hydrido intermediate, one of critical steps in the reaction mechanism. Similarly, the lower ionization potential (IP) value of dppp than any other ligand in the set signifies great basicity which in turn aids insertion reaction as well as facilitating the leaving of product from the catalytic cycle. The observed trend in the catalytic performance of these set of disphosphines for transfer hydrogenation of acetophenone is in agreement with the report by Kamer et al [95] describing nickel-catalyzed hydrocyanation of styrene, using diphosphine ligands. Moreover, the reduction reaction path may probably follow the mechanism highlighted in Scheme 21.

Table 21. TOF and percent yield for different catalytic systems using P- donor ligands

Entry	**Catalyst**	**Ligand**	**TOF (h^{-1})**[a]	**Yield (%)**[b]
1	**1**	dppm	22.1	67
2	**1**	dppe	12.2	51
3	**1**	dppp	29.9	75
4	**1**	dppb	4.4	54
5	**3**	dppm	12.2	69
6	**3**	dppe	2.7	27
7	**3**	dppp	18.8	58
8	**3**	dppb	21.1	82

Conditions: 3 mmol of acetophenone, Ir catalyst (0.03 mmol), ligand (0.06 mmol), KOH (0.09 mmol) and *i*-PrOH (3 mL) at 60 ^{o}C

. [a] TOF calculated for the reaction mixture at 1h. [b] Calculated by GC.

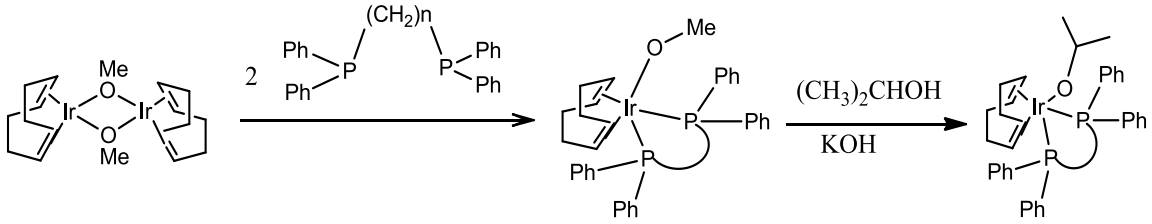

Scheme 20. Formation of active catalyst from $[Ir(\mu\text{-}OMe)(COD)]_2$ / 2 diphosphine system

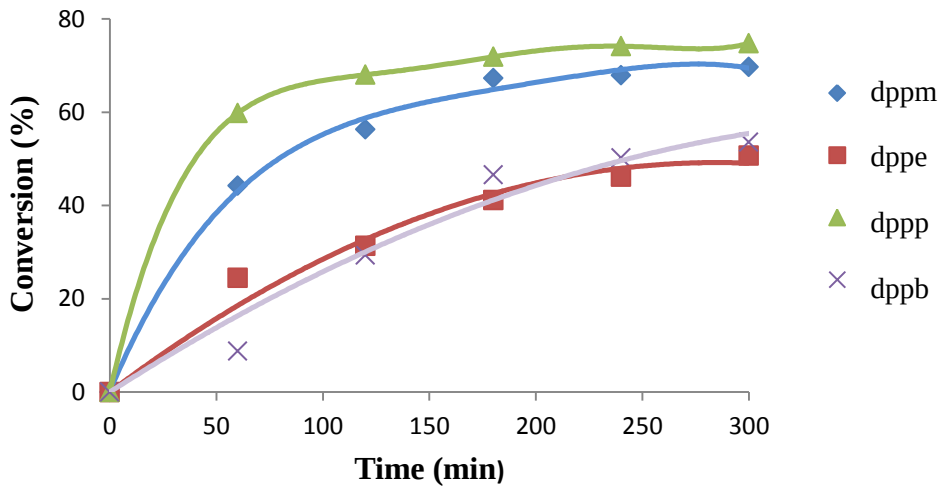

Figure 21. Conversion of acetophenone using $[Ir(\mu\text{-}OMe)(COD)]_2$ with diphosphines

Reaction conditions: 3 mmol of acetophenone, Ir catalyst (0.03 mmol), ligand (0.06 mmol), KOH (0.09 mmol) and *i*-PrOH (3 mL) at 60 ^{o}C

Table 22. Bite angles (^{o}) and stability energies (kcal/mol) of the ligands in the catalyst complex

Ligands	Symmetry	Bite Angle	Binding Energy	Coordination energy
dppm	C_s	69.7	41.21	205.30
dppe	C_2	82.3	54.76	218.85
dppp	C_1	88.7	59.22	223.31
dppb	C_1	90.7	55.50	219.59

Table 23. Ionization potential (IP), electron affinity (EA) hardness (η) and absolute electronegativity (χ) of the diphosphine ligands

Ligand	IP	EA	η	χ
dppm	7.19	0.11	3.54	3.65
dppe	6.46	-0.10	3.28	3.18
dppp	6.22	-0.03	3.12	3.09
dppb	6.76	-0.09	3.42	3.33

6.2.2. $[Ir(\mu\text{-}OMe)(TFBB)]_2$/ Diphosphine Ligand Catalytic System

The influence of diolefin in the catalytic activity of a complex cannot be underestimated. At the same time, the nature of ancillary ligands which stabilize or add electronic or steric effect to complex, matters in complex catalytic performance. As a means of justifying these statements we decided to explore $[Ir(\mu\text{-}OMe)(TFBB)]_2$/diphosphine system for transfer hydrogenation of acetophenone and compared the results with those obtained with $[Ir(\mu\text{-}OMe)(COD)]_2$ system. The results presented in Table 21 as well as Figure 21 and Figure 22 strongly indicate that the nature of diolefin plays a significant role in the order of performance of a catalytic system. It shows that the replacement of 1,5-cyclooctadiene, an acidic diolefin with tetrafluorobenzo-barrelene (TFBB) bearing electron withdrawing substituent modifies order of activity of the diphosphines set used in this work. In addition, different values obtained for each of the corresponding diphosphine with the two catalytic systems (1 and 3) revealed that diolefin remained coordinated during the catalytic reaction. Like the cyclooctadiene system, dppe is also not beneficial with tetrafluorobenzobarrelene. This could be due to the similar reasons earlier said for COD system. In the same manner the dppm gave a good turnout and this could also be due to the similar reasons given for $[Ir(\mu\text{-}OMe)(COD)]_2$ system. Since similar results were obtained for calculated bite angle and binding energy of both systems (see Table 22 and 24). Surprisingly, dppb gave the best performance in diphospine's set for the TFBB system whereas dppp had initial high conversion rate, as indicated by TOF in Table 21 and the plot in Figure 22. This still buttresses the influence of diolefin in the catalytic activity. As evident in Table 25, $[Ir(\mu\text{-}OMe)(TFBB)]_2$ is less basic than $[Ir(\mu\text{-}OMe)(COD)]_2$, also dppb is of low basicity (see Table 23) in the diphosphine's set. This combined effect of dppb ligand and complex in the resulting catalyst favours reductive

elimination which has been reported to be inversely proportional to the basicity [108]. On the other hand the poor performance of dppp could be problem of compatibility with $[Ir(\mu\text{-}OMe)(TFBB)]_2$.

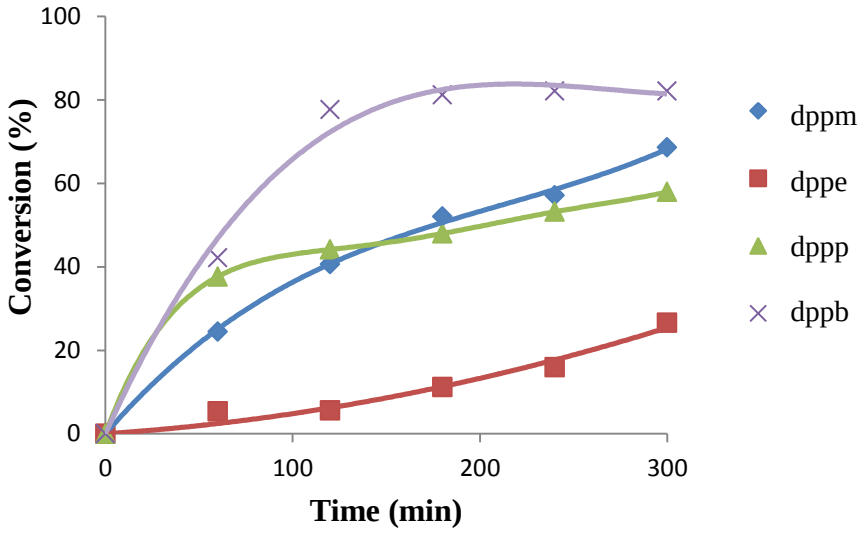

Figure 22. Conversion of acetophenone using $[Ir(\mu\text{-}OMe)(TFBB)]_2$ with diphosphines

Reaction conditions: 3 mmol of acetophenone, Ir catalyst (0.03 mmol), ligand (0.06 mmol), KOH (0.09 mmol) and *i*-PrOH (3 mL) at 60 ^{o}C

Table 24. Bite angles (^{o}) and stability energies (kcal/mol) of the ligands in the catalyst complex

Ligands	Symmetry	Bite Angle	Binding Energy	Coordination energy
dppm	C_s	70.3	47.03	202.41
dppe	C_2	82.8	59.10	214.48
dppp	C_1	88.5	62.91	218.28
dppb	C_1	93.5	62.21	217.59

Table 25. Electronic parameters of the complexes

Complex	IP	EA	η	χ
$[Ir(\mu\text{-}OMe)(COD)]_2$	6.48	-0.34	3.41	3.07
$[Ir(\mu\text{-}OMe)(TFBB)]_2$	6.90	0.61	3.15	3.75

6.2.3. $[Ir(\mu\text{-}OMe)(diolef)]_2$/ N-donor Bidentate Ligand Catalytic System

For this system, 2,2′-bipyridine and 1,10-phenanthroline with $[Ir(\mu\text{-}OMe)(diolef)]_2$ for the acetophenone reduction were tested. The results as shown in Table 26 and Figure 23 revealed that 2,2′-bipyridine outperformed 1,10-phenanthroline in the $[Ir(\mu\text{-}OMe)(COD)]_2$ system as reflected by its higher TOF value (41.1 h^{-1}) and higher % yield (86%). However, with catalyst 3 (Scheme 11) the two ligands have different TOF but the same % yield (see Figure 24). The similar results obtained for 1,10-phenanthroline in both catalyst 1 and 3 suggested that the diolefin might have been replaced by the phenanthroline, giving $[Ir(phen)_2]^+$ as the active catalyst in the system. Similar to diphosphine ligands, 2,2′-bipyridine would coordinate with Ir through its two chelating sites, making the Ir saturated with 18-electrons. However, discoordination of one of the ligand bonds with Ir centre would be required for substrate entry. Consequently, 2,2′-bipyridine system realize transfer hydrogenation of acetophenone via mechanism depicted in Scheme 21. In addition, catalytic activity is enhanced by freed Nitrogen after discoordination which makes them catalytically more beneficial, than the monodentate pyridine ligand. In general, the bidentate N-donor were found to be more catalytically active than the monodentate N-donor when tested in transfer hydrogenation of acetophenone.

Table 26. TOF and percent yield for different catalytic systems using N –donor ligands

Entry	Catalyst	Ligand	TOF[a] (h^{-1})	Yield[b] (%)
1	1	2,2′-Bipyridine	41.1	86
2	1	1,10-Phenathroline	13	66
3	3	2,2′-Bipyridine	18.3	75
4	3	1,10-Phenathroline	12.2	75

Reaction conditions: 3 mmol of acetophenone, Ir catalyst (0.03 mmol), ligand (0.06 mmol), KOH (0.09 mmol) and *i*-PrOH (3 mL) at 60 ^{o}C

[a] TOF at 1 hour [b] Yield at 5 hours

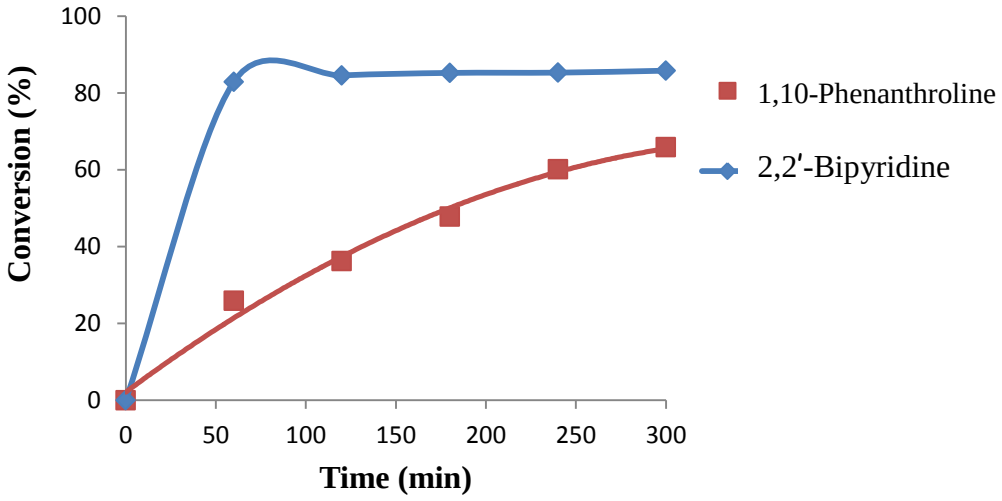

Figure 23. Conversion of acetophenone using $[Ir(\mu\text{-}OMe)(COD)]_2$ with N- donor ligands

Reaction conditions: 3 mmol of acetophenone, Ir catalyst (0.03 mmol), ligand (0.06 mmol), KOH (0.09 mmol) and *i*-PrOH (3 mL) at 60 ^{o}C

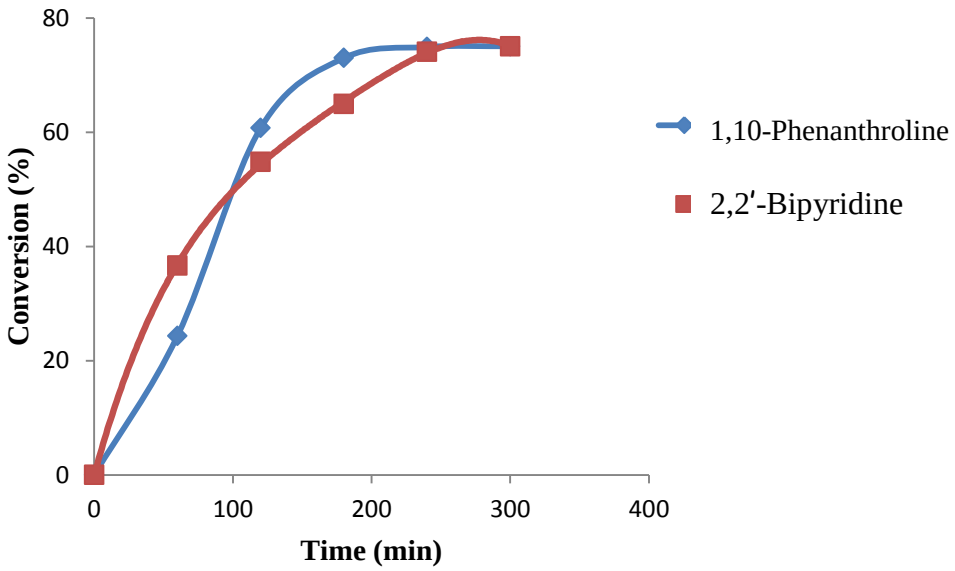

Figure 24. Conversion of acetophenone using $[Ir(\mu\text{-}OMe)(TFBB)]_2$ with N- donor ligands

Reaction conditions: 3 mmol of acetophenone, Ir catalyst (0.03 mmol) ligand (0.06 mmol), KOH (0.09 mmol) and *i*-PrOH (3 mL) at 60 ^{o}C

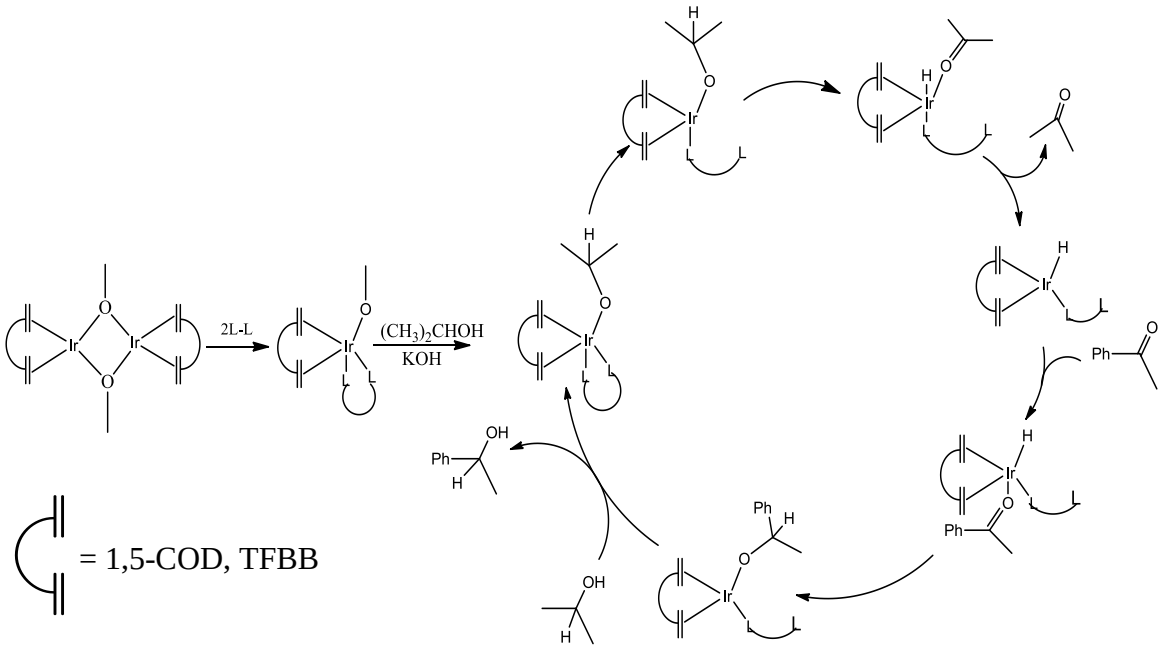

Scheme 21. Proposed mechanism for 18-electron system with diphosphine ligands

6.2.4. Rhodium Based Catalytic Systems

Having noted deposition with monodentate ligands after one hour of reaction, we decided to use bidentate since their bulkiness may help in stabilizing the active catalyst. Consequently, the problem of decomposition was overcome by using bidentate ligands with the exception for dppm in the case of $[Rh(\mu\text{-}OMe)(TFBB)]_2$ system. Using $[Rh(\mu\text{-}OMe)(COD)]_2$ system, the catalytic activity of the ligand was found to increase with the increase in the chains of CH_2 (see Figure 25). However, a different trend was obtained with $[Rh(\mu\text{-}OMe)(TFBB)]_2$ system, as shown in Figure 26. This disparity in the results of both systems further buttresses the influence of diolefin in catalytic activity. Furthermore, it revealed that the diolefin remained coordinated during the course of reaction. With the bidentate ligands used in this study, Rh complex systems generally performed better than their Ir counterparts.

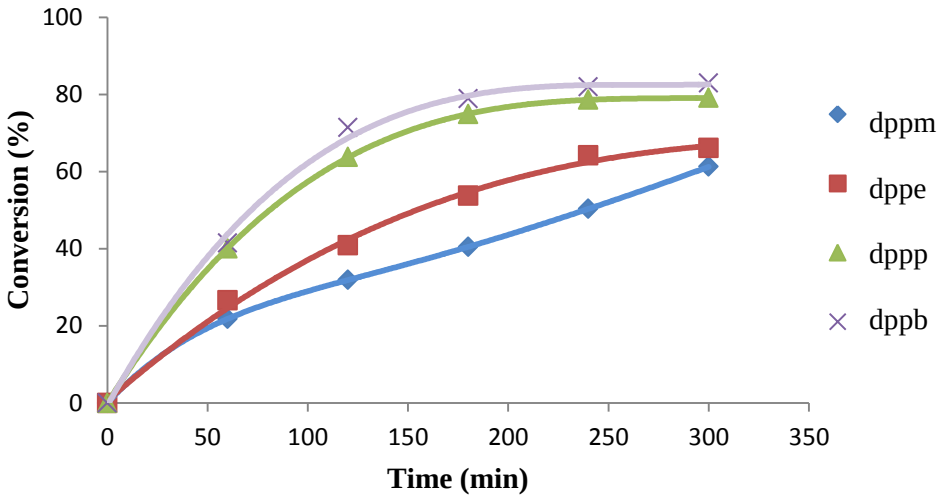

Figure 25. Conversion of acetophenone using $[Rh(\mu\text{-}OMe)(COD)]_2$ with diphosphines

Reaction conditions: 3 mmol of acetophenone, Ir catalyst (0.03 mmol), ligand (0.06 mmol), KOH (0.09 mmol) and *i*-PrOH (3 mL) at 60 ^{o}C

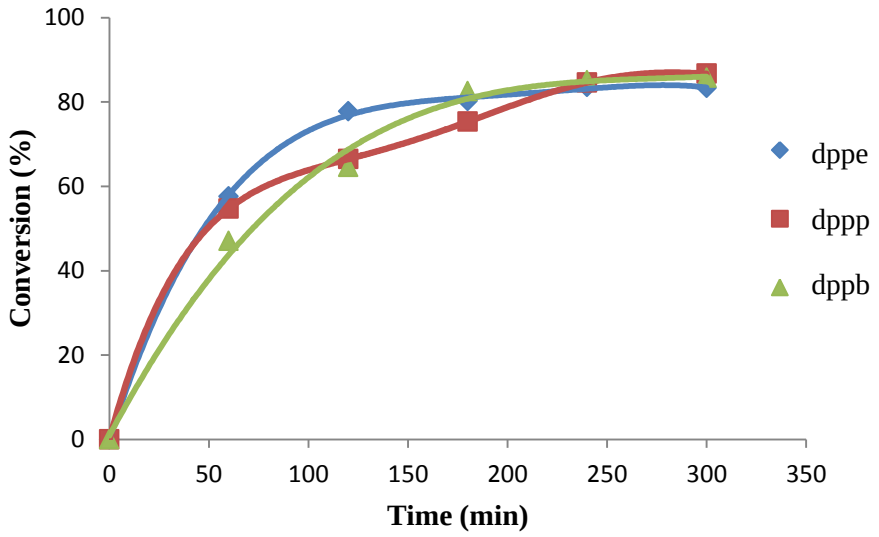

Figure 26. Conversion of acetophenone using $[Rh(\mu\text{-}OMe)(TFBB)]_2$ with diphosphines

Reaction conditions: 3 mmol of acetophenone, Ir catalyst (0.03 mmol), ligand (0.06 mmol), KOH (0.09 mmol) and *i*-PrOH (3 mL) at 60 ^{o}C

6.3. Conclusion

The catalytic activity of the iridium system with diphosphine ligands depends on the interplay of electronic and steric properties of ligands together with nature of diolefin. For the catalyst **1**, the order of performance was found to be dppp > dppm > dppb > dppe whereas a different trend was recorded for catalyst **3**. For both catalyst systems moderate performance was recorded for dppm whereas the performance of dppe was found to be poor. On the other hand, excellent result was obtained for dppp with catalyst **1** whereas dppb gave the best performance with catalyst **3**. The difference in the trend of catalytic activity of the same set of diphosphine with catalyst **1** and **3** affirmed that diolefin remained coordinated during the course of reaction and also that the nature of diolefin has influence on catalytic activity. In case of N- donor ligand, bipyridine was found to be more catalytically beneficial than 1,10-phenanthroline with catalyst **1**. However, similar results recorded for 1,10-phenanthroline in both catalyst systems, suggest the replacement of diolefin by the ligand. For rhodium complex, diphosphine ligands helped in stabilizing the resulting active catalyst while the catalytic activity increased with increasing number of CH_2 in ligand backbone for $[Rh(\mu\text{-}OMe)(COD)]_2$ system with a different trend being followed by TFBB system.

.

CHAPTER 7

CONFORMATIONAL ANALYSIS AND VIBRATIONAL SPECTRA OF SOME PHOSPHINIC ACIDS AND THEIR POSSIBLE USE AS POTENTIAL LIGANDS IN RHODIUM COMPLEXES

7.1. Introduction

Phosphinic acids which are oxyacids of phosphorus are known for their important roles in biological systems [109]. Phosphinic acid can be hypothetically obtained from phosphine oxide molecule H_3PO by replacing one of the hydrogens with a hydroxyl group and its derivatives are obtained by replacing the phosphinic acid hydrogens with alkyl, aryl or other substituents [109]. A few theoretical studied were carried out on phosphinic acids to investigate their molecular and conformational properties [109]. These studies either implemented small basis set or did not thoroughly converge to global minima and as such giving inaccurate energetics for different conformations. Polarization functions on phosphorus were later found essential for accurate structural parameters [109]. In general, the relative stability of conformations was found to be dependent of steric, dipole-dipole and anomeric factors. While the steric effect is due to the electronic repulsion between the different sides of the molecule, the overall molecular dipole moment is minimized by dipole-dipole forces that arrange different regional local dipole moments in the molecule. The anomeric effect was found to play a major role in providing a further stability to the phosphinic acid and its derivatives [110].

One of the most interesting structural features is the strong hydrogen bonding between phosphinic acid monomers taking place between the P=O and OH moieties [112–115]. Such a feature leads to dimerization of monomers which exhibit the ability of phosphinic

acid to act as proton donor and acceptor simultaneously. This significant type of interaction is similar to that in carboxylic acids whose chemical [116-117, 118] and biochemical [118] properties are tied to the hydrogen-bond donor-acceptors behaviour [115]. Several reports [112–116, 120] have pointed out to the of existence of strong hydrogen bonding in phosphinic acids in the condensed and non-condensed states. In the solid state, phosphinic acids appear as spiral polymeric molecules and sometime as cyclic dimeric cluster [113, 120]. Furthermore, a gas-phase IR study of dimethylphosphinic acid by Tokhadze and co-workers [121, 122] showed a typical *ABC* structure; which is an indication of a strong hydrogen bonding existing within the dimers. Empirical studies have predicted the dimerization energy to be in the range of 25-50 kcal/mol at the temperature range of 400-650K for the double hydrogen bond (O-H---O) [120–123]. On the other hand, the theoretical estimated values for both phosphinic and dimethylphosphinic acids were calculated to be 23.2kcal/mole [115]. Experimentally, the dimerization constants for some phosphinic acid derivatives have been found by measuring their distribution between the aqueous and organic phases [123]. Moreover, inductively coupled plasma (ICP) atomic emission spectroscopy using first-order atomic emission line was employed to determine equilibrium constants of bis(2,4,4-trimethylpentyl) phosphinic and diphenylphosphinic acids from which their dimerization constants were determined [124].

The binding abilities as well as stereochemistry of phosphinic acid derivatives have attracted attention because of the important role they play in the choice of metal extractants [113, 126]. In addition to being used as extraction reagents for metals in

leaching solution they are also used in the purification for actinides and lanthanides [113, 127, 128]. Furthermore, bifunctional phosphinic acid resins in which the phosphinic acid is an extractant ligand supported on a polymer was developed for solid-liquid extraction processes [129, 130]. Very interestingly, phosphinic acids have found applications in homogenous catalysis. Rhodium phosphinate was developed by Adjabeng group [11] and used as a catalyst for the decomposition of α-diazo compounds. In another report, phosphinic acid was employed to reverse the regioselectivity in Pd-catalyzed hydrophosphinylation of alkynes.

7.2. Results and Discussion

7.2.1. Geometry

Understanding the molecular structure of phosphinic acids is crucial as it leads to comprehend other properties including the reactivity and biological activity. We carried out conformational analysis on the phosphinic acids by first calculating potential energy scan for OH and phenyl groups for which the results are presented in Figure 27. The optimized structure of the most stable form of phosphinic acids are shown in Figure 28 These results show that only dimethylphopshinic acid can have its most stable conformation at O=P-O-H dihedral of 0^o. Furthermore, the result presented in Table 27 shows that the *cis* and *trans* configurations are possible for the parent phosphinic acid (PA) and dimethyl derivative while other derivatives could only exist in the gauche configuration. This could be due to steric factor. In addition, they are typical of C_1 and C_s symmetry with only dimethyl derivative having its C_s (a *cis* configuration) being more stable than *trans* by 4.66 kcal/mol. This extra stability could be attributed to the existence of intramolecular hydrogen bonding between the OH and P=O moities. In the case of parent phosphinic acid, gauche is more stable than either cis or trans configurations. This is supported by agreement between experimental and calculated NMR results (see Figure 29) which showed that the two hydrogen atoms are at different chemical environment. Like the parent PA, gauche configuration is the most stable configuration for all the derivatives except the dimethyl one. These are supported with the NMR presented in Figure 30 and Figure 31. On the issue of the dihedral angle between the functional group atoms, only the dimethyl derivative has its most stable conformation at 0^o (cis configuration) while the parent PA and others substituted PAs maintain their most stable form with the dihedral angle being in the range of 33 to 54.6^o (gauche configuration).

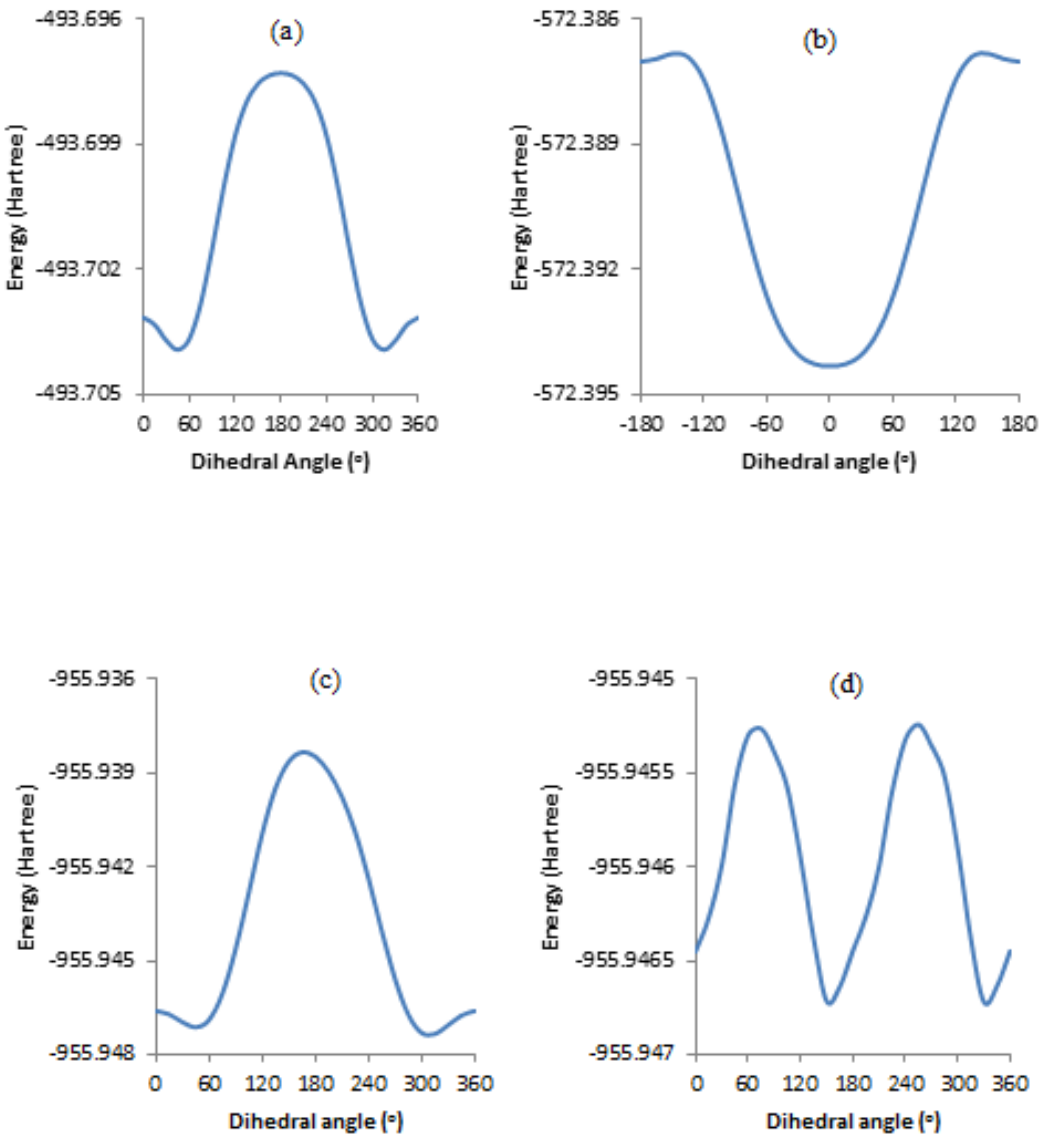

Figure 27. Potential energy scan (PES) for O=P-O-H group of phosphinic acid (a), dimethylphosphinic acid (b), diphenylphospinic acid (c) and phenyl group of diphenylphospinic acid (d).

Table 27. Conformational analysis of phosphinic acid and it derivatives

Molecule	Conformation	OH Dihedral angle (^{o})	Substituent Angle (^{o})	Symmetry	Rel. Energy (kcal/mol)
Phosphinic acid	*Gauche*	40	-	C_1	0.00
	Cis	0	-	C_s	0.38
	Trans	180	-	C_s	4.20
Dimethyphosphinic acid	*Cis*	0	-	C_s	0.00
	Trans	180	-	C_s	4.66
Phenylphosphinic acid	*Gauche*	44.2	168.9	C_1	0.00
	Gauche	41	167.2	C_1	0.47
Diphenylphosphinic acid	*Gauche*	33	77.5, 172.4	C_1	0.00
	Gauche	128.5	27.2, 168.5	C_1	0.31
Bis(4-methoxyphenyl)phosphinic acid	*Gauche*	56.4	9.2, 156.7	C_1	0.00
	Gauche	31.8	74.8, 173.7	C_1	0.31

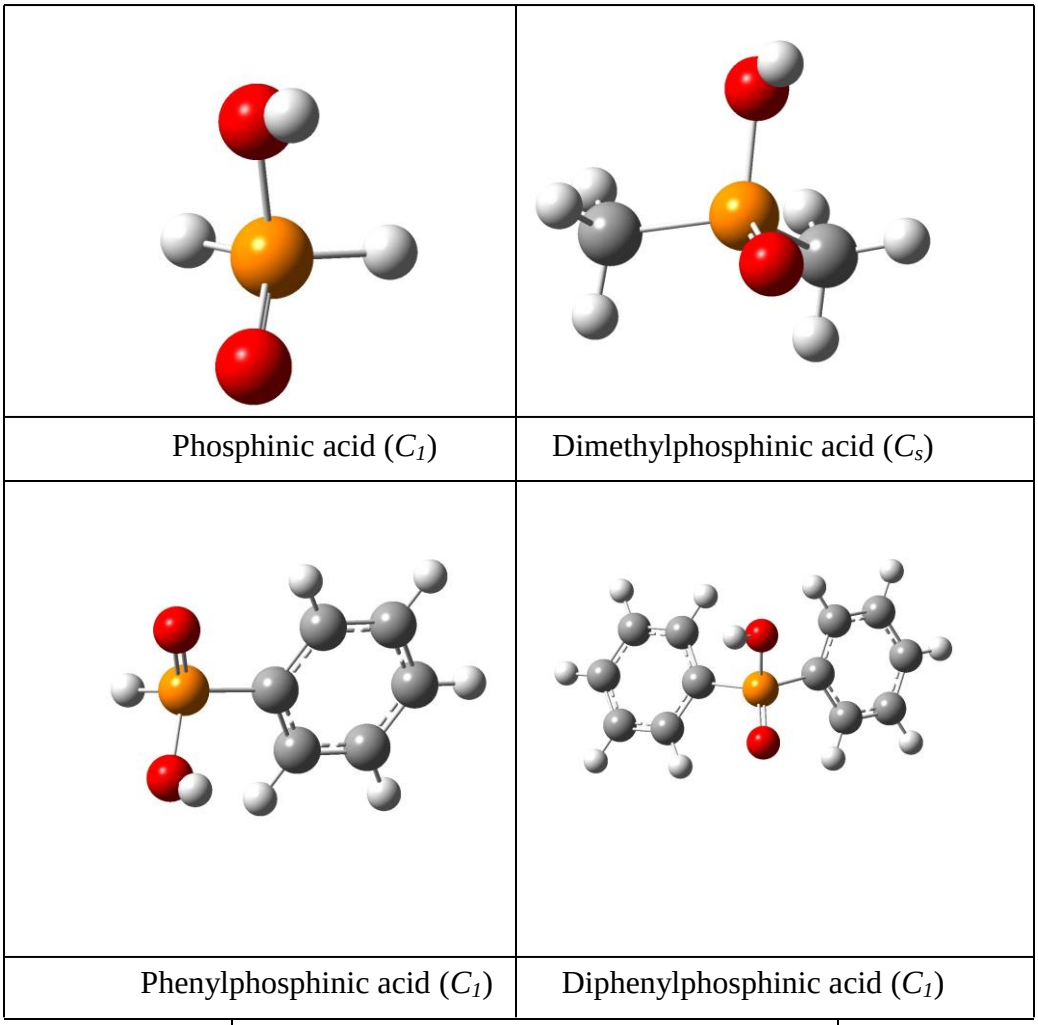

Figure 28. Stable structures for phosphinic acid and its derivatives

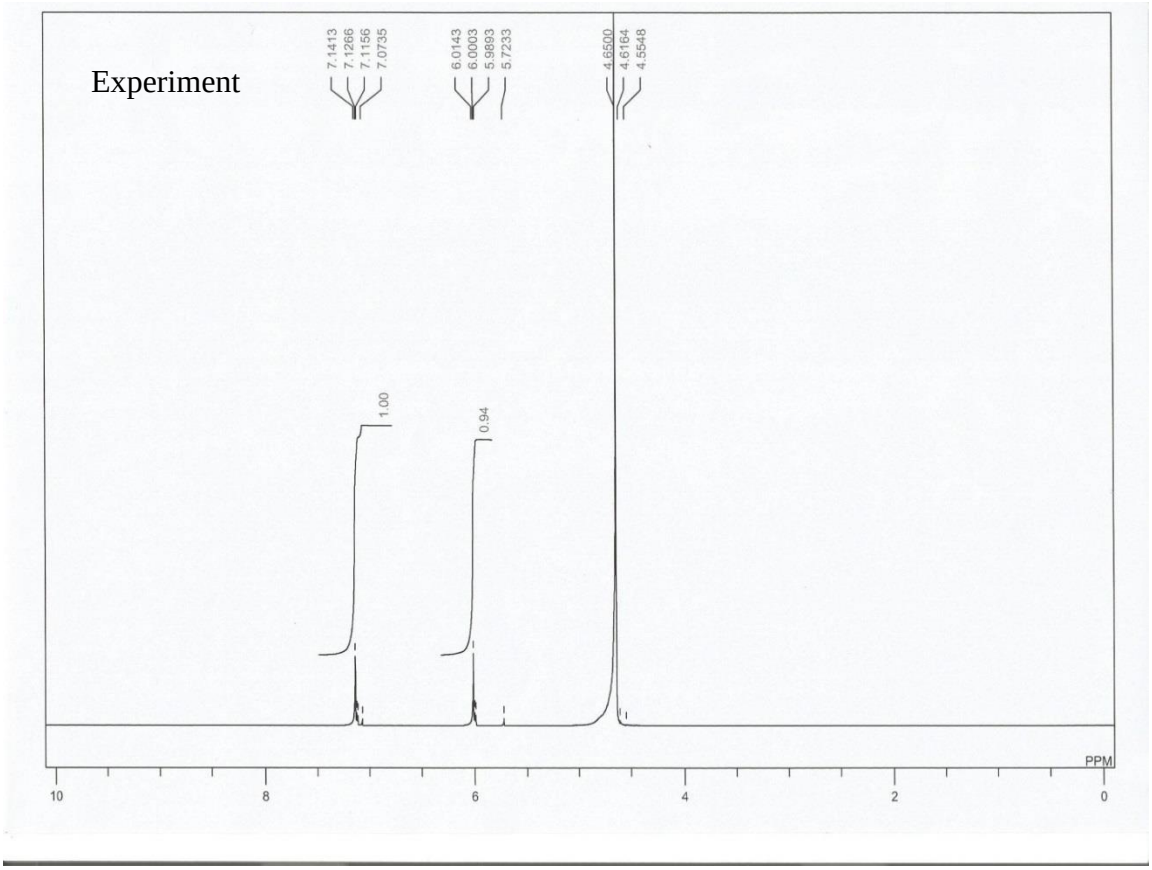

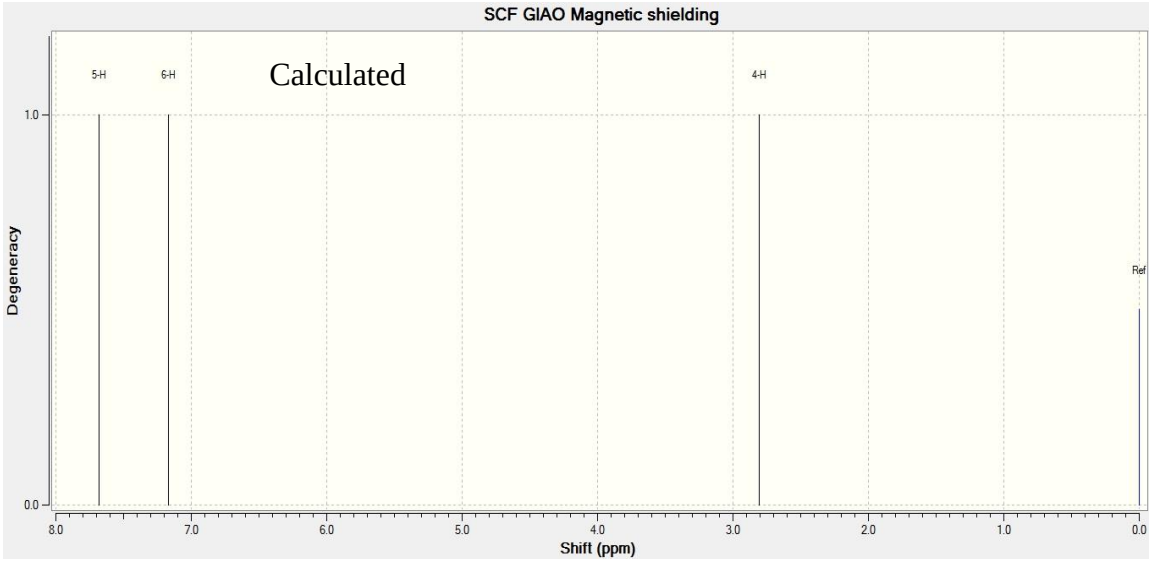

Figure 29. NMR spectra for phosphinic acid

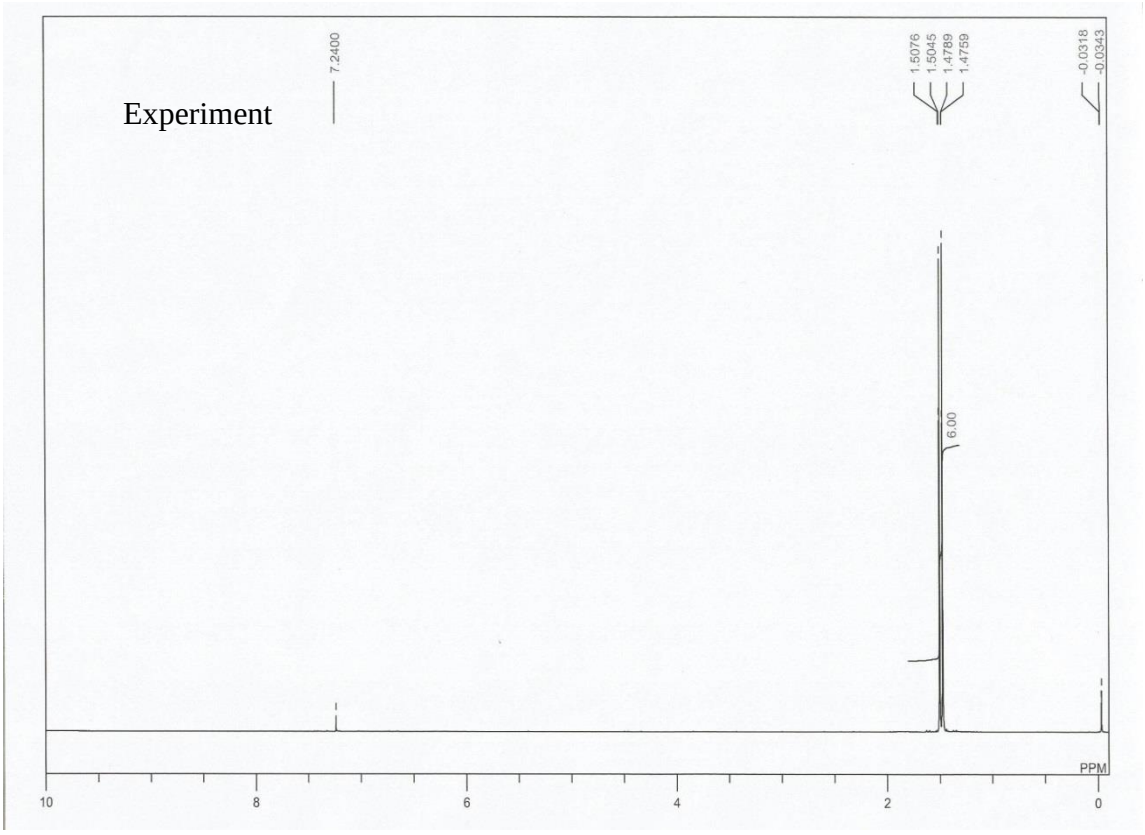

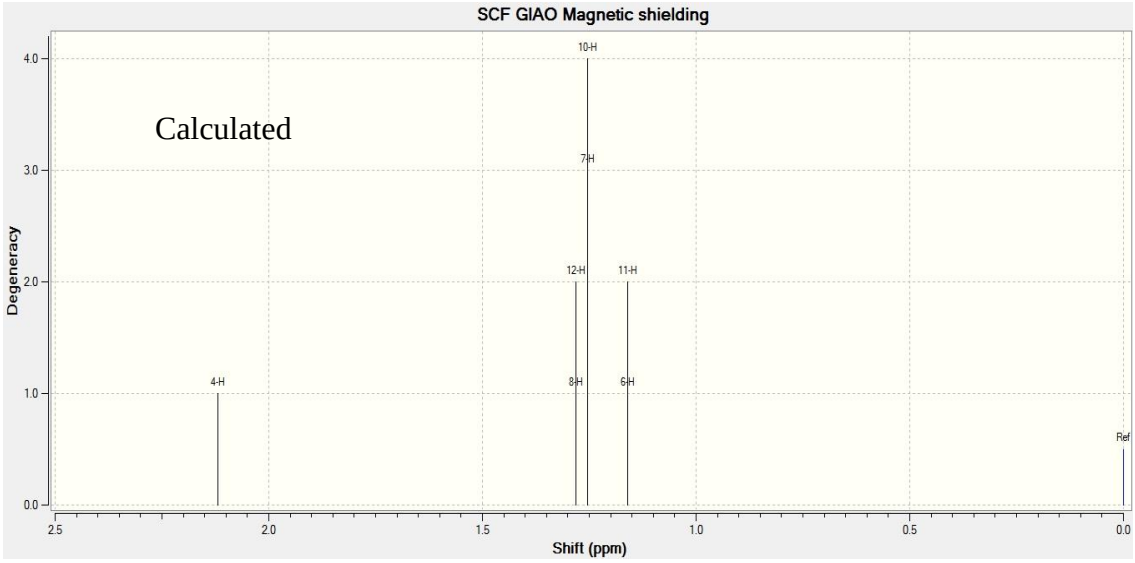

Figure 30. NMR spectra for dimethylphosphinic acid

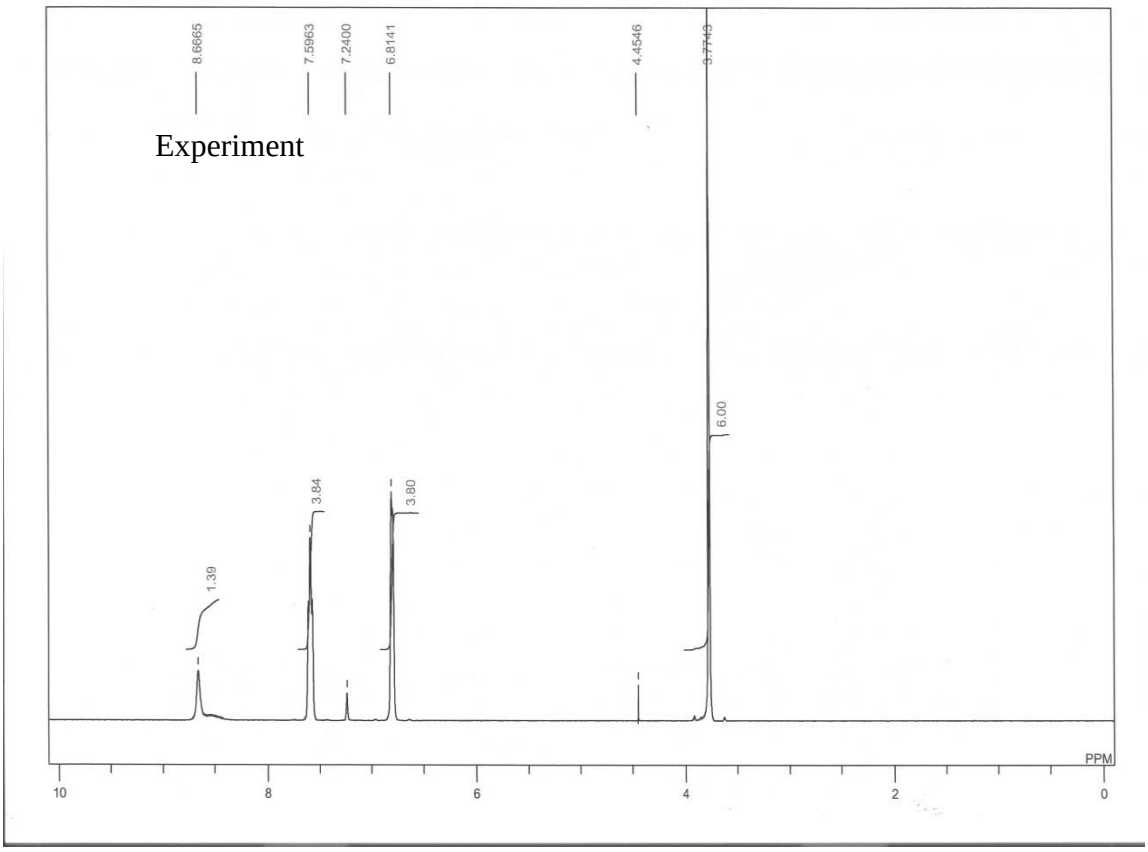

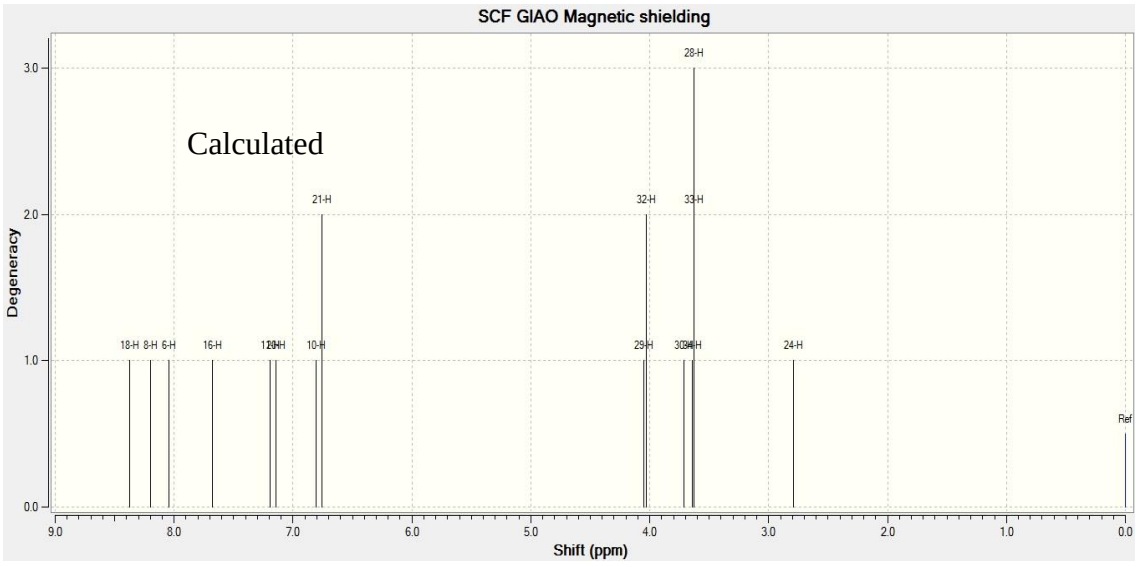

Figure 31. NMR spectra for bis(methoxyphenyl)phosphinic acid

7.2.2. Dimerization

The presence of both a proton donor and acceptor properties in the phosphinic acids facilitates the occurrence of dimerization among monomeric units through hydrogen bonding. The interaction is possible in two ways, one is the single-type interaction which involves The O-H---O=P interaction (Scheme 32a) that results in the common spiral polymeric molecules. The second way is the double-type interaction (Scheme 32b) which results in a cyclic dimer. The dimerization energies obtained from the calculation are presented in Table 28. This result is consistent with experimental values reported in literature for phosphinic acids [120–123]. As can be seen, the magnitude of double-type interaction is almost as twice as that of the single-type of interaction. However, the effect of the nature of substituents on the dimerization energy is more influential in the single-type of interaction. The electron donating substituent (dimethyl) were found to avail more electrons to the P=O oxygen which enhances the strength of the interaction. This interaction consequently causes red shift in vibrational frequencies associated with OH and P=O as reflected in Table 29, because of the hindrance of functional group atoms movement. The frequencies associated with functional groups reduce as the interaction occurs with greater shift being recorded for double interaction. It is important to note that the theoretical results obtained for single interaction are in better agreement with experimental results than double interaction. This is an indication that the single interaction which leads to spiral polymer is the most prominent among the phosphinic acid considered.

(a)

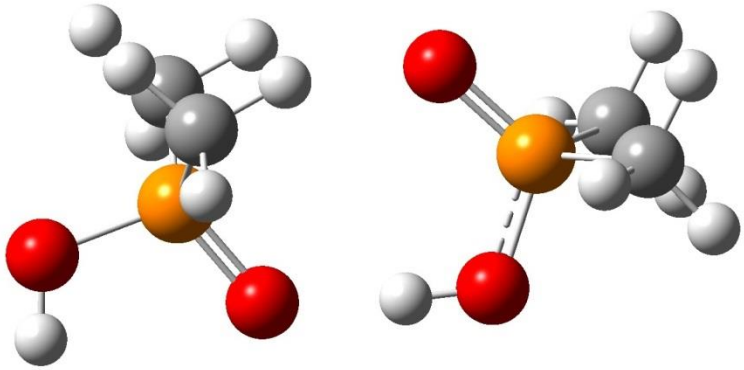

(b)

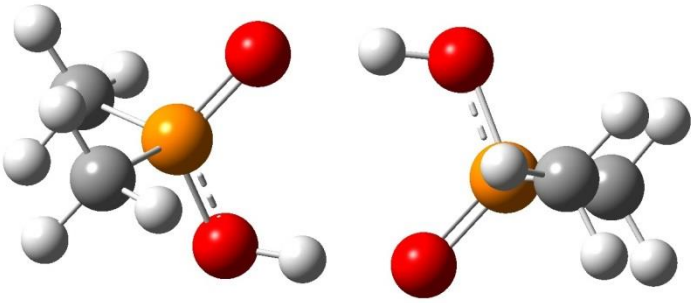

Figure 32. Dimerization between the phosphinic acid molecules, (a) single-type (b) double-type

Table 28. Dimerization energies of single-type and double-type interaction for phosphinic acids

Molecule	Dimerization Energy (kcal/mol)	
	Single	Double
Phosphinic acid	15.59	24.37
Dimethyphosphinic acid	16.22	24.57
Phenylphosphinic acid	12.14	23.94
Diphenylphosphinic acid	15.13	24.47
Bis(4-methoxyphenyl)phosphinic acid	13.82	23.88

Table 29. Frequencies associated with OH and P=O stretching mode

Molecule	Monomer		Dimer				Experiment			
			Double		Single		Raman		IR	
	OH	P=O	OH	P=O	OH	P=O	OH	P=O	OH	P=O
Phosphinic acid	3779	1243	3011	1125	3124	1202	3412	1162	3261	1161
Dimethyphosphinic acid	3684	1221	2872	1109	3048	1145	3000	-	3014	1264
Phenylphosphinic acid	3671	1226	2837	1135	3194	1208	3064	1186	3075	1197
Diphenylphosphinic acid	3677	1218	2786	1130	3118	1158	3061	1186	3074	1183
Bis(4-methoxyphenyl)phosphinic acid	3677	1212	2792	1130	3124	1164	3068	1214	3066	1205

7.2.3. Reactivity

HOMO-LUMO energy gap is an indicator for molecule reactivity, the lower the value is, the more reactive the molecule would be. In this context, the reactivity of these phosphinic acids as shown in Table 30 would be in the order of phosphinic acid > dimethylphosphinic > bis(4-methoxyphenyl)phosphinic > diphenylphosphinic > phenylphosphinic. Orbital feature is another important factor worthy of considering in reactivity. Big size signifies easy molecular orbital overlap and as such, the big shape of parent phosphinic and dimethylphosphinic acid LUMO portrayed in Figure 33, further affirms their higher reactivity over other phosphinic acids. The HOMO is usually related to ionization potential (IP) as it is charged with the responsibility of donating electron while the LUMO which accepts electrons is related to electron affinity (EA). The HOMO energy level of parent PA suggests that it would need more energy than any of it derivatives for electron donation while its LUMO energy level indicates the easy of accepting electrons more than any of them. This assertion is corroborated by the reactivity result data presented in Table 31. The high IP value obtained for PA indicates its low basicity, although they are all generally less basic. On the other hand, their electron affinity values suggest that they are acidic with parent PA being the most acidic. Another parameters worthy of considering are the hardness and electronegative as these are important in choosing ligands for complexation. As it could be seen in Table 33, the hardness is inversely related to size of the molecule. The parent PA which is the smallest among them happened to be the hardest (5.46) while bis(4-methoxyphenyl) phosphinic acid the largest is the softest (3.84) as reflected in the Table. This result is consistent with literature [1] and in this regard, the PA as a ligand would be much compatible with hard metal while the bis(4-methoxyphenyl)phosphinic would prefer soft metal. In the same

sense, PA which is the most electronegative among them (see Table 31) would be a suitable ligand for a system saturated with electrons.

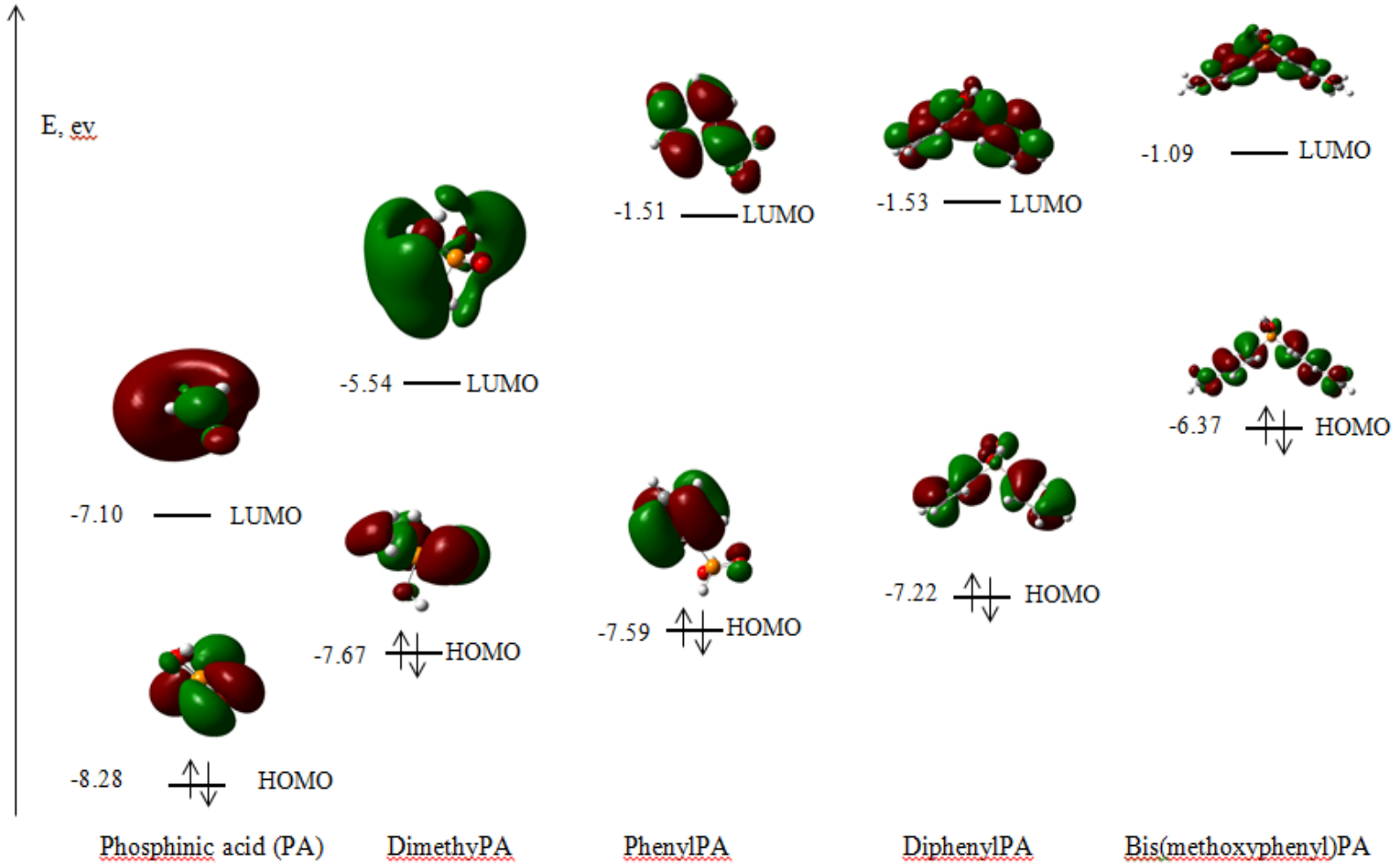

Figure 33. Frontier orbitals for phosphinic acids

Table 30. HOMO – LUMO energy gap of phosphinic acids

Molecule	Energy level (ev)		Energy gap (ev)
	HOMO	LUMO	
Phosphinic acid	-8.28	-7.10	1.18
Dimethyphosphinic acid	-7.67	-5.54	2.13
Phenylphosphinic acid	-7.59	-1.51	6.09
Diphenylphosphinic acid	-7.22	-1.53	5.70
Bis(4-methoxyphenyl)phosphinic acid	-6.37	-1.09	5.28

Table 31. Calculated ionization potential (IP), electron affinity (EA), hardness (η) and absolute electronegativity (χ) in ev

Molecule	IP	EA	η	χ
Phosphinic acid	10.55	-0.38	5.46	5.09
Dimethyphosphinic acid	9.67	-0.38	5.02	4.64
Phenylphosphinic acid	9.22	0.09	4.57	4.66
Diphenylphosphinic acid	8.61	0.24	4.18	4.43
Bis(4-methoxyphenyl)phosphinic acid	7.59	-0.08	3.84	3.76

7.3. $[Rh(\mu\text{-}O_2PMe_2)(COD)]_2$ (Di-μ-dimethylphosphinate bis(1,5-cyclooctadiene) di-rhodium(I))

The synthesis and characterization of this complex were carried out at Department of Inorganic Chemistry, Institute of Chemical Synthesis and Homogeneous Catalysis, University of Zaragoza, Spain. C and H elemental analysis carried out on the complex confirmed the proposed formulation. Furthermore, mass spectrometry gave the exact mass to be 608.0199 with mass/charge ratio being recorded as 608.0199 (100%), 609.0232 (21.6%) and 610.0266 (2.2%). As for the X-ray, the dinuclear unit consists of two rhodium atoms which have square planar geometry with 1,5-cyclooctadiene if the middles of C=C are considered as vertexes (see Figure 34). Unlike the common dinulear complexes, the bridging atoms in this complex are two oxygen atoms bonded with phosphorus atom to give octagonal shaped bridging centre. Rh Rh separation is 3.892 Å while the four Rh-O bond lengths are not uniform (2.076 Å, 2.089 Å, 2.090 Å and 2.106 Å). The other bond lengths as well as bond angles can be seen in Table 32 and Table 33 respectively. As it can be seen in the Tables for selected bond lengths and bond angles there is a good agreement between the X-ray data and theoretical calculation. For spectroscopy analysis, Raman spectrum was recorded as presented in Figure 35. Frequencies in the range of 3000-2830cm^{-1} are those associated with vibrational modes in cycloocadiene while the one of 1470cm^{-1} is for distorted double bond due to coordination with metal centre. On the other hand those associated with dimethylphosphinic acid are found from 1431cm^{-1} downward. On the issue of reactivity, the complex was found to have limited catalytic activity. It has poor activity towards transfer hydrogenation reaction. When it was made to undergo carbonylation reaction, its diolefins were replaced by carbon monoxide to give unstable complex **2** as illustrated in Figure 32. This complex

2 latter lost CO to atmosphere to give back dimethylphosphinic acid, which formed the bridging ligand for complex **1**. Figure 36 summarizes other ways of carbonylation reactions which were carried out on complex **1** but ended up in producing dimethylphosphinic acid.

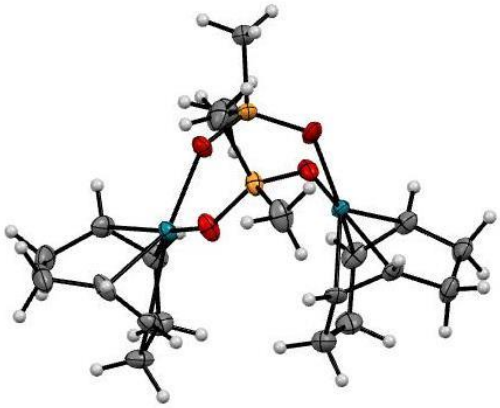

Figure 34. ORTEP view of $[Rh(\mu\text{-}O_2PMe_2)(COD)]_2$

Crystal data:

$[C_{20}H_{36}O_4P_2Rh_2]$, triclinic, *P-1*, a = 9.5370(15) Å, b = 9.7552 Å, c= 14.656(2) Å, α = 103.267(2)°, β = 95.938(2)°, γ = 117.358(2)°, Z = 2, M_r = 608.25, V = 1143.8(3) Å^3, D_{calcd} = 1.766 gcm^{-3}, λ(Mo Kα) = 0.71073 Å, T = 100K, μ = 1.606 mm^{-1}, 12054 reflections collected, 5799 unique (R_{int} = 0.0783), 4355 observed, $R1(F_o)$ = 0.0393 [$I > 2\sigma(I)$], $wR2(F_o^2)$ = 0.0862 (all data), GOF = 1.063.

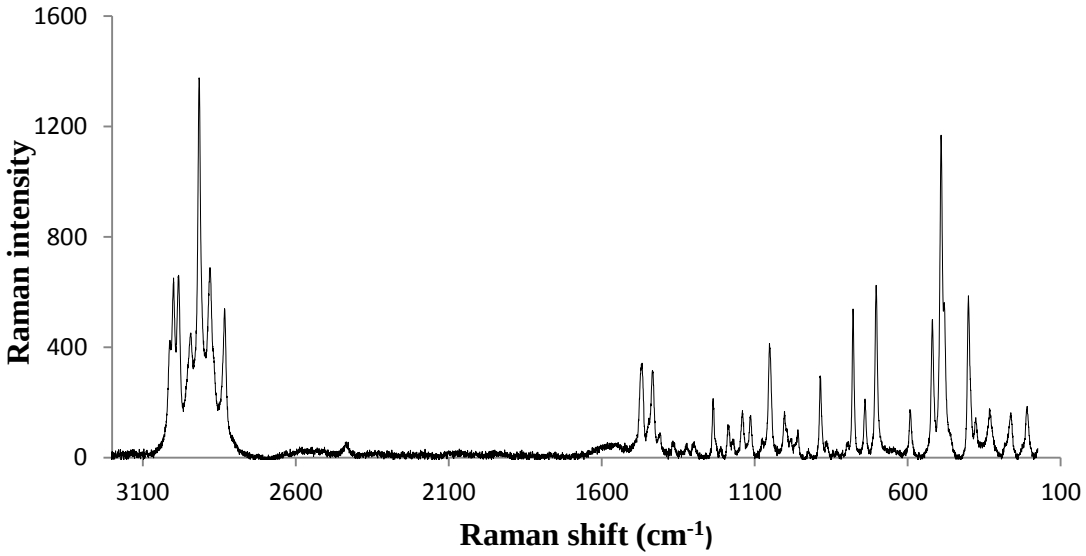

Figure 35. Raman spectrum for $[Rh(\mu\text{-}O_2PMe_2)(COD)]_2$

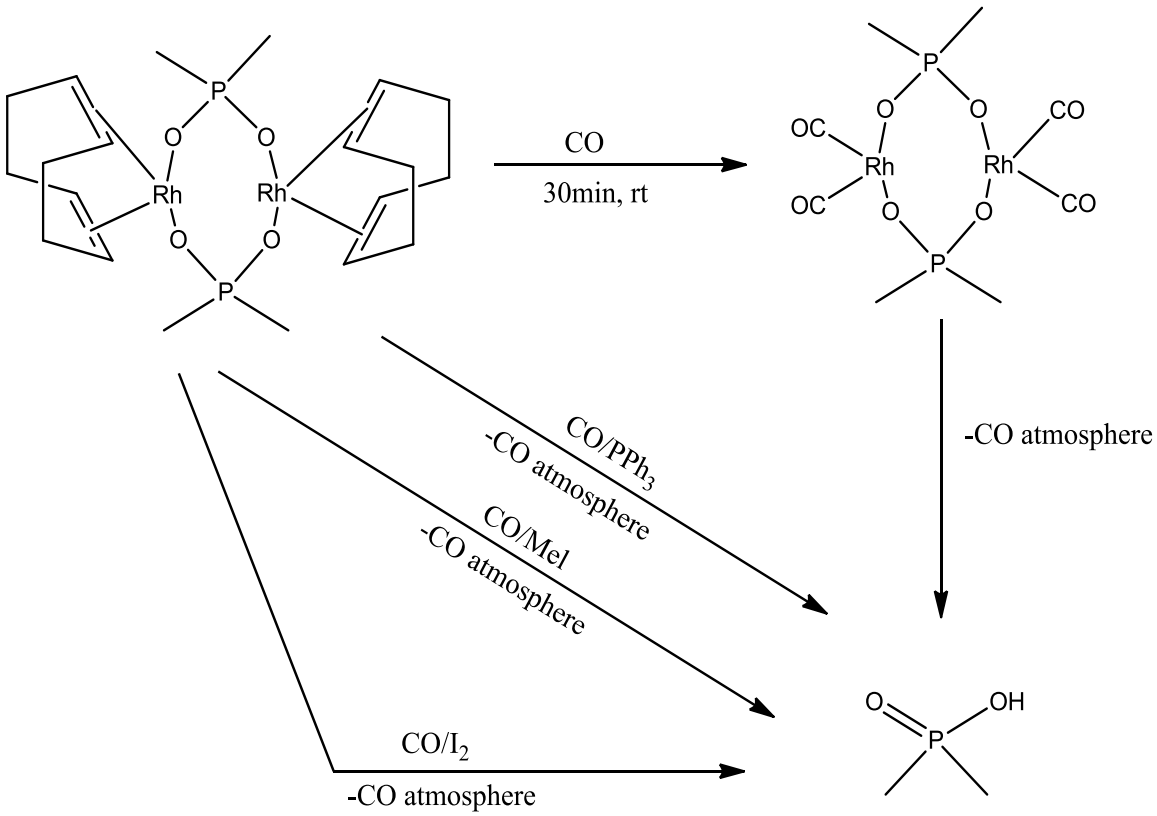

Figure 36. Reactivity schemes for $[Rh(\mu\text{-}O_2PMe_2)(COD)]_2$

Table 32. Selected bond lengths for $[Rh(\mu\text{-}O_2PMe_2)(COD)]_2$ complex

Bond	Bond length (Å)	
	X-Ray	Calculated
Rh_1-O_3	2.106(2)	2.138
Rh_1-O_8	2.090(3)	2.117
Rh_1-C_9	2.084(4)	2.129
Rh_1-C_{10}	2.078(3)	2.108
Rh_1-C_{11}	2.109(5)	2.133
Rh_1-C_{12}	2.086(5)	2.107
Rh_2-O_5	2.076(3)	2.121
Rh_2-O_6	2.076(3)	2.136
Rh_2-C_{13}	2.076(3)	2.112
Rh_2-C_{14}	2.099(4)	2.124
Rh_2-C_{15}	2.074(5)	2.108
Rh_2-C_{16}	2.106(4)	2.129
P_4-O_3	1.512(3)	1.543
P_4-O_5	1.505(4)	1.543
P_4-C_{25}	1.813(4)	1.822
P_4-C_{26}	1.777(5)	1.818
P_7-O_6	1.509(4)	1.542
P_7-O_8	1.523(4)	1.543
P_7-C_{27}	1.786(5)	1.818
P_7-C_{28}	1.797(3)	1.822
C_9-C_{10}	1.429(8)	1.408
C_{11}-C_{12}	1.503(9)	1.408
C_{13}-C_{14}	1.509(7)	1.408
C_{15}-C_{16}	1.530(6)	1.409

Table 33. Selected bond angles for $[Rh(\mu\text{-}O_2PMe_2)(COD)]_2$ complex

	Bond Angle (^{o})	
	X-ray	Calculated
O_3-Rh_1-O_8	90.7(1)	91.0
O_3-Rh_1-C_9	161.3(2)	160.6
O_3-Rh_1-C_{10}	157.6(2)	160.6
O_3-Rh_1-C_{11}	89.0(2)	94.3
O_3-Rh_1-C_{12}	86.0(2)	89.6
O_8-Rh_1-C_9	92.7(2)	86.8
O_8-Rh_1-C_{10}	94.5(2)	89.5
O_8-Rh_1-C_{11}	168.7(2)	162.2
O_8-Rh_1-C_{12}	152.9(2)	158.5
C_9-Rh_1-C_{10}	40.2(2)	38.8
C_9-Rh_1-C_{11}	91.3(2)	99.5
C_9-Rh_1-C_{12}	82.7(2)	82.6
C_{10}-Rh_1-C_{11}	81.8(2)	83.0
C_{10}-Rh_1-C_{12}	98.8(2)	91.2
C_{11}-Rh_1-C_{12}	38.3(2)	38.8
O_5-Rh_2-O_6	88.6(1)	91.6
O_5-Rh_2-C_{13}	167.4(2)	160.3
O_5-Rh_2-C_{14}	153.0(2)	160.3
O_5-Rh_2-C_{15}	92.0(2)	85.9
O_5-Rh_2-C_{16}	93.0(2)	89.9
O_6-Rh_2-C_{13}	91.6(2)	92.0
O_6-Rh_2-C_{14}	90.0(2)	91.3
O_6-Rh_2-C_{15}	163.3(2)	167.0
O_6-Rh_2-C_{16}	157.2(2)	154.1
C_{13}-Rh_1-C_{14}	39.6(2)	38.8
C_{13}-Rh_1-C_{15}	91.4(2)	99.0
C_{13}-Rh_1-C_{16}	82.0(2)	82.4
C_{14}-Rh_1-C_{14}	81.9(2)	83.0
C_{14}-Rh_1-C_{15}	98.6(2)	91.6
C_{15}-Rh_1-C_{16}	39.4(2)	38.8
O_3-P_4-O_5	117.2(2)	116.1

Table 33

Continued

	Bond Angle (^{o})	
	X-ray	Calculated
O_3-P_4-C_{25}	106.0(2)	108.5
O_3-P_4-C_{26}	109.6(2)	109.1
O_5-P_4-C_{25}	107.9(2)	106.7
O_5-P_4-C_{26}	109.9(2)	109.7
C_{25}-P_4-C_{26}	105.4(2)	106.2
O_6-P_7-O_8	116.2(2)	116.2
O_6-P_7-C_{27}	107.9(2)	109.1
O_6-P_7-C_{28}	110.8(2)	108.6
O_8-P_7-C_{27}	108.6(2)	106.7
O_8-P_7-C_{28}	107.2(2)	109.9
C_{27}-P_7-C_{28}	105.6(2)	105.9

7.4. Conclusion

Steric nature of substituents plays a key role in the phosphinic acids configuration. Cis and trans conformations are possible for methyl substituent while only gauche conformation is possible for aryl and other more bulky substituents. The presence of OH and P=O moieties in the phosphinic acid warranted dimerization due to hydrogen bonding and this made them to occur in either spiral or cyclic form depending on the type of interactions. These interactions cause reduction in frequencies associated with OH and P=O modes of vibration with greater effect being felt in double interaction. However, the calculated vibrational frequencies for single interactional are in good agreement with the experiment. On the other hand, the HOMO-LUMO energy gap indicated the reactivity of phosphinic acid to be in the order of phosphinic acid > dimethylphosp-hinic > bis(4-methoxyphenyl)phosphinic > diphenylphosphinic >phenylphosphin-ic. Theoretical calculation also shows that parent phosphinic and dimethylphosphinic acid are acidic in nature and are favoured by easy molecular orbital overlap. However, the rhodium binuclear complex produced from dimethylphosphinic was found to be of limited reactivity.

REFERENCES

[1] R.H. Crabtree, *The Organometallic Chemistry of the Transition Metals*. John Wiley and Sons, 2009.

[2] L.A. Oro and C. Claver, *Iridium Complexes in Organic Synthesis*. Wiley-VCH (Weinheim), 2009.

[3] S.A. Popoola, E.A. Jaseer, A.A. Al-Saadi, V. Polo, M.A. Casado, and L.A. Oro, "Iridium Complexes as Catalysts in the Hydrogen Transfer of Isopropanol to Acetophenone: Ligand Effects and DFT Studies," *Inorg. Chim. Acta*, vol. 436, pp. 146–151, 2015.

[4] I. Mena, E.A Jaseer, M.A Casado, P. García-Orduña, F.J. Lahoz, and L.A. Oro, "Terminal and Bridging Parent Amido 1,5-cyclooctadiene Complexes of Rhodium and Iridium.," *Chem. Eur. J.*, vol. 19, pp. 5665–5675, 2013.

[5] E.L. Kolychev, S. Kronig, K. Brandhorst, M. Freytag, P.G. Jones, and M. Tamm, "Iridium(I) Complexes with Anionic N-heterocyclic Carbene Ligands as Catalysts for the Hydrogenation of Alkenes in Nonpolar Media.," *J. Am. Chem. Soc.*, vol. 135, pp. 12448–12459, 2013.

[6] L.D. Field, B.A. Messerle, K.Q. Vuong, and P. Turner, "Rhodium(I) and Iridium(I) Complexes Containing Bidentate Phosphine-Imidazolyl Donor Ligands as Catalysts for the Hydroamination and Hydrothiolation of alkynes.," *Dalton Trans.*, no. 18, pp. 3599–3614, 2009.

[7] A.R. Chianese and R.H. Crabtree, "Axially Chiral Bidentate N-Heterocyclic Carbene Ligands Derived from BINAM: Rhodium and Iridium Complexes in Asymmetric Ketone Hydrosilylation," *Organometallics*, vol. 24, pp. 4432–4436, 2005.

[8] Y. Kishimoto, P. Eckerle, T. Miyatake, M. Kainosho, A. Ono, T. Ikariya, and R. Noyori, "Well-Controlled Polymerization of Phenylacetylenes with Organorhodium(I) Complexes: Mechanism and Structure of the Polyenes," *J. Am. Chem. Soc.*, vol. 121, pp. 12035–12044, 1999.

[9] Y. Kishimoto, T. Miyatake, T. Ikariya, and R. Noyori, "An Efficient Rhodium(I) Initiator for Stereospecific Living Polymerization of Phenylacetylenes," *Macromolecules*, vol. 29, pp. 5054–5055, 1996.

[10] Y. Kishimoto, P. Eckerle, T. Miyatake, T. Ikariya, and R. Noyori, "Living Polymerization of Phenylacetylenes Initiated by $Rh(C{\equiv}CC_6H_5)$(2,5-norbornadiene)$[P(C_6H_5)_3]_2$," *J. Am. Chem. Soc.*, vol. 116, pp. 12131–12132, 1994.

[11] G.M. Adjabeng, D.A. Gerritsma, H. Bhanabhai, C.S. Frampton, and A. Capretta, "Rhodium Phosphinates as Catalysts for Metal-Stabilized Carbene Chemistry: Synthesis, Characterization, and Application of $Rh_2(O_2PMe_2)_4$," *Organometallics*, vol. 25, pp. 32–34, 2006.

[12] M. Gasperini, F. Ragaini, C. Remondini, A. Caselli, and S. Cenini, "The Palladium–Phenanthroline Catalyzed Carbonylation of Nitroarenes to Diarylureas:

Effect of Chloride and Diphenylphosphinic Acid," *J. Organomet. Chem.*, vol. 690, pp. 4517–4529, 2005.

[13] D.W. Wertz and M.A. Moseley, "Vibrational Study of the Metal-Olefin Bond in 1,5-Cyclooctadiene Complexes of Rhodium(I), Palladium(II), and Platinum(II)," *Inorg. Chem.*, vol. 19, pp. 705–708, 1980.

[14] D. Breitinger, H. Meinberg, and A. Bogner, "Vibrational Spectra of Ammine–Sulfito Complexes of Rhodium," *J. Mol. Struct.*, vol. 482–483, pp. 131–135, 1999.

[15] P. Stein, M.K. Dickson, and D.M. Roundhill, "Raman and Infrared Spectra of Binuclear Platinum(II) and Platinum(III) Octaphosphite Complexes. A Characterization of the Intermetallic Bonding," *J. Am. Chem. Soc.*, vol. 105, pp. 3489–3494, 1983.

[16] M.J. Grogan and K. Nakamoto, "Infrared Spectra and Normal Coordinate Analysis of Metal-Olefin Complexes. I. Zeise's Salt Potassium Trichloro(ethylene)platinate(II) Monohydrate," *J. Am. Chem. Soc.*, vol. 88, pp. 5454–5460, 1966.

[17] W.J. van Zeist and F.M. Bickelhaupt, "Steric Nature of the Bite Angle. A Closer and a Broader Look," *Dalton Trans.*, vol. 40, pp. 3028–3038, 2011.

[18] P. Dierkes and P.W.N.M. van Leeuwen, "The Bite Angle Makes the Difference: a Practical Ligand Parametre for Diphosphine Ligands," *J. Chem. Soc. Dalt. Trans.*, no. 10, pp. 1519–1529, 1999.

[19] P.W.N.M. van Leeuwen, P.C.J. Kamer, J.N.H. Reek, and P. Dierkes, "Ligand Bite Angle Effects in Metal-catalyzed C-C Bond Formation," *Chem. Rev.*, vol. 100, pp. 2741–2769, 2000.

[20] W. van Zeist, R. Visser, and F.M. Bickelhaupt, "The Steric Nature of the Bite Angle," *Chem. Eur. J.*, vol. 15, pp. 6112–6115, 2009.

[21] R. Uson, L.A. Oro, R. Sariego, M.A. Esteruelas, "Catalytic Transfer Hydrogenation by Cationic Rhodium(I) Complexes," *J. Organomet. Chem.*, vol. 214, pp. 399–404, 1981.

[22] J.S.M. Samec, J.E. Bäckvall, P.G. Andersson, and P. Brandt, "Mechanistic Aspects of Transition Metal-Catalyzed Hydrogen Transfer Reactions.," *Chem. Soc. Rev.*, vol. 35, pp. 237–48, 2006.

[23] S. Yasar, S. Cekirdek, N.A. Tas, S. Yildirim, "An Efficient Ligand-Free Method for the Transfer Hydrogenation of Ketones and Aldehydes Catalyzed by Different Complexes," *Turk. J. Chem.*, vol. 37, pp. 292–298, 2013.

[24] R. Spogliarich, A. Tencich, J. Kaspar, and M. Graziani, "Hydrogenation of Ketones and Olefins via Hydrogen Transfer Catalyzed by Rhodium and Iridium Phosphine Complexes," *J. Organomet. Chem.*, vol. 240, pp. 453–459, 1982.

[25] G. Zassinovich, G. Mestroni, and S. Gladiali, "Asymmetric Hydrogen Transfer Reactions Promoted by Homogeneous Transition Metal Catalysts," *Chem. Rev.*, vol. 92, pp. 1051–1069, 1992.

[26] S.H. Oakley, M.P. Coogan, and R.J. Arthur, "Synthesis of Bis(imino)aryl Iridium Pincer Complexes and Demonstration of Catalytic Hydrogen-Transfer Activity," *Organometallics*, vol. 26, pp. 2285–2290, 2007.

[27] J.R. Miecznikowski and R.H. Crabtree, "Transfer Hydrogenation Reduction of Ketones, Aldehydes and Imines using Chelated Iridium(III) N-heterocyclic Bis-carbene Complexes," *Polyhedron*, vol. 23, pp. 2857–2872, 2004.

[28] S. Gladiali, G. Mestroni, M. Beller, and C. Bolm, *Transition Metals for Organic Synthesis*. Wiley-VCH (Weinheim), 2004.

[29] S. Ogo, N. Makihara, and Y. Watanabe, "pH-Dependent Transfer Hydrogenation of Water-Soluble Carbonyl Compounds with $[Cp^*Ir^{III}(H_2O)_3]^{2+}$ ($Cp^* = \eta^5$-C_5Me_5) as a Catalyst Precursor and HCOONa as a Hydrogen Donor in Water," *Organometallics*, vol. 18, pp. 5470–5474, 1999.

[30] C. Bianchini, L. Glendenning, F. Zanobini, M. Graziani, and E. Nagy, "Asymmetric Hydrogen-Transfer Reduction of Prochiral and α,β-Unsaturated Ketones by Iridium Complexes Containing Optically Pure Aminodiphosphine Ligands," *J. Mol. Catal. A Chem.*, vol. 132, pp. 13–19, 1998.

[31] D.G.I. Petra, P.C.J. Kamer, A.L. Spek, H.E. Schoemaker, and P.W.N.M. van Leeuwen, "Aminosulf(ox)ides as Ligands for Iridium(I)-Catalyzed Asymmetric Transfer Hydrogenation," *J. Org. Chem.*, vol. 65, pp. 3010–3017, 2000.

[32] X. Wu, J. Liu, X. Li, A. Zanotti-Gerosa, F. Hancock, D. Vinci, J. Ruan, and J. Xiao, "On Water and in Air: Fast and Highly Chemoselective Transfer Hydrogenation of Aldehydes with Iridium Catalysts," *Angew. Chem. Int. Ed.*, vol. 45, pp. 6718–6722, 2006.

[33] Z.E. Clarke, P.T. Maragh, T.P. Dasgupta, D.G. Gusev, A.J. Lough, K. Abdur-rashid, V. Uni, W. Indies, C. Street, M. Centre, S. Tower, and O. Mg, "A Family of Active Iridium Catalysts for Transfer Hydrogenation of Ketones," *Organometallics*, vol. 25, pp. 4113–4117, 2006.

[34] Y. Ishii, M. Takeno, Y. Kawasaki, A. Muromachi, Y. Nishiyama, and S. Sakaguchi, "Acylation of Alcohols and Amines with Vinyl Acetates Catalyzed by $Cp^*_2Sm(thf)_2$," *J. Org. Chem.*, vol. 61, pp. 3088–3092, 1996.

[35] J.L. Herde, J.C. Lambert, and C.V. Senoff, "Cyclooctene and 1,5-Cyclooctadiene Complexes of Iridium(1)," *Inorg. Synth.*, vol. 15, pp. 18–20, 1974.

[36] G. Giordano and R. H. Crabtree, "Di-μ-chloro-bis(η^4- 1,5-Cyclooctadiene)-Dirhodium(1)," *Inorg. Synth.*, vol. 19, pp. 218–219, 1979.

[37] R. Uson, L.A. Oro, and J.A. Cabeza, "Dinuclear Methoxy, Cyclooctadiene, and Barrelene Complexes of Rhodium(I) and Iridium(I)," *Inorg. Synth.*, vol. 23, pp. 126–130, 1985.

[38] M.A. Esteruelas and L.A. Oro, "Iridium and Rhodium Complexes with Tetrafluorobenzobarrelene Diolefins," *Coord. Chem. Rev.*, vol. 193–195, pp. 557–618, 1999.

[39] G.E.S.M.J. Frisch, G.W. Trucks, H.B. Schlegel, B.M.M.A. Robb, J.R. Cheeseman, G. Scalmani, V. Barone, H.P.H.G.A. Petersson, H. Nakatsuji, M. Caricato, X. Li, M.H.A.F. Izmaylov, J. Bloino, G. Zheng, J.L. Sonnenberg, T.N.M. Ehara, K. Toyota, R. Fukuda, J. Hasegawa, M. Ishida, J.Y. Honda, O. Kitao, H. Nakai, T. Vreven, J.A. Montgomery, E.B.J.E. Peralta, F. Ogliaro, M. Bearpark, J.J. Heyd, J.N.K.N. Kudin, V.N. Staroverov, T. Keith, R. Kobayashi, J.T.K. Raghavachari, A. Rendell, J.C. Burant, S.S. Iyengar, J.B.C.M. Cossi, N. Rega, J.M. Millam, M. Klene, J.E. Knox, R.E.S.V. Bakken, C. Adamo, J. Jaramillo, R. Gomperts, J.W.O.O. Yazyev, A.J. Austin, R. Cammi, C. Pomelli, G.A.V.R.L. Martin, K. Morokuma, V.G. Zakrzewski, A.D.D.P. Salvador, J.J. Dannenberg, S. Dapprich, J.C.O. Farkas, J.B. Foresman, J.V. Ortiz, and D.J. Fox, Gaussian, Inc., Wallingford CT, "Gaussian 09, Revision D.01." 2013.

[40] S. Grimme, J. Antony, S. Ehrlich, and H. Krieg, "A Consistent and Accurate Ab Initio Parametrization of Density Functional Dispersion Correction (DFT-D) for the 94 Elements H-Pu," *J. Chem. Phys.*, vol. 132, pp. 154104, 2010.

[41] T. Chen, X. Liu, and M. Shi, "Synthesis of New NHC–Rhodium and Iridium Complexes Derived from 2,2′-Diaminobiphenyl and Their Catalytic Activities Toward Hydrosilylation of Ketones," *Tetrahedron*, vol. 63, pp. 4874–4880, 2007.

[42] M.P. Garcia, J.L. Millan, M.A. Esteruelas, and L.A. Oro, "Rhodium(I) Complexes with the 2,2′-Bipyrimidine Ligand," *Polyhedron*, vol. 6, pp. 1427–1431, 1987.

[43] E. Mas-Marza, M. Sanau, and E. Peris, "Synthesis and Reactivity of New Complexes of Rhodium and Iridium with Bis(dichloroimidazolylidene) Ligands . Electronic and Catalytic Implications of the Introduction of the Chloro Substituents in the NHC Rings," *Organometallics*, vol. 25, pp. 3063–3069, 2006.

[44] D.J.A. De Ridder and P. Imhoff, "Di-μ-chloro-bis[(cis,cis-η4-1,5-cyclooctadiene)rhodium(I)]: a Redetermination," *Acta Crystallogr. Sect. C Cryst. Struct. Commun.*, vol. 50, pp. 1569–1572, 1994.

[45] J.A. Ibers and R.G. Snyder, "Crystal Structure of the Dimer of Rhodium Chloride 1,5-Cyclooctadiene," *Acta Crystallogr.*, vol. 15, pp. 923–930, 1962.

[46] G. Pannetier Et, D.Tabrizi, "Etude Radiocristallographique Du Di-μ-chloro-bis (π-cyclooctadiene-1,5) Diiridium [(COD-1,5)lrCl]$_2$, Variété Orthorhombique (Rouge-Rubis)," *J. Less Common Met.*, vol. 23, pp. 110–112, 1971.

[47] F.A. Cotton, P. Lahuerta, M. Sanau, and W. Schwotzer, "Air oxidation of $Ir_2(Cl)_2(COD)_2$ Revisited. The structures of $[Ir(\mu_2\text{-}Cl)(COD)]_2$(Ruby Form) and its Oxidation Product, $Ir_2Cl_2(COD)_2(\mu_2\text{-}OH)_2(\mu_2\text{-}O)$," *Inorg. Chim. Acta*, vol. 120, pp. 153–157, 1986.

[48] G.G. Barna and I.S. Butler, "Vibrational Spectra of 1,5-Cyclooctadiene, Di-μ-chlorobis[(1,5-cyclooctadiene)rhodium(I)], Di-μ-chlorobis[(1,5-cyclooctadiene)copper(I)] and Bis(1,5-cyclooctadiene)copper(I) Perchlorate," *J. Raman Spectrosc.*, vol. 7, pp. 168–172, 1978.

[49] D.B. Powell and T.J. Leedham, "Infrared and Raman Spectra of 1,5-

Cyclooctadiene Complexes of Rhodium, Palladium and Platinum," *Spectrochim. Acta Part A Mol. Spectrosc.*, vol. 28, pp. 337–341, 1972.

[50] X. Zhou, P. Pulay, R. Hargitai, A. Stirling, and J. Mink, "Complete Assignment of Vibrational Spectra of 1,5-Cyclooctadiene - A Theoretical and Experimental Infrared and Raman Study," *Spectrochim. Acta Part A Mol. Spectrosc.*, vol. 49, pp. 257–270, 1993.

[51] R.G. Pearson, "Absolute Electronegativity and Hardness Correlated with Molecular Orbital Theory," *Proc. Natl. Acad. Sci. U. S. A.*, vol. 83, pp. 8440–8441, 1986.

[52] A.K. Guha, C. Das, and A.K. Phukan, "Heterocyclic Carbenes of Diverse Flexibility: A Theoretical Insight," *J. Organomet. Chem.*, vol. 696, pp. 586–593, 2011.

[53] J.C.A. Boeyens, L. Denner, S.W. Orchard, I. Rencken, and B.G. Rose, "Crystal Structures of the Cis,Cis-1,5-Cyclooctadiene Complexes of Copper(I)chloride and Rhodium(I) chloride," South Afr. J. Chem., vol. 39, pp.229-232, 1986.

[54] S. Sudha, M. Karabacak, M. Kurt, M. Cinar, and N. Sundaraganesan, "Molecular Structure, Vibrational Spectroscopic, First-order Hyperpolarizability and HOMO, LUMO Studies of 2-Aminobenzimidazole.," *Spectrochim. Acta. A. Mol. Biomol. Spectrosc.*, vol. 84, pp. 184–95, 2011.

[55] D.W. Wertz and M.A. Moseley, "A Vibrational Study of the Metal-Olefin Bond in Norbornadiene Complexes of Rh(I), Pd(II) and Pt(II)," *Spectrochim. Acta Part A Mol. Spectrosc.*, vol. 36, pp. 467–472, 1980.

[56] R. Dennington, T. Keith, and J. Millam, "GaussView, Version 5.," *Semichem Inc. , Shawnee Mission, KS*. Semichem Inc, 2009.

[57] A.A. Al-Saadi and J. Laane, "Ab Initio and DFT Calculations for the Structure and Vibrational Spectra of Cyclopentene and its Isotopomers," *J. Mol. Struct.*, vol. 830, pp. 46–57, 2007.

[59] C.K. Kim, K.A. Lee, C.K. Kim, B.S. Lee, and H.W. Lee, "NBO Analyses of the Back-Bonding in Metal-Olefin Complexes," *Chem. Phys. Lett.*, vol. 391, pp. 321–324, 2004.

[60] D.N. Schlappi and D.L. Cedeno, "Metal-Olefin Bond Energies in $M(CO)_5(C_2H_{4-n}Cl_n)$ M = Cr, Mo, W; n = 0 - 4: Electron-Withdrawing Olefins Do Not Increase the Bond Strength," *J. Phys. Chem. A*, vol. 113, pp. 9692–9699, 2009.

[61] D.L. Cedeno and E. Weitz, "Experimental Determination of the Cr-C_2Cl_4 Bond Dissociation Enthalpy in $Cr(CO)_5(C_2Cl_4)$: Quantifying Metal-Olefin Bonding Interactions," *J. Am. Chem. Soc.*, vol. 123, pp. 12857–12865, 2001.

[62] J. Dewar, "A Review of the pi-Complex Theory," *Bull. Soc. Chim. Fr.*, vol. 18, pp. C71–C79, 1951.

[63] J. Chatt and L.A. Duncanson, "Olefin Co-ordination Compounds. Part III. Infra-red Spectra and Structure: Attempted Preparation of Acetylene Complexes," *J.*

Chem. Soc., pp. 2939–2947, 1953.

[64] G. Pannetier, R. Bonnaire, P. Fougeroux, and P. Alépée, "Complexes De l'iridium Avec Le Cyclooctadiène-1,5 1. Propriétés Physicochimiques De $[(COD\text{-}1,5)IrCl]_2$ Variété Orange Et De $[(COD\text{-}1,5)IrHCl_2]_2$," *J. Less Common Met.*, vol. 21, pp. 103–113, 1970.

[65] D.B. Powell, J.G.V. Scott, and N. Sheppard, "Infrared and Raman Spectra and the vC=C Stretching Frequencies of Some Silver-Olefin and Platinum-Olefin Complexes," *Spectrochim. Acta Part A Mol. Spectrosc.*, vol. 28, pp. 327–335, 1972.

[66] A.L. Gavrilova and B. Bosnich, "Principles of Mononucleating and Binucleating Ligand Design," *Chem. Rev.*, vol. 104, pp. 349–383, 2004.

[67] I. Mena, M.A. Casado, V. Polo, P. García-Orduña, F.J. Lahoz, and L.A. Oro, "P-H Activation of Secondary Phosphanes on a Parent Amido Diiridium Complex.," *Dalton Trans.*, vol. 43, pp. 1609–19, 2014.

[68] F.A. Cotton, P. Lahuerta, J. Latorre, M. Sanau, S. Isabel, and S. Willi, "A New Sulfur-Bridged Ir(I)-Ir(I) Compound and Its Conversion to a Compound Containing a Metal-Metal Bond. Crystal Structures of $Ir_2(SPh)_2(COD)_2$ and $Ir_2Cl_2(\mu_2\text{-}SPh)_2(COD)_2$," *Inorg. Chem.*, vol. 27, pp. 2131–2135, 1988.

[69] J. Zhou and J.F. Hartwig, "Iridium-Catalyzed H/D Exchange at Vinyl Groups without Olefin Isomerization," *Angew. Chem.*, vol. 120, pp. 5867–5871, 2008.

[70] C. Cheng and J.F. Hartwig, "Iridium-Catalyzed Silylation of Aryl C–H Bonds," *J. Am. Chem. Soc.*, vol. 137, pp. 592–595, 2015.

[71] T.A. Boebel and J.F. Hartwig, "Iridium-Catalyzed Preparation of Silylboranes by Silane Borylation and Their Use in the Catalytic Borylation of Arenes," *Organometallics*, vol. 27, pp. 6013–6019, 2008.

[72] C.W. Liskey and J.F. Hartwig, "Iridium-Catalyzed C-H Borylation of Cyclopropanes," *J. Am. Chem. Soc.*, vol. 135, pp. 3375–3378, 2013.

[73] L.V.A. Hale, K.A. McGarry, M.A. Ringgold, and T.B. Clark, "Role of Hemilabile Diamine Ligands in the Amine-Directed C–H Borylation of Arenes," *Organometallics*, vol. 34, pp. 51–55, 2015.

[74] S.G. Bratsch, "Electronegativity Equalization with Pauling Units," *J. Chem. Educ.*, vol. 61, pp. 588-589, 1984.

[75] S.G. Bratsch, "A Group Electronegativity Method with Pauling Units," *J. Chem. Educ.*, vol. 62, pp. 101-103, 1985.

[76] I. Mena, M. A. Casado, P. Garcia-Orduna, V. Polo, F. J. Lahoz, A. Fazal, and L. A. Oro, "Direct Access to Parent Amido Complexes of Rhodium and Iridium through N-H Activation of Ammonia," *Angew. Chem. Int. Ed.*, vol. 50, pp. 11735–11738, 2011

[77] I. Tanaka, N. Jin-No, and T. Kushida, N. Tsutsui, T. Ashida, H. Suzuki, H.

Sakurai, Y. Moro-Oka and T, Ikawa "Crystal Structures of (1,5-cyclooctadiene) di-μ-methoxo-dirhodium (I) and Tetrakis(η^3-allyl)di-μ-hydroxo-dirhodium(III)," *Bull. Chem. Soc.,* vol. 56, pp. 657–661, 1983.

[78] J.M. Smith, D.A. Hrovat, and W.T. Borden, "Synthesis and Spectroscopy of Tricycle[3 .3.3.$0^{3.7}$]undec-3(7)-ene: Confirmation of Computational Predictions Regarding the Effects of Byramidalization on Alkene Ionization Energies and Electron Affinities," *J. Am. Chem. Soc.*, vol. 115, pp. 3816–3817, 1993.

[79] M. Aydemir, A. Baysal, N. Meric, C. Kayan, B. Gümgüm, S. Özkar, and E. Şahin, "Organometallic Ruthenium, Rhodium and Iridium Complexes Containing a P-bound Thiophene-2-(N-diphenylphosphino)methylamine Ligand: Synthesis, Molecular Structure and Catalytic Activity," *J. Organomet. Chem.*, vol. 696, pp. 2584–2588, 2011.

[80] M.V. Jiménez, J. Fernández-Tornos, J.J. Pérez-Torrente, F.J. Modrego, S. Winterle, C. Cunchillos, F.J. Lahoz, and L.A. Oro, "Iridium(I) Complexes with Hemilabile N-Heterocyclic Carbenes: Efficient and Versatile Transfer Hydrogenation Catalysts," *Organometallics*, vol. 30, pp. 5493–5508, 2011.

[81] S. Sakaguchi, T. Yamaga, and Y. Ishii, "Iridium-Catalyzed Transfer Hydrogenation of α,β-Unsaturated and Saturated Carbonyl Compounds with 2-Propanol," *J. Org. Chem.*, vol. 66, pp. 4710–2, 2001.

[82] R. Marčec, "Ligand Effects in the Rhodium Acetate Catalyzed Hydrogen Transfer," *React. Kinet. Catal. Lett.*, vol. 31, pp. 337–341, 1986.

[83] R. Uson, L.A. Oro, R. Sariego, and M.A. Esteruelas, "Catalytic Transfer Hydrogenation by Cationic Rhodium(I) Complexes," *J. Organomet. Chem.*, vol. 214, pp. 399–404, 1981.

[84] C.M. Thomas and G. Süss-Fink, "Ligand Effects in the Rhodium-Catalyzed Carbonylation of Methanol," *Coord. Chem. Rev.*, vol. 243, pp. 125–142, 2003.

[85] O. Pàmies and J.E. Bäckvall, "Studies on the Mechanism of Metal-Catalyzed Hydrogen Transfer from Alcohols to Ketones," *Chem. Eur. J.*, vol. 7, pp. 5052–5058, 2001.

[86] A. Tencich, J. Kaspar, and M. Graziani, "Hydrogenation of Ketones and Olefins via Hydrogen Transfer Catalyzed by Rhodium and Iridium Phosphine Complexes," *J. Organomet. Chem.*, vol. 240, pp. 453–459, 1982.

[87] C. Bianchini, L. Glendenning, F. Zanobini, E. Farnetti, M. Graziani, and E. Nagy, "Asymmetric Hydrogen-Transfer Reduction of Prochiral and α,β,-Unsaturated Ketones by Iridium Complexes Containing Optically Pure Aminodiphosphine Ligands," *J. Mol. Catal. A Chem.*, vol. 132, pp. 13–19, 1998.

[88] C. Tejel, M. Ciriano, S. Jiménez, and L.A. Oro, "Reactions of Phosphine Ligands with Iridium Complexes Leading to C(sp^3)-H Bond Activation," *Organometallics*, vol. 24, pp. 1105–1111, 2005.

[89] U. Hintermair, T.P. Brewster, L.M. Pratt, N.D. Schley, and R.H. Crabtree,

"Hydrogen-Transfer Catalysis with Cp * Ir^{III} Complexes: The Influence of the Ancillary Ligands," *ACS Catal.*, vol. 4, pp. 99–108, 2014.

[90] R. Uson, L.A. Oro, D. Carmona, amd M.A. Esteruelas, "Cationic Iridium(I) Complexes with 1,5-Cyclooctadiene and Nitrogen Ligands," *Inorg. Chim. Acta*, vol. 73, pp. 215–219, 1983.

[91] M.A. Esteruelas, M.P. Garcia, F.J. Lahoz, M. Martin, J. Modrego, E. Onate, and L.A. Oro, "Synthesis and Characterization of New Hydridoiridium Complexes Containing Carboxylate Ligands," *Inorg. Chem.*, vol. 33, pp. 3473–3480, 1994.

[92] D. Totev, A. Salzer, D. Carmona, and L. Oro, "Synthesis and Characterization of Ru(II), Rh(III) and Ir(III) Complexes of the 'Daniphos' Ligands and Their Application in the Hydrogen Transfer Catalysis," *Inorg. Chim.* , vol. 357, pp. 2889–2898, 2004.

[93] S.H. Oakley, M.P. Coogan, and R.J. Arthur, "Synthesis of Bis(imino)aryl Iridium Pincer Complexes and Demonstration of Catalytic Hydrogen-Transfer Activity," *Organometallics*, vol. 26, pp. 2285–2290, 2007.

[94] S. Kozuch and S. Shaik, "How to Conceptualize Catalytic Cycles? The Energetic Span Model," *Acc. Chem. Res.*, vol. 44, pp. 101–110, 2011.

[95] P.C. Kamer, P.W. van Leeuwen, and J.N. Reek, "Wide Bite Angle Diphosphines: Xantphos Ligands in Transition Metal Complexes and Catalysis," *Acc. Chem. Res.*, vol. 34, pp. 895–904, 2001.

[96] L. Zeng, F. Wu, Y.Y. Li, Z.R. Dong, and J.X. Gao, "Synthesis and Characterization of Novel Chiral Bidentate P,N-Containing Ligands and Ruthenium(II) Complex. The Application in Asymmetric Transfer Hydrogenation of Ketones," *J. Organomet. Chem.*, vol. 762, pp. 34–39, 2014.

[97] O. Dayan, S. Dayan, I. Kani, and B. Çetinkaya, "Ruthenium(II) Complexes Bearing Pyridine-Based Tridentate and Bidentate Ligands: Catalytic Activity for Transfer Hydrogenation of Aryl Ketones," *Appl. Organomet. Chem.*, vol. 26, pp. 663–670, 2012.

[98] A.L. Müller, T. Bleith, T. Roth, H. Wadepohl, and L.H. Gade, "Iridium Half-Sandwich Complexes with Di- and Tridentate Bis(pyridylimino)isoindolato Ligands: Stoichiometric and Catalytic Reactivity," *Organometallics*, vol. 34, pp. 2326-2342, 2015.

[99] P.W.N.M. van Leeuwen, *Homogeneous Catalysis: Understanding the Art*. Kluwer Academic Publishers, 2006.

[100] P. Dierkes and P.W.N.M. van Leeuwen, "The Bite Angle Makes the Difference: A Practical Ligand Parameter for Diphosphine Ligands," *J. Chem. Soc., Dalton Trans.*, no. 10. pp. 1519–1530, 1999.

[101] C.A Tolman, "Steric Effects of Phosphorus Ligands in Organometallic Chemistry and Homogeneous Catalysis," *Chem. Rev.*, vol. 77, pp. 313–348, 1977.

[102] C. Casey and G. Whiteker, "The Natural Bite Angle of Chelating Diphosphines,"

Isr. J. Chem., vol. 30, pp. 299–304, 1990.

[103] M.N. Birkholz, Z. Freixa, and P.W.N.M. van Leeuwen, "Bite Angle Effects of Diphosphines in C-C and C-X Bond Forming Cross Coupling Reactions," *Chem. Soc. Rev.*, vol. 38, pp. 1099–1118, 2009.

[104] D.L. Thorn and R. Hoffmann, "The Olefin Insertion Reaction," *J. Am. Chem. Soc.*, vol. 100, pp. 2079–2090, 1978.

[105] G.P.C.M. Dekker, C.J. Elsevier, K. Vrieze, P.W.N.M. van Leeuwen, and C.F. Roobeek, "Influence of Ligands and Anions on the Insertion of Alkenes into Palladium-Acyl and Palladium-Carbomethoxy Bonds in the Neutral Complex (dppp)Pd(C(O)CH_3)Cl and the Ionic Complexes [(P-P)PdR(L)]$^{+}SO_3CF_3^{-}$ (P-P = dppe, dppp, dppb; R = C(O)CH_3, L = CH_3CN, PPh_3; R = C(O)CH_3, L = PPh_3," *J. Organomet. Chem.*, vol. 430, pp. 357–372, 1992.

[106] A.M.A. Rocha Gonsalves, J.C. Bayón, M.M. Pereira, M.E.S. Serra, and J.P.R. Pereira, "Asymmetric Transfer Hydrogenation of Acrylic Acids Catalyzed by Rhodium(I) Complexes of Diphosphine Ligands," *J. Organomet. Chem.*, vol. 553, pp. 199–204, 1998.

[107] R.H.M. Weiwei Zuo, Alan J. Lough, Young Feng Li, "Amine(imine)diphosphine Iron Catalysts for Asymmetric Transfer Hydrogenation of Ketones and Imines," *Science*, vol. 342, pp. 1080–1083, 2013.

[108] E. Zuidema, P.W.N.M. van Leeuwen, and C. Bo, "Reductive Elimination of Organic Molecules from Palladium-Diphosphine Complexes," *Organometallics*, vol. 24, pp. 3703–3710, 2005.

[109] C.S. Ewig and J.R. Van Wazer, "Ab Initio Structures of Phosphorus Acids and Esters. 1. Phosphinic, Phosphonic, and Phosphoric Acids," *J. Am. Chem. Soc.*, vol. 107, pp. 1965–1971, 1985.

[110] A.J. Kirby, *The Anomeric Effect and Related Stereoelectronic Effects at Oxygen*: *Reactivity and Structure Concepts in Organic Chemistry*, vol. 15. Springer Science and Business Media, 2012.

[111] S. Detoni and D. Hadži, "Hydroxyl Bands in the Infra-red Spectra of Organophosphoric and Phosphinic Acids," *Spectrochim. Acta*, vol. 20, pp. 949–955, 1964.

[112] M.E. Druyan, A.H. Reis, E. Gebert, S.W. Peterson, G.W. Mason, and D.F. Peppard, "Dimeric Structure of Di-tert-butylphosphinic Acid," *J. Am. Chem. Soc.*, vol. 98, pp. 4801–4805, 1976.

[113] J.A. Walmsley, "Self-Association of Phosphinic Acids in Nonpolar Solvents. The Origin of the Apparent Dipole Moment in Symmetric Dimers," *J. Phys. Chem.*, vol. 88, pp. 1226–1231, 1984.

[114] A.H. Reis, S.W. Peterson, M.E. Druyan, E. Gebert, G.W. Mason, and D.F. Peppard, "Sterically Hindered Solvent Extractants. 2. A Neutron-Diffraction Study of the Di-tert-butylphosphinic Acid Dimer Showing Strong Asymmetric Hydrogen

Bonding," *Inorg. Chem.*, vol. 15, pp. 2748–2752, 1976.

[115] L. González, O. Mó, M. Yáñez, and J. Elguero, "Very Strong Hydrogen Bonds in Neutral Molecules: The Phosphinic Acid Dimers," *J. Chem. Phys.*, vol. 109, pp. 2685-2693, 1998.

[116] G. Pistolis, C. M. Paleos, and A. Malliaris, "Molecular Recognition in Organic Solvents. The Importance of Excimer Fluorescence Spectroscopy," *J. Phys. Chem.*, vol. 99, pp. 8896–8902, 1995.

[117] P.L. Wash, E. Maverick, J. Chiefari, and D.A. Lightner, "Acid−Amide Intermolecular Hydrogen Bonding," *J. Am. Chem. Soc.*, vol. 119, pp. 3802–3806, 1997.

[118] A.J. Beveridge and G.C. Heywood, "A Quantum Mechanical Study of the Active Site of Aspartic Proteinases," *Biochemistry*, vol. 32, pp. 3325–3333, 1993.

[119] R.E. Asfin, G.S. Denisov, and K.G. Tokhadze, "The Infrared Spectra and Enthalpies of Strongly Bound Dimers of Phosphinic Acids in the Gas Phase. $(CH_2Cl)_2POOH$ and $(C_6H_5)_2POOH$," *J. Mol. Struct.*, vol. 608, pp. 161–168, 2002.

[120] G.S. Denisov and K.G. Tokhadze, "Utrastrong Hydrogen Bond in Gas Phase. Dimer of Dimethylphosphinic Acid," *Dokl. Phys. Chem.*, vol. 337, pp. 117–119, 1994.

[121] K.G. Tokhadze, G.S. Denisov, M. Wierzejewska, and M. Drozd, "First Example of the ABC ν(OH) Absorption Structure for Both Gaseous and Crystalline Phase: Infrared Studies of Dimethylphosphinic Acid," *J. Mol. Struct.*, vol. 404, pp. 55–62, 1997.

[122] L.S. Khaikin, O.E. Grikina, A.V. Golubinskii, L.V. Vilkov, E.G. Atavin, R.E. Asfin, and G.S. Denisov, "Geometry of a Strong Hydrogen Bond As Determined by Gas-Phase Electron Diffraction: The Cyclic Dimer of Dimethylphosphinic Acid," *Dokl. Phys. Chem.*, vol. 390, pp. 158–162, 2003.

[123] Z. Kolarik, "Review: Dissociation, Self-Association, and Partition of Monoacidic Organophosphorus Extractants," *Solvent Extr. Ion Exch.*, vol. 28, pp. 707–763, 2010.

[124] L.K. An, S. Muralidharan, and H. Freiser, "Determination of the Equilibrium Constants of Organophosphorus Liquid-Liquid Extractants by Inductively Coupled Plasma-Atomic Emission Spectroscopy," *Solvent Extr. Ion Exch.*, vol. 3, pp. 895–908, 1985.

[125] P.R. Danesi, L. Reichley-Yinger, G. Mason, L. Kaplan, E.P. Horwltz, and H. Diamond, "Selectivity-Structure Trends in the Extraction of Co(II) and Ni(II) by Dialkyl Phosphoric, Alkyl Alkylphosphonic,and Dialkylphosphinic Acids," *Solvent Extr. Ion Exch.*, vol. 3, pp. 435–452, 1985.

[126] Y. Komatsu and H. Freiser, "Extraction Separation of Tervalent Lanthanide Metals with Bis(2,4,4-trimethylpentyl)phosphinic Acid," *Anal. Chim. Acta*, vol. 227, pp. 397–404, 1989.

[127] M. Aguilar, N. Miralles, and A.M. Sastre, “Metal Complexes with Phosphonic and Phosphinic Acids,” *Rev. Inorg. Chem.*, vol. 10, pp. 93–120, 1989.

[128] S.D. Alexandratos, M.A. Strand, D.R. Quillen, and A.J. Walder, “Synthesis and Characterization of Bifunctional Phosphinic Acid Resin,” *Macromolecules*, vol. 18, pp. 829–835, 1985.

[129] S.D. Alexandratos, D.L. Wilson, M.A. Strand, D.R. Quillen, A.J. Walder, and W.J. McDowell, “Metal Ion Extraction Capability of Phosphinic Acid Resins: Comparative Study of Phosphinic, Sulfonic, and Carboxylic Resins Using Zinc Ions,” *Macromolecules*, vol. 18, pp. 835–840, 1985.

VITAE

Name :Saheed Abiodun Popoola

Nationality :Nigerian

Date of Birth :2/11/1978

Email :popsa02@yahoo.com

Address :Department of Chemistry, KFUPM.

Academic Background :BSc. (Chemistry), University of Agriculture Abeokuta, Nigeria (2003), MSc. (Industrial Chemistry), University of Agriculture Abeokuta, Nigeria (2009) PhD (Chemistry), King Fahd University of Petroleum and Minerals, Dhahran, Saudi Arabia (2016)